

ISSN 1881-7831 Online ISSN 1881-784X



Drug Discoveries & Therapeutics

Volume 17, Number 5
October, 2023



www.ddtjournal.com



Drug Discoveries & Therapeutics



ISSN: 1881-7831
Online ISSN: 1881-784X
CODEN: DDTBX
Issues/Year: 6
Language: English
Publisher: IACMHR Co., Ltd.

Drug Discoveries & Therapeutics is one of a series of peer-reviewed journals of the International Research and Cooperation Association for Bio & Socio-Sciences Advancement (IRCA-BSSA) Group. It is published bimonthly by the International Advancement Center for Medicine & Health Research Co., Ltd. (IACMHR Co., Ltd.) and supported by the IRCA-BSSA.

Drug Discoveries & Therapeutics publishes contributions in all fields of pharmaceutical and therapeutic research such as medicinal chemistry, pharmacology, pharmaceutical analysis, pharmaceutics, pharmaceutical administration, and experimental and clinical studies of effects, mechanisms, or uses of various treatments. Studies in drug-related fields such as biology, biochemistry, physiology, microbiology, and immunology are also within the scope of this journal.

Drug Discoveries & Therapeutics publishes Original Articles, Brief Reports, Reviews, Policy Forum articles, Case Reports, Communications, Editorials, News, and Letters on all aspects of the field of pharmaceutical research. All contributions should seek to promote international collaboration in pharmaceutical science.

Editorial Board

International Field Chief Editors:

Fen-Er CHEN
Fudan University, Shanghai, China

Takashi KARAKO
National Center for Global Health and Medicine, Tokyo, Japan

Hongzhou LU
National Clinical Research Centre for Infectious Diseases, Shenzhen, Guangdong, China

Munehiro NAKATA
Tokai University, Hiratsuka, Japan

Sven SCHRÖDER
University Medical Center Hamburg Eppendorf(UKE), Hamburg, Germany

Kazuhisa SEKIMIZU
Teikyo University, Tokyo, Japan

Corklin R. STEINHART
CAN Community Health, FL, USA

Executive Editor:

Hongzhou LU
National Clinical Research Centre for Infectious Diseases, Shenzhen, Guangdong, China

Associate Editors:

Nobuyoshi AKIMITSU
The University of Tokyo, Tokyo, Japan

Feihu CHEN
Anhui Medical University, Hefei, Anhui, China

Jianjun GAO
Qingdao University, Qingdao, Shandong, China

Hiroshi HAMAMOTO
Teikyo University, Tokyo, Japan

Chikara KAITO
Okayama University, Okayama, Japan

Gagan KAUSHAL
Jefferson College of Pharmacy, Philadelphia, PA, USA

Xiao-Kang LI
National Research Institute for Child Health and Development, Tokyo, Japan

Yasuhiko MATSUMOTO
Meiji Pharmaceutical University, Tokyo, Japan

Atsushi MIYASHITA
Teikyo University, Tokyo, Japan

Masahiro MURAKAMI
Osaka Ohtani University, Osaka, Japan

Tomofumi SANTA
The University of Tokyo, Tokyo, Japan

Tianqiang SONG
Tianjin Medical University, Tianjin, China

Sanjay K. SRIVASTAVA
Texas Tech University Health Sciences Center, Abilene, TX, USA

Hongbin SUN
China Pharmaceutical University, Nanjing, Jiangsu, China

Fengshan WANG
Shandong University, Jinan, Shandong, China.

Proofreaders:

Curtis BENTLEY
Roswell, GA, USA
Thomas R. LEBON
Los Angeles, CA, USA

Editorial and Head Office:

Pearl City Koishikawa 603,
2-4-5 Kasuga, Bunkyo-ku,
Tokyo 112-0003, Japan
E-mail: office@ddtjournal.com

Drug Discoveries & Therapeutics

Editorial and Head Office

Pearl City Koishikawa 603, 2-4-5 Kasuga, Bunkyo-ku,
Tokyo 112-0003, Japan

E-mail: office@ddtjournal.com
URL: www.ddtjournal.com

Editorial Board Members

Alex ALMASAN (Cleveland, OH)	Youcui HU (Beijing)	Sridhar MANI (Bronx, NY)	Yong XU (Guangzhou, Guangdong)	
John K. BUOLAMWINI (Memphis, TN)	Yu HUANG (Hong Kong)	Tohru MIZUSHIMA (Tokyo)	Bing YAN (Jinan, Shandong)	
Jianping CAO (Shanghai)	Zhangjian HUANG (Nanjing Jiangsu)	Jasmin MONPARA (Philadelphia, PA)	Chunyan YAN (Guangzhou, Guangdong)	
Shousong CAO (Buffalo, NY)	Amrit B. KARMARKAR (Karad, Maharashtra)	Yoshinobu NAKANISHI (Kanazawa, Ishikawa)	Xiao-Long YANG (Chongqing)	
Jang-Yang CHANG (Tainan)	Toshiaki KATADA (Tokyo)	Siriporn OKONOGI (Chiang Mai)	Yun YEN (Duarte, CA)	
Zhe-Sheng CHEN (Queens, NY)	Ibrahim S. KHATTAB (Kuwait)	Weisan PAN (Shenyang, Liaoning)	Yongmei YIN (Tianjin)	
Zilin CHEN (Wuhan, Hubei)	Shiroh KISHIOKA (Wakayama, Wakayama)	Chan Hum PARK (Eumseong)	Yasuko YOKOTA (Tokyo)	
Xiaolan CUI (Beijing)	Robert Kam-Ming KO (Hong Kong)	Rakesh P. PATEL (Mehsana, Gujarat)	Yun YOU (Beijing)	
Saphala DHITAL (Clemson, SC)	Nobuyuki KOBAYASHI (Nagasaki, Nagasaki)	Shivanand P. PUTHLI (Mumbai, Maharashtra)	Rongmin YU (Guangzhou, Guangdong)	
Shaofeng DUAN (Lawrence, KS)	Toshiro KONISHI (Tokyo)	Shafiqur RAHMAN (Brookings, SD)	Tao YU (Qingdao, Shandong)	
Hao FANG (Jinan, Shandong)	Peixiang LAN (Wuhan, Hubei)	Gary K. SCHWARTZ (New York, NY)	Guangxi ZHAI (Jinan, Shandong)	
Marcus L. FORREST (Lawrence, KS)	Chun-Guang LI (Melbourne)	Luqing SHANG (Tianjin)	Liangren ZHANG (Beijing)	
Tomoko FUJIYUKI (Tokyo)	Minyong LI (Jinan, Shandong)	Yuemao SHEN (Jinan, Shandong)	Lining ZHANG (Jinan, Shandong)	
Takeshi FUKUSHIMA (Funabashi, Chiba)	Xun LI (Jinan, Shandong)	Rong SHI (Shanghai)	Na ZHANG (Jinan, Shandong)	
Harald HAMACHER (Tübingen, Baden-Württemberg)	Dongfei LIU (Nanjing, Jiangsu)	Chandan M. THOMAS (Bradenton, FL)	Ruiwen ZHANG (Houston, TX)	
Kenji HAMASE (Fukuoka, Fukuoka)	Jian LIU (Hefei, Anhui)	Michihisa TOHDA (Sugitani, Toyama)	Xiu-Mei ZHANG (Jinan, Shandong)	
Junqing HAN (Jinan, Shandong)	Jikai LIU (Wuhan, Hubei)	Li TONG (Xining, Qinghai)	Xuebo ZHANG (Baltimore, MD)	
Xiaojiang HAO (Kunming, Yunnan)	Jing LIU (Beijing)	Murat TURKOGLU (Istanbul)	Yingjie ZHANG (Jinan, Shandong)	
Kiyoshi HASEGAWA (Tokyo)	Xinyong LIU (Jinan, Shandong)	Hui WANG (Shanghai)	Yongxiang ZHANG (Beijing)	
Waseem HASSAN (Rio de Janeiro)	Yuxiu LIU (Nanjing, Jiangsu)	Quanxing WANG (Shanghai)	Haibing ZHOU (Wuhan, Hubei)	
Langchong HE (Xi'an, Shaanxi)	Hongxiang LOU (Jinan, Shandong)	Stephen G. WARD (Bath)	Jian-hua ZHU (Guangzhou, Guangdong)	
Rodney J. Y. HO (Seattle, WA)	Hai-Bin LUO (Haikou, Hainan)	Zhun WEI (Qingdao, Shandong)	(As of October 2022)	
Hsing-Pang HSIEH (Zhunan, Miaoli)	Xingyuan MA (Shanghai)	Tao XU (Qingdao, Shandong)		
Yongzhou HU (Hangzhou, Zhejiang)	Ken-ichi MAFUNE (Tokyo)	Yuhong XU (Shanghai)		

Original Article

- 304-311** **Inhaled ciclesonide does not affect production of antibodies or elimination of virus in patients with COVID-19: Subanalysis of a multicenter, open-label randomized trial.**
Manabu Suzuki, Akihiro Matsunaga, Tohru Miyoshi-Akiyama, Junko Terada-Hirashima, Kenji Sadamasu, Mami Nagashima, Jin Takasaki, Shinya Izumi, Masayuki Hojo, Yukihito Ishizaka, Haruhito Sugiyama
- 312-319** **Elevated indoleamine 2,3-dioxygenase activity is associated with endothelial dysfunction in people living with HIV and ROS production in human aortic endothelial cells *in vitro***
Junyang Yang, Rentian Cai, Jingna Xun, Renfang Zhang, Li Liu, Yinzhang Shen, Tangkai Qi, Zhenyan Wang, Wei Song, Yang Tang, Jianjun Sun, Shuibao Xu, Bihe Zhao, Hongzhou Lu, Jun Chen
- 320-327** **Effects of plant-based copper nanoparticles on the elimination of ciprofloxacin.**
Tanongsak Sassa-deepaeng, Wachira Yodthong, Nattakanwadee Khumpirapang, Songyot Anuchapreeda, Siriporn Okonogi
- 328-339** **FASN promotes gallbladder cancer progression and reduces cancer cell sensitivity to gemcitabine through PI3K/AKT signaling.**
Haihong Cheng, Yuxin Sun, Xiaopeng Yu, Di Zhou, Jun Ding, Shouhua Wang, Fei Ma

Brief Report

- 340-345** **Efficacy of *Andrographis paniculata* spray in acute pharyngitis: A randomized controlled trial.**
Risa Okonogi, Vich Thampanya, Siriporn Okonogi
- 346-350** **Hypofibrinolytic phenotype in Tsumura Suzuki Obese Diabetes (TSOD) mice unrelated to hyperglycemia.**
Naoki Ohkura, Riyo Morimoto-Kamata, Yuichi Kamikubo, Yoshihisa Takahashi, Katsutaka Oishi
- 351-356** **Effectiveness of an artificial intelligence-based training and monitoring system in prevention of nosocomial infections: A pilot study of hospital-based data.**
Ting Huang, Yue Ma, Shaxi Li, Jianchao Ran, Yifan Xu, Tetsuya Asakawa, Hongzhou Lu
- 357-362** **A pilot study comparing the disinfecting effects of commercialized stable ClO₂ solution (free of activation) with conventional H₂O₂ on dental unit waterlines in the dental practice setting.**
Xiaolei Zhang, Jingjing Sha, Zefan Huang, Sisi Chen, Xufei Luo, Ruijun Liu, Tetsuya Asakawa, Qiang Zhang

Correspondence

- 363-364 **EQUIBIND: A geometric deep learning-based protein-ligand binding prediction method.**
Yuze Li, Li Li, Shuang Wang, Xiaowen Tang

Letter to the Editor

- 365-367 **Complete trisomy 9 detected by noninvasive prenatal testing and confirmed by amniocentesis.**
Feixiang Huang, Jing Zhou, Zheyun Xu, Qing Qi, Hongmei Sun, Lei Chen, Ling Wang

Inhaled ciclesonide does not affect production of antibodies or elimination of virus in patients with COVID-19: Subanalysis of a multicenter, open-label randomized trial

Manabu Suzuki^{1,*}, Akihiro Matsunaga², Tohru Miyoshi-Akiyama³,
Junko Terada-Hirashima¹, Kenji Sadamasu⁴, Mami Nagashima⁴, Jin Takasaki¹,
Shinya Izumi¹, Masayuki Hojo¹, Yukihito Ishizaka², Haruhito Sugiyama¹

¹ Department of Respiratory Medicine, National Center for Global Health and Medicine, Tokyo, Japan;

² Department of Intractable Diseases, Research Institute, National Center for Global Health and Medicine, Tokyo, Japan;

³ Pathogenic Microbe Laboratory, Research Institute, National Center for Global Health and Medicine, Tokyo, Japan;

⁴ Tokyo Metropolitan Institute of Public Health, Tokyo, Japan.

SUMMARY During an earlier multicenter, open-label, randomized controlled trial designed to evaluate the effectiveness of high-dose inhaled ciclesonide in patients with asymptomatic or mild coronavirus disease 2019 (COVID-19), we observed that worsening of shadows on CT without worsening of clinical symptoms was more common with ciclesonide. The present study sought to determine if an association exists between worsening CT shadows and impaired antibody production in patients treated with inhaled ciclesonide. Eighty-nine of the 90 patients in the original study were prospectively enrolled. After exclusions, there were 36 patients each in the ciclesonide and control groups. We analyzed antibody titers against severe acute respiratory syndrome coronavirus 2 (SARS-CoV-2) nucleocapsid protein at various time points. Changes in viral load during treatment were compared. There was no significant difference in age, sex, body mass index, background clinical characteristics, or symptoms between the two groups. Although evaluation on day 8 suggested a greater tendency for worsening shadows on CT in the ciclesonide group ($p = 0.072$), there was no significant difference between them in the ability to produce antibodies ($p = 0.379$) or the maximum antibody titer during the clinical course. In both groups, worsening CT shadows and higher viral loads were observed on days 1–8, suggesting ciclesonide does not affect clearance of the virus ($p = 0.134$). High-dose inhaled ciclesonide did not impair production of antibodies against SARS-CoV-2 or affect elimination of the virus, suggesting that this treatment can be used safely in patients with COVID-19 patients who use inhaled steroids for asthma and other diseases.

Keywords SARS-CoV-2 nucleocapsid protein antibody, asymptomatic or mild COVID-19, randomized clinical trial, anti-viral effect, viral load

1. Introduction

In 2019, severe acute respiratory syndrome coronavirus 2 (SARS-CoV-2) emerged and seriously threatened human health and socioeconomic activity worldwide. Clinical manifestations of SARS-CoV-2 infection vary depending on the presence of risk factors that include obesity, cardiovascular disease, diabetes, older age, and comorbidities (1). The rationale for using steroids in patients who are hospitalized with coronavirus disease 2019 (COVID-19) is based on the finding in a clinical trial that administration of dexamethasone reduced mortality in these patients, suggesting that the anti-

inflammatory effects of the compound overcome its negative immunosuppression effects (2).

Interestingly, ciclesonide is thought to ameliorate inflammation by inhibiting the pathogenic kinase PAK1 (RAC/CDC42-activated kinase 1) (3). Basic research has suggested that ciclesonide may have potent antiviral activity against SARS-CoV-2 (4), and case reports have also shown the effectiveness of ciclesonide (5). Moreover, several lines of evidence suggest that inhaled ciclesonide has anti-viral activity (6,7). Although it is unclear whether asthma is a risk factor for severe SARS-CoV-2 infection (8), several clinical trials of ciclesonide have been conducted in outpatients or hospitalized

patients based on these results (9-11). However, it has not been confirmed that ciclesonide improves outcomes in patients with severe clinical symptoms. We performed a clinical trial to evaluate the effects of ciclesonide 400 µg inhaled three times daily for 7 consecutive days in patients with mild clinical signs of COVID-19 at the time of enrollment (12). Surprisingly, we found that worsening of shadows on CT was more common in patients treated with ciclesonide (39%, $n = 16$) than in those who received symptomatic treatment alone (18.8%, $n = 9$). Given that antibody production has been reported to be impaired after SARS-CoV-2 vaccination in patients on corticosteroids (13), it is necessary to clarify whether ciclesonide causes worsening of CT shadows and impairs antibody production.

The aim of this study was to determine if there is an association of worsening CT shadows with impaired antibody production in patients treated with inhaled ciclesonide.

2. Materials and Methods

2.1. Study population and protocol

This study is a subanalysis of a multicenter, open-labelled randomized trial (RACCO study). The complete study protocol has been described previously (12). This trial was approved by the Clinical Research Review Board at The University of Tokyo (protocol number: 2019017SP). Written informed consent was obtained from all patients before participation.

2.2. Demographic characteristics

Eighty-nine of the 90 patients who participated in our previously reported trial (12) were enrolled in the present study (Table S1 in the Supplementary Data, <http://www.ddtjournal.com/action/getSupplementalData.php?ID=173>)

and were divided into a ciclesonide group ($n = 41$, 20 men, mean age 38.7 ± 17.0 years) and a control group ($n = 48$, 24 men, mean age 42.7 ± 18.7 years). One patient was excluded from the analysis due to lack of baseline CT. There was no between-group difference in body mass index, mean age, or duration of hospitalization after onset of clinical signs of SARS-CoV-2 infection. After excluding 2 patients whose condition deteriorated and required additional medications, 3 who were discharged on day 7 (with a medication compliance rate of < 90%), and 12 who were negative on day 1 of the study but positive before hospitalization (ciclesonide group, $n = 3$; control group, $n = 9$), this left 72 patients for this study (ciclesonide group, $n = 36$; control group, $n = 36$) (Figure 1).

2.3. Exacerbation of pneumonia and production of antibodies against SARS-CoV-2 nucleocapsid protein

Antibody titers against SARS-CoV-2 nucleocapsid protein were measured by enzyme-linked immunosorbent assay on hospital days 1, 8, 15, and 22 and then compared between patients with exacerbation of pneumonia in the ciclesonide group and their counterparts in the control group. Exacerbation of pneumonia was judged on CT scans obtained on day 1 (pretreatment) and day 8 (12). The actual dates for antibody measurement were calculated from the date of onset of clinical signs of SARS-CoV-2 infection.

2.4. Measurement of antibody titers

A plate coated in recombinant nucleocapsid protein was incubated with a serum/plasma sample diluted to 1/800 for 1 h at 37°C after blocking with 1% BlockAce (KAC, Kyoto, Japan). Following washing with phosphate-

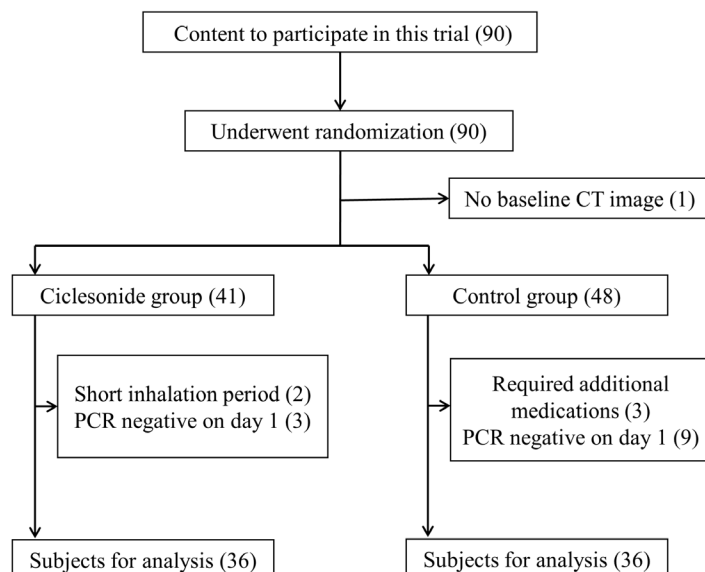


Figure 1. Flow diagram of participant recruitment in this study.

buffered saline containing 0.2% Tween 20, the plate was incubated with anti-human IgG conjugated with horseradish peroxidase (GeneTex, Irvine, CA) for 30 min at 37°C. The captured antibodies were detected with 3,3',5,5'-tetramethylbenzidine substrate solution (Nacalai Tesque, Kyoto, Japan) and measured at a wavelength of 450 nm by a microplate reader (Bio-Rad, Irvine, CA, USA). Samples from a healthy volunteer without SARS-CoV-2 infection were used as a negative control. Anti-nucleocapsid human IgG (ACROBiosystems, Newark, DE) was used as a positive control and a standard curve was created. Each sample was assayed in triplicate, and all measurements were normalized to the value of the positive control. The positive and negative cut-off values for the antibody titer were set to a value of the mean plus three times the standard deviation of the negative control.

2.5. SARS-CoV-2 copy numbers

Nasopharyngeal swab fluid was collected on days 1 and 8. Nucleic acid RNA was extracted from the nasopharyngeal swab fluid using a QIAamp virus RNA mini kit. To determine the amount of SARS-CoV-2 per mL of universal transport medium (14), quantitative real-time reverse transcription-polymerase chain reaction (qRT-PCR) was performed with QuantStudio 12K (Thermo Fisher Scientific, Waltham, MA) using primer/probe nucleocapsid protein set no. 2 (N2) (15). EDX SARS-CoV-2 standard (BR code: COV019, Bio-Rad Laboratories, Inc. Japan, 200,000 copies/mL of N-region

RNA) was used as a quantitation standard to correct the calibration curve in real-time PCR quantification.

2.6. Statistical analysis

The anti-nucleocapsid IgG titer was compared between the placebo and ciclesonide groups using the nonparametric Mann-Whitney *U* test. For statistical analysis of the viral load, the value under the limit of quantification was set to 50 copy/mL and the value under the level detectable by qRT-PCR was set to 1 copy/mL. Categorical variables were compared between the groups using Fisher's exact test. A nonparametric Kruskal-Wallis test was performed to compare more than three groups followed by a post-hoc Dunn's multiple comparisons test to identify significant differences between specific groups. All statistical analyses were performed using Prism software (version 9; GraphPad Software, La Jolla, CA). A *p*-value < 0.05 was considered statistically significant.

3. Results

3.1. Patient characteristics

The clinical characteristics of the ciclesonide group (*n* = 36) and the control group (*n* = 36) are shown in Table 1. Age tended to be younger in the ciclesonide group, with a median age of 44 years in the control group and 32.5 years in the ciclesonide group, but there were no significant differences. The control group consisted

Table 1. Clinical characteristics of the study participants

Items	Control group (<i>n</i> = 36)	Ciclesonide group (<i>n</i> = 36)	<i>p</i> -value
Age, years [†]	44.0 [25.3, 60.8]	32.5 [27.0, 46.3]	0.2284 ^a
Sex			
Female	18	19	> 0.9999 ^b
Male	18	17	
BMI [†]	22.0 [20.2, 25.7]	22.0 [19.7, 24.4]	0.448 ^a
Days from symptom onset to day 1 [†]	5.0 [3.0, 7.0]	5.0 [3.0, 6.0]	0.7977 ^a
Clinical features on day 1 ^{††}			
Body temperature (> 37.5°C)	13 (36.1) ^{††}	14 (38.9)	> 0.9999 ^b
Dry cough	16 (44.4)	22 (61.1)	0.2377 ^b
Productive cough	5 (13.9)	6 (16.7)	> 0.9999 ^b
Haemoptysis	0 (0.0)	0 (0.0)	> 0.9999 ^b
Sore throat	6 (16.7)	11 (30.6)	0.2668 ^b
Runny nose	7 (19.4)	5 (13.9)	0.7531 ^b
Wheezing	0 (0.0)	0 (0.0)	> 0.9999 ^b
Dyspnoea	9 (25.0)	6 (16.7)	0.5628 ^b
Chest pain	3 (8.3)	3 (8.3)	> 0.9999 ^b
Muscle pain	6 (16.7)	6 (16.7)	> 0.9999 ^b
Joint pain	3 (8.3)	4 (11.1)	> 0.9999 ^b
Headache	8 (22.2)	9 (25.0)	> 0.9999 ^b
Altered consciousness	0 (0.0)	1 (2.8)	> 0.9999 ^b
Fatigue	13 (36.1)	13 (36.1)	> 0.9999 ^b
Abdominal pain	3 (8.3)	1 (2.8)	0.6142 ^b
Vomiting/nausea	2 (5.6)	1 (2.8)	> 0.9999 ^b
Diarrhoea	7 (19.4)	7 (19.4)	> 0.9999 ^b

Data are presented as the [†]median [interquartile range] or ^{††}number (percentage). ^aMann-Whitney *U* test. ^bFisher's exact test. BMI, body mass index.

of 18 males while the ciclesonide group consisted of 17 males. Both groups had a median body mass index (BMI) of 22.0, and the interval between symptom onset and hospitalization was 5 days for both groups, with no significant differences. Regarding clinical symptoms on the first day of admission, 13 (36.1%) patients in the control group and 14 (38.9%) in the ciclesonide group had fever. Dry cough was more common in the ciclesonide group, 16 (44.4%) in the control group and 22 (61.1%) in the ciclesonide group, but the difference between the two groups was not significant. Other respiratory symptoms such as sore throat, runny nose and dyspnoea were observed in 6 (16.7%), 7 (19.4%) and 9 (25.0%) patients in the control group respectively. In contrast, 11 (30.6%), 5 (13.9%) and 6 (16.7%) patients in the ciclesonide group showed no difference between the two groups. There were also no differences in systemic symptoms such as headache, muscle pain, joint pain and fatigue between the two groups: 8 (22.2%), 6 (16.7%), 3 (8.3%) and 13 (36.1%) patients in the control group and 9 (25.0%), 6 (16.7%), 4 (11.1%) and 13 (36.1%) patients in the ciclesonide group, respectively. In addition, gastrointestinal symptoms such as abdominal pain and diarrhoea occurred in 3 (8.3%) and 7 (19.4%) patients in the control group and 1 (2.8%) and 7 (19.4%) patients in the ciclesonide group, respectively, with no significant differences between the two groups.

3.2. Induction of antibodies against SARS-CoV-2 nucleocapsid protein

Enzyme-linked immunosorbent assay data confirmed that seroconversion was induced in both groups (Figure 2A). The maximum antibody titer was reached in 2-3 weeks (Figure 2B). Although induction of antibodies tended to be weaker in the ciclesonide group (Figure 2A), there was no significant difference in the days taken to reach the maximum antibody titer and the amount of antibodies (Figure 2C left, $p = 0.187$; right, $p = 0.158$, respectively). Furthermore, there was no between-group difference in the fold increase of antibody titres on day 8 compared to those detected on day 1 (Figure 2D, $p = 0.379$). These data indicate that inhaled ciclesonide did not impair seroconversion against SARS-CoV-2.

3.3. Association between exacerbation of pneumonia and impaired antibody production

Worsening CT shadows on day 8 was observed in 15 patients (41.7%) in the ciclesonide group and 7 (19.4%) in the control group, indicating a greater likelihood of worsening CT shadows with ciclesonide (Figure 3A, $p = 0.072$). However, there was no between-group difference in antibody titers on day 8 among patients with worsening CT shadows (Figure 3B left, $p = 0.178$ for control; $p = 0.505$ for ciclesonide). Moreover, there was

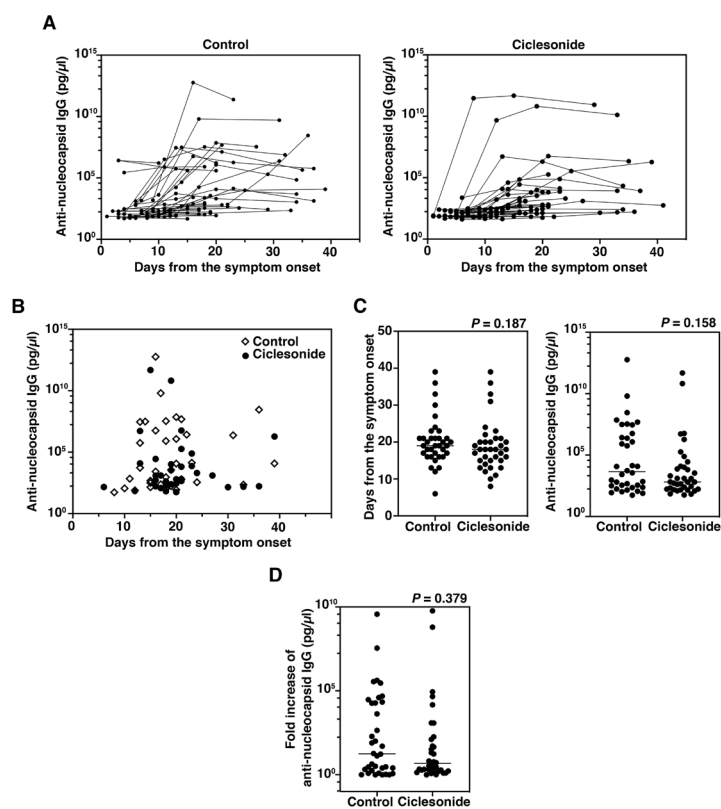


Figure 2 Comparison of anti-nucleocapsid antibody acquisition and quantity change and comparison of maximum antibody titers between the control and ciclesonide groups. (A) Anti-nucleocapsid antibody titer over time starting at symptom onset. **(B)** Comparison of number of days from symptom onset to maximum antibody titer. **(C)** Days until maximum antibody value is reached. **(D)** Fold increase of antibody titers on day 8.

no significant between-group difference in the maximum antibody titer (Figure 3B right, $p = 0.388$ for control; $p = 0.102$ for ciclesonide). These data suggest that the worsening CT shadows observed in the ciclesonide group was not the result of impaired antibody production.

We also analyzed the viral load and frequency of detection of the virus on day 1 and 8. First, in the control group, we observed that the viral load was higher on both days 1 and 8 in cases with worsening CT shadows than in cases with amelioration (Figure 3C, $p = 0.007$ and $p = 0.022$, respectively). The frequency of detection on day 8 was significantly higher in cases with worsening CT shadows than in those with amelioration (Figure 3D left, $p = 0.034$). These data suggest that the worsening CT shadows in the control group were attributable to delayed elimination of the virus. In the ciclesonide group, we observed that the viral load was higher on day 1 in cases with worsening CT shadows than in cases with amelioration (Figure 3C left, $p = 0.046$), but there were no significant between-group differences on day 8 (Figure 3C, $p = 0.568$). There were also no between-group differences in the frequency of detection on day 8 (Figure 3D right, $p = 0.134$), and there was no significant difference in the time to discharge between cases with

worsening CT shadows and those with amelioration in the control group or ciclesonide group (Figure 3E, $p = 0.482$ and $p = 0.118$, respectively). Furthermore, there were no significant between-group differences in clinical observations or laboratory findings on day 8 or at the time of discharge. Although there were more cases with worsening of CT shadows in the ciclesonide group, because there was no delay in viral clearance in the ciclesonide group compared with the control group, these data may indicate a therapeutic effect of ciclesonide.

4. Discussion

In this study, we prospectively compared the antibody production capacity between the ciclesonide group and control group in the RACCO study to determine whether administration of ciclesonide affects induction of antibodies against the SARS-CoV-2 nucleocapsid protein. We found that patients in both groups reached their peak antibody titers within 2-3 weeks, with no difference between them in peak values or number of days taken to reach them. There was also no significant difference in antibody production capacity, maximum antibody titer, or change in viral load between worsening

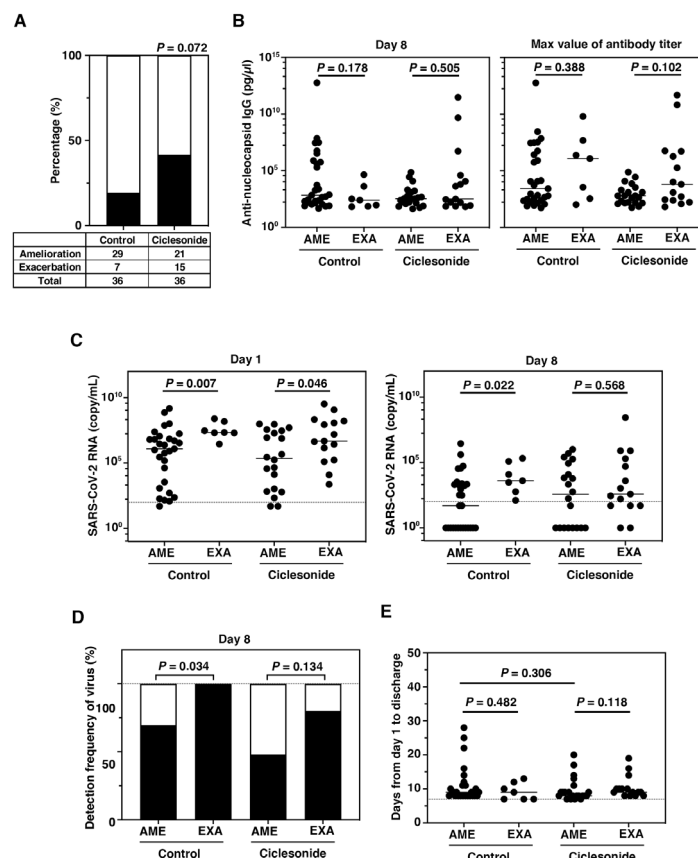


Figure 3 Comparison of the relationships between amelioration and exacerbation of CT images, viral antibody titers, and viral load between the control and ciclesonide groups. (A) Comparison of the amelioration and exacerbation groups: 15 of 46 patients (41.7%) in the ciclesonide group and 7 of 36 (19.4%) in the control group showed worsening CT shadows on day 8. (B) Comparison of antibody titers on day 8 and maximum antibody in the control and ciclesonide groups between the amelioration and exacerbation groups. (C) Viral load and detection frequency of SARS-CoV-2 in the nasopharyngeal swabs at days 1 and 8. (D) Detection frequency of the viruses. (E) Comparison of days from symptom onset to discharge.

CT shadows and improvement. These observations suggest that the influence of inhaled ciclesonide on antibody production capacity was neither statistically nor clinically significant.

Representative CT shadows in each group are compared in Figure 4. Both groups showed worsening CT shadows on day 8, suggesting a possible exacerbation of COVID-19 pneumonia. However, the shadows had disappeared at the 3-month follow-up. Although worsening CT shadows on day 8 were more common in the ciclesonide group, exacerbation of COVID-19 pneumonia during the clinical course was not observed in the ciclesonide group but was observed in 3 controls (Table 2). This discrepancy was addressed in a subsequent study by Inui *et al.*, who found lung abnormalities even in asymptomatic cases, with 54% having pneumonia-like changes (16), suggesting a significant discrepancy between initial CT findings and subjective symptoms. Such imaging changes are reported to be distinct from changes indicative of the progression of severe pneumonia. Therefore, it is hypothesized that

the changes induced by ciclesonide might be different from these imaging-related changes.

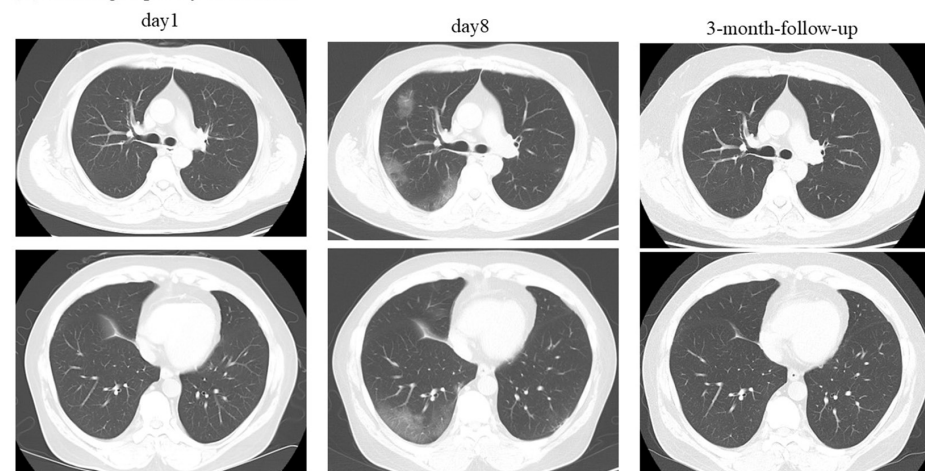
Ciclesonide has been demonstrated to inhibit the intracellular enzyme PAK1, which is implicated in the pathogenesis of COVID-19 associated with angiotensin-converting enzyme 2. By inhibiting PAK1, ciclesonide is reported to alleviate immune suppression and reduce

Table 2. Comparison of exacerbations of COVID-19 pneumonia between the ciclesonide group and the control group

Adverse event	Control group (n = 48)	Ciclesonide group (n = 41)
COVID-19 pneumonia	3	0
Mild	0	0
Moderate	2	0
Severe	1	0

Exacerbations were more common on computed tomography scans on day 8 in the ciclesonide group. However, exacerbation of COVID-19 pneumonia was not clinically diagnosed in any patients in the ciclesonide group but was diagnosed in 3 patients in the control group. COVID-19, coronavirus disease 2019.

(A) Control group: 57-year-old man.



(B) Ciclesonide group: 27-year-old woman.

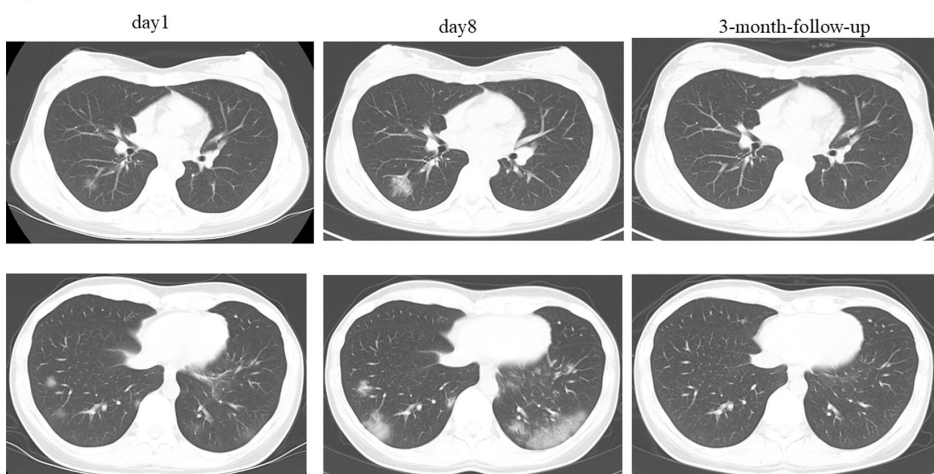


Figure 4. Representative cases of changes in CT image findings in the control and ciclesonide groups. (A) Control group: 57-year-old man. (B) Ciclesonide group: 27-year-old woman. Worsening CT shadows at day 8 in both cases are no longer evident at the 3-month follow-up.

lung inflammation (3). Furthermore, it is believed that ciclesonide targets the non-structural proteins of this novel coronavirus. This target has been shown to hinder viral replication *in vitro* (4,6,7).

Song *et al.* performed a randomized non-blinded multicenter phase II clinical trial of inhaled ciclesonide in patients with mild-to-moderate COVID-19 and found a significantly higher SARS-CoV-2 clearance rate on day 14 in their ciclesonide group ($p = 0.021$). Inhaled ciclesonide was found to shorten the SARS-CoV-2 shedding period and demonstrated the potential to inhibit progression to acute respiratory failure in patients with mild-to-moderate COVID-19 (17).

Ciclesonide has been identified as a potential treatment for COVID-19 in several studies, including ours. However, there is still no clear research demonstrating its efficacy. Indeed, Clemency *et al.* reported that the median time to relief of all COVID-19-related symptoms in outpatients with symptomatic COVID-19 was 19.0 days in both a ciclesonide group and a placebo group. Although there was no significant difference in symptom improvement, patients in the ciclesonide group were less likely to make subsequent visits to the emergency room or be hospitalized for COVID-19-related reasons by day 30 than those in the placebo group (1.0% vs. 5.4%; $p = 0.03$) (10). Furthermore, in the COVERAGE study, which evaluated ciclesonide in adults at risk of severe progression of COVID-19, there was no significant difference in the primary endpoint of worsening COVID-19 (hospitalization, home oxygen therapy, or death) up to day 14 (9). Studies targeting hospitalized patients have also been conducted, but there was also no reduction in the duration of oxygen administration in patients hospitalized with COVID-19 receiving oxygen therapy (11).

In terms of safety, a study by Lee *et al.* in South Korea indicated that prior use of ICS did not increase the likelihood of SARS-CoV-2 positivity. Moreover, the dosage and type of ICS did not impact the positivity rate (18). Meta-analyses have also found that use of ICS, either as monotherapy or in combination with bronchodilators, does not influence the risk of SARS-CoV-2 infection (19). Therefore, antibodies are produced in patients with asymptomatic to mild COVID-19, even those on high-dose ICS, with no significant difference in antibody titers according to whether or not these agents are used. This finding suggests that patients with asthma can safely use high-dose ICS containing ciclesonide if they contract COVID-19.

The study has several limitations. The first is its small sample size. When planning the RACCO study, the number of infected individuals in Japan was not particularly high, so the study focused on a smaller number of cases that allowed the results to be delivered more rapidly. The present analysis is based on sera samples that were carefully selected in that study

because we believed that there was an association between inhaled ciclesonide and antibody titers. The second limitation is the uncertainty regarding the dosage of ciclesonide needed for patients to achieve intracellular concentrations equal to the concentrations found to induce antiviral effects in previous studies. In basic research, ciclesonide powder is directly dispersed onto infected cells. However, we used inhaled ciclesonide, and there have been no definitive experiments to confirm how much of the drug is absorbed through the respiratory mucosa after inhalation and whether an adequate amount reaches the infected cells. Therefore, in this study, we used high-dose ciclesonide to ensure an adequate dosage. The third limitation is the choice of the primary endpoint. The RACCO study focused on CT images obtained at day 8 rather than clinical symptoms. A relationship between worsening on imaging and progression to severe disease has not been clearly established, making this assessment complex. There have been several studies of ciclesonide but the endpoints have varied.

It is reasonable to conclude that high doses of inhaled ciclesonide do not affect antibody production even in patients with asymptomatic to mild COVID-19. Furthermore, we found no significant difference in antibody titers according to whether or not ciclesonide was inhaled. Therefore, in the event of COVID-19 infection in patients with asthma, it can be inferred that high-dose ICS are safe to use.

Acknowledgements

The authors thank the patients who participated in the RACCO study for their cooperation with sample collection for antibody titers and virus measurements.

Funding: This work was supported by a grant from Ministry of Health, Labour and Welfare (grant No. 19HA1003).

Conflict of Interest: The authors have no conflicts of interest to disclose.

References

- Williamson EJ, Walker AJ, Bhaskaran K, *et al.* Factors associated with COVID-19-related death using OpenSAFELY. *Nature*. 2020; 584:430-436.
- Horby P, Lim WS, Emberson JR, *et al.* Dexamethasone in hospitalized patients with Covid-19. *N Engl J Med*. 2021; 384:693-704.
- Indari O, Jakhmola S, Manivannan E, Jha HC. An update on antiviral therapy against SARS-CoV-2: How far have we come? *Front Pharmacol*. 2021; 12:632677.
- Matsuyama S, Kawase M, Nao N, Shirato K, Ujike M, Kamitani W, Shimojima M, Fukushi S. The inhaled steroid ciclesonide blocks SARS-CoV-2 RNA replication by targeting the viral replication-transcription complex in cultured cells. *J Virol*. 2020; 95:e01648-20.
- Iwabuchi K, Yoshie K, Kurakami Y, Takahashi K, Kato

- Y, Morishima T. Therapeutic potential of ciclesonide inhalation for COVID-19 pneumonia: report of three cases. *J Infect Chemother.* 2020; 26:625-632.
6. Jeon S, Ko M, Lee J, Choi I, Byun SY, Park S, Shum D, Kim S. Identification of antiviral drug candidates against SARS-CoV-2 from FDA-approved drugs. *Antimicrob Agents Chemother.* 2020; 64:e00819-20.
 7. Ko M, Chang SY, Byun SY, Ianevski A, Choi I, Pham Hung d'Alexandry d'Orengiani A-L, Ravlo E, Wang W, Bjørås M, Kainov DE, Shum D, Min JY, Windisch MP. Screening of FDA-approved drugs using a MERS-CoV clinical isolate from South Korea identifies potential therapeutic options for COVID-19. *Viruses.* 2021; 13:651.
 8. Hojo M, Terada-Hirashima J, Sugiyama H. COVID-19 and bronchial asthma: Current perspectives. *Glob Health Med.* 2021; 3:67-72.
 9. Duvignaud A, Lhomme E, Onaisi R, et al. Inhaled ciclesonide for outpatient treatment of COVID-19 in adults at risk of adverse outcomes: A randomised controlled trial (COVERAGE). *Clin Microbiol Infect.* 2022; 28:1010-1016.
 10. Clemency BM, Varughese R, Gonzalez-Rojas Y, Morse CG, Phipatanakul W, Koster DJ, Blaiss MS. Efficacy of inhaled ciclesonide for outpatient treatment of adolescents and adults with symptomatic COVID-19: a randomized clinical trial. *JAMA Intern Med.* 2022; 182:42-49.
 11. Brodin D, Tornhammar P, Ueda P, et al. Inhaled ciclesonide in adults hospitalised with COVID-19: A randomised controlled open-label trial (HALT COVID-19). *BMJ Open.* 2023; 13:e064374.
 12. Terada-Hirashima J, Suzuki M, Tsujimoto Y, et al. Impact of inhaled ciclesonide on asymptomatic or mild COVID-19: a randomized trial. *Drug Discov Ther.* 2022; 16:225-232.
 13. Runnstrom MC, Morrison-Porter A, Ravindran M, Quehl H, Ramonell RP, Woodruff M, Patel R, Kim C, Haddad NS, Lee FE. Reduced COVID-19 vaccine response in patients treated with biologic therapies for asthma. *Am J Respir Crit Care Med.* 2022; 205:1243-1235.
 14. Akiyama Y, Kinoshita N, Sadamasu K, Nagashima M, Yoshida I, Kusaba Y, Suzuki T, Nagashima M, Ishikane M, Takasaki J, Yoshimura K, Ohmagari N. A pilot study on viral load in stool samples of patients with COVID-19 suffering from diarrhea. *Jpn J Infect Dis.* 2022; 75:36-40.
 15. Shirato K, Nao N, Katano H, Takayama I, Saito S, Kato F, Katoh H, Sakata M, Nakatsu Y, Mori Y, Kageyama T, Matsuyama S, Takeda M. Development of genetic diagnostic methods for detection for novel coronavirus 2019 (nCoV-2019) in Japan. *Jpn J Infect Dis.* 2020; 73:304-307.
 16. Inui S, Fujikawa A, Jitsu M, Kunishima N, Watanabe S, Suzuki Y, Umeda S, Uwabe Y. Chest CT findings in cases from the cruise ship "Diamond Princess" with coronavirus disease 2019 (COVID-19). *Radiol Cardiothorac Imaging.* 2020; 2:e204002.
 17. Song JY, Yoon JG, Seo YB, Lee J, Eom JS, Lee JS, Choi WS, Lee EY, Choi YA, Hyun HJ, Seong H, Noh JY, Cheong HJ, Kim WJ. Ciclesonide inhaler treatment for mild-to-moderate COVID-19: A randomized, open-label, phase 2 trial. *J Clin Med.* 2021; 10:3545.
 18. Lee SC, Son KJ, Han CH, Jung JY, Park SC. Association between inhaled corticosteroid use and SARS-CoV-2 infection: A nationwide population-based study in South Korea. *Tuberc Respir Dis.* 2022; 85:80-88.
 19. Chen CH, Chen CY, Lai CC, Wang YH, Chen KH, Wang CY, Wei YF, Fu PK. The association between inhaled corticosteroid and the risks of SARS-CoV-2 infection: A systematic review and meta-analysis. *J Infect Public Health.* 2023; 16:823-830.

Received September 27, 2023; Revised October 23, 2023;
Accepted October 25, 2023.

*Address correspondence to:

Manabu Suzuki, Department of Respiratory Medicine, National Center for Global Health and Medicine, 1-21-1 Toyama, Shinjuku-ku, Tokyo 162-8655, Japan.
E-mail: manabu@nms.ac.jp

Released online in J-STAGE as advance publication October 30, 2023.

Elevated indoleamine 2,3-dioxygenase activity is associated with endothelial dysfunction in people living with HIV and ROS production in human aortic endothelial cells *in vitro*

Junyang Yang^{1,§}, Rentian Cai^{2,§}, Jingna Xun¹, Renfang Zhang¹, Li Liu¹, Yinzhang Shen¹, Tangkai Qi¹, Zhenyan Wang¹, Wei Song¹, Yang Tang¹, Jianjun Sun¹, Shuibao Xu¹, Bihe Zhao¹, Hongzhou Lu^{3,*}, Jun Chen^{1,*}

¹ Department of Infectious and Immune Diseases, Shanghai Public Health Clinical Center, Fudan University, Shanghai, China;

² Department of Infectious Disease, The Second Hospital of Nanjing, Affiliated to Nanjing University of Chinese Medicine, Nanjing, China;

³ Department of Infectious Diseases and Nursing Research Institution, National Clinical Research Center for Infectious Diseases, The Third People's Hospital of Shenzhen, Shenzhen, China.

SUMMARY The precise role of indoleamine 2,3-dioxygenase (IDO) in cardiovascular diseases (CVD) among people living with HIV (PLWH) is still under debate, despite recognized links. This study aimed to investigate the impact of elevated IDO activity on endothelial dysfunction in PLWH. A total of 38 PLWH, who had not previously received anti-retroviral therapy (ART), were enrolled in the study. These participants were monitored for 36 months following the initiation of ART. Measurements including plasma levels of IDO activity, markers of endothelial dysfunction, inflammatory factors, and lipids. *In vitro*, human aortic endothelial cells (HAEC) were exposed to interferon- γ , an IDO inhibitor, a kynurenine 3-hydroxylase (KMO) inhibitor, as well as different concentrations of kynurenine. Pre-ART, PLWH demonstrated notably elevated plasma concentrations of soluble intercellular adhesion molecule 1 (sICAM-1), soluble vascular cell adhesion molecule 1(sVCAM-1), and IDO activity in comparison to healthy controls. Post-ART, both IDO activity and sICAM-1 levels experienced a significant decrease, with IDO activity reaching levels comparable to those observed in healthy controls. Furthermore, a positive correlation was observed between IDO activity and sICAM-1 ($p = 0.0002$), as well as sVCAM-1 ($p < 0.0001$) before ART. *In vitro*, the augmentation of kynurenine concentration in the medium and the induction of IDO expression in HAEC resulted in increased production of reactive oxygen species (ROS), with minimal impact on endothelial dysfunction. From these findings, it can be concluded that long-term ART has the potential to restore the heightened IDO activity observed in PLWH. The overexpression of IDO primarily influences the expression of ROS in HAEC.

Keywords Tryptophan metabolism, indoleamine 2,3-dioxygenase, endothelial dysfunction, human immunodeficiency virus (HIV)

1. Introduction

Cardiovascular disease (CVD) is a commonly occurring chronic complication in people living with HIV (PLWH) (1,2). The introduction of widespread antiretroviral therapy (ART) has yielded a significant enhancement in the life expectancy of PLWH, which may potentially contribute to an increased prevalence of CVD among this demographic (3). Several factors have been associated with the increased occurrence of CVD (4,5), encompassing hypertension, hyperlipidemia, smoking, alcohol abuse, diabetes, physical inactivity,

overweightness, unhealthy lifestyle behaviors, HIV infection, and the use of ART medications, among others.

Tryptophan (Trp), an indispensable amino acid, plays a crucial role in protein synthesis, as well as the production of 5-hydroxytryptamine and melatonin in the human body. The kynurenine (Kyn) synthesis pathway (KP) is responsible for the metabolism of approximately 90% of Trp (6). Indoleamine 2,3 oxygenase (IDO) serves as the catalyst for the initial and rate-limiting step in the degradation of Trp through the KP, resulting in the generation of immunomodulatory tryptophan metabolites and subsequent suppression of immune function.

Recent research indicates that IDO may play a role in the development of atherosclerosis through multiple mechanisms (7,8). In non-HIV populations, there have been reports of decreased levels of serum Trp and increased Kyn/Trp ratios (K/T ratios) in those with coronary heart disease (9). Additionally, elevated plasma Kyn levels have been linked to acute myocardial infarction in patients with stable angina pectoris (10,11).

Overexpression of IDO activity is frequently observed in PLWH (12), with the HIV-1 Tat protein directly stimulating IDO production in human monocyte-derived dendritic cells (13). The potential correlation between this modification and the increased occurrence of CVD in PLWH is still a matter of discussion, necessitating additional research into the underlying mechanisms. Therefore, this study was conducted to investigate the association between the KP and endothelial dysfunction, a crucial initial step in CVD development.

2. Materials and Methods

2.1. Study population

In this study, a total of 50 PLWH and 18 HIV-negative healthy individuals as controls were recruited. The inclusion criteria required a positive HIV test, age above 16 years, and no prior ART exposure. Exclusion criteria included a history of opportunistic infections, cancer, pregnancy, hypertension, diabetes, or known CVD. At the time of enrollment, whole blood samples (10 mL) were obtained from both healthy controls and PLWH. After a three-year period of ART, 38 PLWH were effectively monitored and subsequently provided with 10 mL whole blood samples. These samples were subsequently employed to evaluate lipid profiles, HIV RNA, inflammatory markers, tryptophan, and tryptophan metabolites. All subjects gave their informed consent for inclusion before they participated in the study. The study was conducted in accordance with the Declaration of Helsinki, and the protocol was approved by the Ethics Committee of Shanghai Public Health Clinical Center (2016-S028-01).

2.2. Quantification of lipid profiles, HIV RNA, and CD4 and CD8 T-cell counts

Total cholesterol (TCH), high-density lipoprotein cholesterol (HDL-C), and low-density lipoprotein cholesterol (LDL-C) were determined using the ultracentrifugation Abell-Levy-Brodie-Kendall method. Triglyceride (TG) levels were measured using the glycerol lipase oxidase method. HIV-1 RNA loads were quantified using polymerase chain reaction (PCR) with the Cobas Amplicor system (Roche, Basel, Switzerland). CD4 and CD8 T-cell counts were evaluated using flow cytometry (BD Biosciences, Franklin Lakes, New Jersey).

2.3. Quantification of tryptophan and kynurenine levels

Plasma levels of tryptophan and kynurenine were quantified by high performance liquid chromatography as previously described (14). IDO activity was calculated using the plasma K/T ratio.

2.4. Quantification of plasma markers of immune activation and endothelial dysfunction

Plasma levels of markers including angiopoietin-2 (R&D Systems, Minneapolis, Minnesota), sCD14 (R&D Systems, Minneapolis, Minnesota), sCD163 (R&D Systems, Minneapolis, Minnesota), endogenous endotoxin-core antibody (EndoCAb) (Hycult Biotech, Uden, the Netherlands), LPS-binding protein (LBP) (Hycult Biotech, Uden, the Netherlands), IL-6 (Raybiotech, Norcross, America), sICAM-1/sCD54 (R&D Systems, Minneapolis, Minnesota) and sVCAM-1/sCD106 (R&D Systems, Minneapolis, Minnesota), were determined using enzyme-linked immunosorbent assays in accordance with the manufacturers' instructions.

2.5. Cell Culture

Human aortic endothelial cells (HAECs) (ScienCell, Carlsbad, USA) were cultured in Endothelial Cell Medium (ScienCell, Carlsbad, USA) supplemented with 5% FBS (ScienCell, Carlsbad, USA), 1% Endothelial Cell Growth Supplement (ScienCell, Carlsbad, USA), and 1% penicillin/ streptomycin (ScienCell, Carlsbad, USA) as per the manufacturer's instructions. Cells within passages 3 to 8 were utilized and allowed to reach 70-80% confluence before exposure to various agents.

HAECs were subjected to pretreatment with 0.2% dimethyl sulfoxide (DMSO), IDO inhibitor (1-methyl-DL-tryptophan (1-MT) (Sigma-Aldrich, Stockholm, Sweden)), or KMO inhibitor (Ro61-8048) (MedChem Express, Monmouth Junction, USA), for a duration of one hour. Subsequently, the cells were stimulated with Kyn (10 µM or 100 µM) (Sigma-Aldrich, Stockholm, Sweden) or IFN-γ (100 ng/ml) (PEPROTECH, Rocky Hill, USA) for 48 hours. All experiments were conducted in triplicate.

The levels of sICAM-1/sCD54 (R&D Systems, Minneapolis, Minnesota), sVCAM-1/sCD106 (R&D Systems, Minneapolis, Minnesota), Tryptophan (MyBioSource, California, USA), and Kynurenine (MyBioSource, California, USA) were quantified in the cell supernatant using ELISA. Additionally, the levels of caspase-3 and reactive oxygen species (ROS) were quantified in the cell suspension using the PE Active Caspase-3 Apoptosis Kit (BD Biosciences, Franklin Lakes, New Jersey) and the Reactive Oxygen Species Assay Kit (Yisheng, Shanghai, China) respectively, through flow cytometry.

2.6. Data analysis

The data analysis was conducted using IBM SPSS version 19.0 (IBM SPSS, Inc., Armonk, NY, USA), while the figures were generated using GraphPad Prism 6.0 software (GraphPad Software Inc., San Diego, CA, USA). Categorical variables were presented as n (%). For continuous data with a normal distribution, means \pm SD were presented, whereas non-normally distributed data were described using the median with interquartile range (IQR). The statistical tests employed in this study included the *t*-test and Mann-Whitney rank-sum test to identify significant differences between pre- and post-ART conditions, as well as healthy controls. Additionally, Pearson correlation and Spearman rank correlation tests were utilized to assess the relationship between IDO activity and other variables. Statistical significance was determined by *p*-values less than 0.05.

3. Results

3.1. Demographic and clinical characteristics of the study participants

The demographic and clinical characteristics of PLWH who have not yet received ART and healthy controls are presented in Table 1. Out of the 38 PLWH included in the study, a substantial majority of 89.5% (34/38) were male, with a median age of 32. The majority of PLWH were prescribed a regimen consisting of two nucleoside reverse transcriptase inhibitors (NRTIs) in combination with one nonnucleoside reverse transcriptase inhibitor (NNRTI).

3.2. Characteristics changes in PLWH at pre- and on-ART

After ART, all PLWH achieved viral suppression (< 50 copies/ μ L), accompanied by a significant increase in the CD4/CD8 ratio (0.42 (0.32-0.51) vs. 0.74 (0.51-0.97), *p* < 0.001), indicating an improvement in immune function. However, there was no significant change observed

Table 1. Study participants

Characteristics	PLWH (<i>n</i> = 38)	HIV-negative controls (<i>n</i> = 18)
Age, year, median (year)	32 (26-50)	31 (26-41)
Male sex, No. (%)	34 (89.47)	12 (66.67)
CD4 T-cell count (cells/ μ L)	357 (264-527)	N/A
CD4/CD8 ratio	0.42 (0.32-0.51)	N/A
ART regimen (No, %)		
TDF+3TC+EFV	32 (84.2)	N/A
TDF+3TC+LPV/r	2 (5.3)	N/A
AZT+3TC+EFV	3 (7.9)	N/A
TDF+3TC+RAL	1 (2.6)	N/A

Abbreviations: PLWH, people living with HIV; TDF, tenofovir disoproxil fumarate; 3TC, lamivudine; EFV, efavirenz; LPV/r, lopinavir/ritonavir; RAL, raltegravir.

in the CD4 cell count (357 (264-527) cells/ μ L vs. 400 (307-530) cells/ μ L, *p* = 0.117). Prior to initiating ART, PLWH exhibited higher plasma Kyn concentrations and IDO activity compared to healthy control. However, after three years of ART, these levels were reduced to a similar extent as observed in healthy controls (Figure 1). Additional information pertaining to changes in lipid profiles, markers of endothelial dysfunction, microbial translocation, and chronic inflammation following ART in PLWH can be found in Table 2.

3.3. Plasma Kyn concentration and IDO activity was associated with endothelial dysfunction in PLWH

Prior to ART, PLWH displayed notably higher plasma concentration of sICAM-1 and sVCAM-1 compared to the control group of healthy individuals (217.00 ng/mL (156.80-241.80 ng/mL) vs. 187.90 ng/mL (117.70-209.40 ng/mL), *p* = 0.0317; 712.40 ng/mL (416.70-1168.00 ng/mL) vs. 467.80 ng/mL (284.40-522.70 ng/mL), *p* = 0.0052; for sICAM-1 and sVCAM-1 respectively). Post-ART, a significant decrease was observed in plasma sICAM-1 concentration, bringing it in line with the level observed in the healthy control group, while the sVCAM-1 level remained unchanged (Figure 2A). The plasma level of ANG-II in PLWH, both before and after ART, was found to be similar to that of healthy controls. However, a decrease in plasma ANG-II concentration was observed after ART (255.90 pg/mL (206.80-454.60 pg/mL) vs. 241.40 pg/mL (166.60-289.70 pg/mL), *p* = 0.0075) (Figure 2A).

Prior to ART, IDO activities and plasma Kyn concentration were positively correlated with plasma sVCAM-1 and sICAM-1 concentration in PLWH. However, the correlation between IDO activities and sICAM-1 lost significance after ART. Neither plasma Kyn concentration nor IDO activities showed any correlation with Ang-II in PLWH (Figures 2B and 2C). Furthermore, the changes in IDO activities and plasma Kyn concentration were positively correlated with the concentrations of sVCAM-1, sICAM-1, and Ang-II (Figure S1, <http://www.ddtjournal.com/action/getSupplementalData.php?ID=172>).

3.4. Kyn and IDO activity was not associated with lipids, microbial translocation, and chronic inflammation markers

A significant increase in plasma HDL levels was observed after ART (0.94 mmol/L (0.80-1.08 mmol/L) pre-ART vs. 1.08 mmol/L (0.90-1.30 mmol/L) post-ART; *p* = 0.0082). However, these levels remained lower than those observed in healthy controls (1.08 mmol/L (0.90-1.30 mmol/L) vs. 1.24 mmol/L (1.11-1.57 mmol/L); *p* = 0.0148). Plasma levels of TG, TCH, and LDL were comparable to those of the healthy controls, both before and after ART. No significant correlations were found

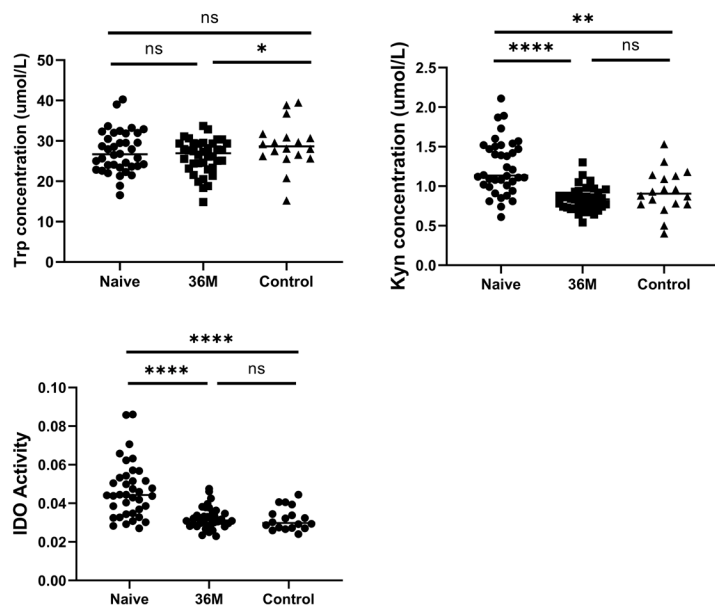


Figure 1. The impact of ART on plasma concentrations of Trp (A), Kyn (B), and IDO activity (C) in PLWH. ns, not significant; * $p < 0.05$; ** $p < 0.01$; *** $p < 0.001$; **** $p < 0.0001$. Abbreviations: Trp, Tryptophan; Kyn, Kynurenine; IDO activity, Kyn/Trp ratio

Table 2. Characteristics changes in PLWH pre- and on-ART

Characteristics	Pre-ART	On-ART	<i>p</i> value
CD4 T-cell count (cell/ μ L)	357.50 (264.80-527.50)	399.50 (307.80-530.80)	0.117
CD4/CD8 rate	0.42 (0.32-0.51)	0.74 (0.51-0.97)	< 0.001
sICAM-1 (ng/mL)	217.00 (156.80-241.80)	172.00 (135.60-231.10)	0.008
sVCAM-1 (ng/mL)	712.40 (416.70-1168.00)	668.50 (578.90-778.50)	0.278
ANG-II(pg/mL)	255.90 (206.80-454.60)	241.40 (166.60-289.70)	0.008
TG (mmol/L)	1.15 (0.88-1.55)	1.51 (0.90-2.07)	0.086
TCH (mmol/L)	4.21 (3.35-5.11)	4.12 (3.47-4.98)	0.468
LDL (mmol/L)	2.40 (1.77-3.2)	2.73 (2.26-3.45)	0.086
HDL (mmol/L)	0.94 (0.80-1.08)	1.08 (0.90-1.30)	0.009
Tryptophan (μ mol/L)	23.68 (23.57-31.87)	26.96 (23.31-29.35)	0.145
Kynurenine (μ mol/L)	1.14 (1.01-1.51)	0.84 (0.73-0.92)	< 0.001
IDO Activity (nM/ μ M)	44.32 (34.72-53.56)	31.10 (28.76-34.81)	< 0.001
Endocab (MMu/mL)	72.30 (34.88-111.50)	169.50 (89.80-293.70)	0.001
LBP (ng/mL)	5623.00 (3362.00-7936.00)	5896.00 (5047.00-7289.00)	0.24
sCD14 (ng/mL)	1450.00 (490.20-2111.00)	1514.00 (1218.00-1829.00)	0.396
sCD163 (ng/mL)	774.30 (578.30-1081.00)	712.10 (579.20-895.90)	0.236
IL-6 (pg/mL)	77.39 (23.93-124.10)	27.67 (14.33-47.08)	0.005

Abbreviations: ART, anti-retroviral therapy; sICAM-1, soluble intercellular adhesion molecule 1; sVCAM-1, soluble vascular cell adhesion molecule 1; ANG-II, angiopoietin-2; TG, triglyceride; TCH, total cholesterol; LDL, low-density lipoprotein; HDL, high-density lipoprotein; IDO, indoleamine 2,3-dioxygenase; EndoCAb, endogenous endotoxin-core antibody; LBP, LPS-binding protein; IL-6, interleukin-6.

between TG, TCH, HDL, LDL, and plasma Kyn levels or IDO activity.

Plasma concentration of sCD14 and sCD163 were found to be significantly elevated, while plasma IL-6 levels were comparable, and plasma EndoCAb and LBP level were lower among untreated PLWH compared to healthy controls. However, apart from sCD14, which demonstrated a significant correlation with IDO activity prior to the initiation of ART ($R^2 = 0.154$, $p = 0.01$), there is no observed correlation between plasma Kyn concentration or IDO activity and plasma levels of LBP, sCD163, EndoCAb, and IL-6, both before and after ART in PLWH.

3.5. Activation of KP induces ROS production in HAECs *in vitro*

To further elucidate the impact of IDO activity on endothelial cells, HAECs were pretreated with 1-MT or Ro61-8048 for 1 hour prior to stimulation with 100 ng/mL IFN- γ for 48 hours. Our observations revealed that IFN- γ effectively induced KP activation in HAECs, an effect that could be mitigated by the administration of 1-MT and Ro61-8048 (Figure 3A). Furthermore, these interventions yielded comparable results in terms of ROS production and IDO activity, while exerting minimal impact on sICAM-1, sVCAM-1, and caspase3

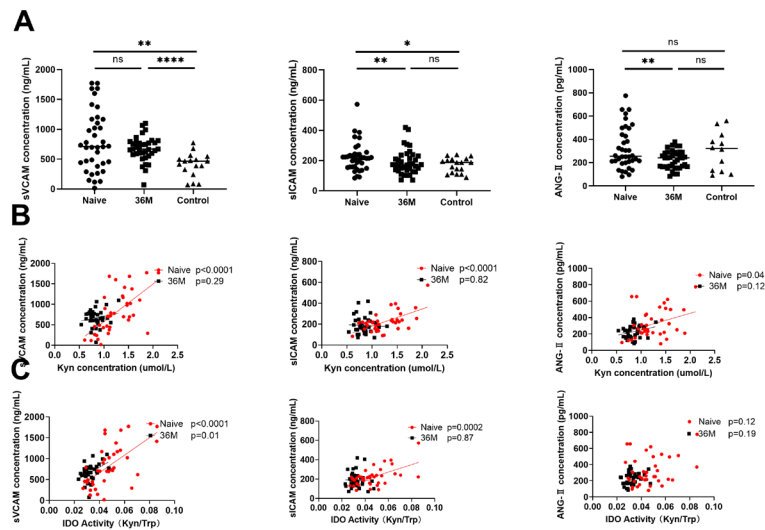


Figure 2. The impact of ART on endothelial dysfunction and its correlation with the metabolites of tryptophan. A tripartite panel representation delineating the impact of ART on plasma concentrations of sVCAM-1, sICAM-1, and ANG-II, sequentially from left to right (A). A series of three scatter plots demonstrating the relationships between plasma KYN levels and the respective plasma concentrations of sVCAM-1, sICAM-1, and ANG-II, arranged from left to right (B). A series of three scatter plots demonstrating the associations between IDO activity and the corresponding plasma concentrations of sVCAM-1, sICAM-1, and ANG-II, sequentially from left to right (C). ns, not significant; * $p < 0.05$; ** $p < 0.01$; *** $p < 0.001$; **** $p < 0.0001$. Abbreviations: sICAM-1, soluble intercellular adhesion molecule 1; sVCAM-1, soluble vascular cell adhesion molecule 1; ANG-II, Angiopoietin-2; Kyn, Kynurenone; IDO, indoleamine 2,3-dioxygenase.

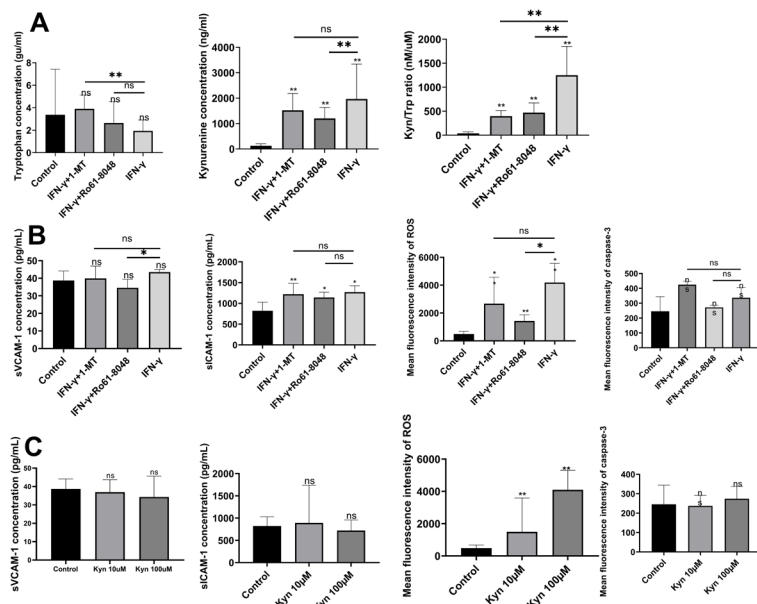


Figure 3. The impact of tryptophan and its metabolic products on HAEC in vitro. A set of three bar graphs, arranged from left to right, depicting the effects of IFN- γ , 1-MT, and Ro61-8048 on tryptophan concentration, kynurenone concentration, and Kyn/Trp ratio in HAEC in vitro, respectively (A). A set of four bar graphs, arranged from left to right, depicting the effects of IFN- γ , 1-MT, and Ro61-8048 on sVCAM concentration, sICAM concentration, ROS production, and caspase-3 activity in HAEC in vitro, respectively (B). A set of four bar graphs, arranged from left to right, depicting the effects of 10 μ M and 100 μ M KYN on sVCAM concentration, sICAM concentration, ROS production, and caspase-3 activity in HAEC in vitro, respectively (C). ns, not significant; * $p < 0.05$; ** $p < 0.01$; *** $p < 0.001$; **** $p < 0.0001$. Abbreviations: Kyn/Trp ratio, kynurenone/tryptophan ratio; sICAM-1, soluble intercellular adhesion molecule 1; sVCAM-1, soluble vascular cell adhesion molecule 1.

(Figure 3B).

In order to provide additional evidence for the hypothesis that KP activation may initiate the generation of ROS, we exposed HAECs to exogenous Kyn at concentrations of 10 μ M or 100 μ M for a duration of 48 hours. It was observed that Kyn had the ability to

induce the production of ROS, with the intensity of ROS production increasing proportionally with higher concentrations of Kyn. However, it is worth noting that both interventions had minimal impact on the production of sICAM-1 and sVCAM-1, as well as HAEC apoptosis, as depicted in Figure 3C.

4. Discussion

Endothelial dysfunction plays a crucial role in the development of atherosclerosis and other vascular disorders (15). Understanding the factors involved in HIV-related endothelial dysfunction is vital for the effective long-term management of AIDS. Our study revealed a significant association between IDO activity, plasma Kyn concentration and endothelial dysfunction in PLWH. Additionally, we confirmed that activation of KP in increased production of ROS in HAECs *in vitro*. These findings suggest that targeting this pathway could potentially reduce the risk of CVD in individuals with HIV.

In our study, we noted a notable increase in markers of endothelial dysfunction in PLWH who had not received ART, as compared to healthy controls. After ART, only levels of sVCAM-1 remained higher in PLWH compared to the healthy controls. Similarly, prior to ART, there was a significant elevation in IDO activity and plasma KYN concentration, which returned to normal levels after treatment. Consistent with our previous findings and those of Routy *et al.*, it was observed that IDO activity did not fully recover even after antiviral therapy (12,16). The observed disparity between our present findings and prior research can be ascribed to variances in the demographics of the study cohorts. Specifically, the individuals included in this investigation displayed comparatively elevated CD4 levels, which previous studies have established to have an inverse association with IDO activity (12). Interestingly, a previous study has documented that PLWH who exhibited persistently low CD4 levels after receiving treatment exhibited a notably heightened susceptibility to cardiovascular events (17). This finding may partially account for the heightened association observed between pre-treatment IDO activity and plasma Kyn levels, as well as endothelial damage biomarkers in our investigation, which diminished following treatment. Subsequent research endeavors should prioritize the inclusion of populations with lower CD4 levels to gain further insight into these associations.

Both the beneficial and detrimental effects of CVD on Trp and its metabolites have been documented (18). Zhang *et al.* (8) determined the atheroprotective effects of 3-hydroxybutyrate anthranilic acid, while Kynurenic acid and aryl hydrocarbon receptor were found to inhibit the immune response, thereby enhancing the stability of carotid plaques (19). Conversely, Wang *et al.* argued that 3-hydroxyanthranilic acid activated the nuclear factor-kappa B transcription factor, leading to increased expression of matrix metallopeptidase 2 in vascular smooth muscle cells and contributing to AngII-induced abdominal aortic aneurysm *in vivo* (20). K/ ratio demonstrated a positive association with BMI, LDL, TG, carotid intima-media thickness, and abdominal

circumference, while exhibiting a negative association with HDL (10,21,22). Furthermore, increased plasma Kyn concentrations were found to be positively associated with the likelihood of experiencing an acute coronary event among older individuals (23). In the context of this study, IDO activity exhibited a positive correlation with plasma sICAM-1 and sVCAM-1 levels in ART-naïve PLWH. These findings are consistent with previous research conducted on PLWH (11,24).

Based on the aforementioned studies, it appears that the overexpression of IDO may contribute to endothelial dysfunction and have detrimental effects on CVD. However, an inexplicable phenomenon was observed *in vitro*, where the activation of IDO and the introduction of exogenous Kyn had minimal impact on endothelial dysfunction and apoptosis in HAEC. Interestingly, in hypercholesterolemic ApoE^{-/-} mice, the deficiency of IDO resulted in a significant increase in lesion size and a decrease in blood levels of IL10 (25). Furthermore, the inhibition of IDO led to heightened vascular inflammation and an upregulation of monocyte chemoattractant protein-1 and sVCAM-1 expression in ApoE^{-/-} mice (26). Regulatory T cells and KP exhibit reciprocal regulation within the vessel wall, thereby facilitating vascular tolerance mechanisms and mitigating inflammation and atherosclerosis (27).

Our investigation further revealed that the activation of IDO and elevation of Kyn concentration resulted in the generation of ROS in HAEC *in vitro*, without causing any endothelial dysfunction. Furthermore, the treatment of mouse and human myoblasts with Kyn led to a two-fold increase in ROS levels (28). ROS, functioning as a subcellular messenger in signal transduction pathways, has been found to exert both advantageous and detrimental effects on the cardiovascular system (29). Under normal physiological conditions, the production of ROS at low levels has been observed to play a regulatory role in gene expression, excitation-contraction coupling, cell growth, migration, differentiation, and programmed cell death. However, in pathological scenarios, ROS can lead to oxidative modifications of crucial cellular macromolecules (29). Lubrano's research (30) has demonstrated that elevated levels of ROS can directly enhance the production of lectin-like oxidized low-density lipoprotein. This increase in LOX-1 has been linked to apoptosis induction in various cell types when present in high concentrations, while low concentrations have been associated with cell proliferation.

Our previous research has demonstrated the prevalence of dyslipidemia, microbial translocation, and chronic inflammation in PLWH (31,32), which have been considered to be associated with endothelial dysfunction (15, 33). In Apet^{-/-} mice, inhibition of IDO resulted in an increase in the level of TCH and the ratio of VLDL/HDL (26). The involvement of Kyn metabolites in regulating lipid metabolism, thermogenic

gene expression, and anti-inflammatory gene expression in adipose tissue has been observed through the activation of G protein-coupled receptor Gpr35 or aryl hydrocarbon receptor/signal transducer or transcription 3/interleukin-6 signaling (34,35). Catabolism of tryptophan (Trp) plays a significant role in the precise regulation of intestinal physiology (36), and it has also been linked to CVD (37). Numerous studies have reported the involvement of IDO in the pathophysiology of various inflammatory conditions, such as infection, allergy, autoimmunity, chronic inflammation, and inflammatory neurological diseases (38,39). Based on the aforementioned evidence, it is justifiable to postulate that KP might potentially contribute to the development of endothelial dysfunction through its influence on lipid metabolism, microbial translocation, or chronic inflammatory response. However, this conjecture was promptly refuted as our study revealed minimal association between IDO activity and plasma lipid levels, as well as plasma markers for inflammation or microbial translocation.

Our study is subject to several limitations and deficiencies. Firstly, the majority of participants were young and middle-aged men, thus limiting the generalizability of our findings to women and the elderly. Secondly, the assessment of atherosclerosis was incomplete as we did not measure carotid artery intima-media thickness, a crucial parameter for evaluating this condition. Thirdly, the utilization of the K/T ratio as a representative measure of IDO activity may lead to erroneous conclusions, as it does not fully capture the complexity of IDO activity. Additionally, the verification of our results through *in vitro* experiments using HAEC may be deemed less persuasive compared to *in vivo* studies.

In summary, long-term ART has the potential to restore normal levels of IDO activity that is elevated due to HIV infection. The activity of IDO is found to be positively associated with endothelial dysfunction in PLWH. The excessive expression of IDO primarily impacts the production of ROS, while its direct influence on endothelial dysfunction in HAEC is limited.

Acknowledgements

We thank all workers for their diagnosis, nursing and treatment of HIV/AIDS patients at Shanghai Public Health Clinical Center.

Funding: This work was supported by a grant from the Shanghai Public Health Clinical Center (KY-GW-2022-10; KY-GW-2022-10); Shanghai Science and Technology Committee (20MC1920100); Shanghai Talent Development Fund (2020089).

Conflict of Interest: The authors have no conflicts of interest to disclose.

References

- Paisible AL, Chang CC, So-Armah KA, et al. HIV infection, cardiovascular disease risk factor profile, and risk for acute myocardial infarction. *J Acquir Immune Defic Syndr.* 2015; 68:209-216.
- Freiberg MS, Chang CC, Kuller LH, et al. HIV infection and the risk of acute myocardial infarction. *JAMA Intern Med.* 2013; 173:614-622.
- So-Armah K, Benjamin LA, Bloomfield GS, Feinstein MJ, Hsue P, Njuguna B, Freiberg MS. HIV and cardiovascular disease. *Lancet HIV.* 2020; 7:e279-e293.
- Jokinen E. Obesity and cardiovascular disease. *Minerva Pediatr.* 2015; 67:25-32.
- Leong DP, Joseph PG, McKee M, Anand SS, Teo KK, Schwalm JD, Yusuf S. Reducing the global burden of cardiovascular disease, Part 2: Prevention and treatment of cardiovascular disease. *Cir Res.* 2017; 121:695-710.
- King NJ, Thomas SR. Molecules in focus: indoleamine 2,3-dioxygenase. *Int J Biochem Cell Biol.* 2007; 39:2167-2172.
- Liu G, Chen S, Zhong J, Teng K, Yin Y. Crosstalk between tryptophan metabolism and cardiovascular disease, mechanisms, and therapeutic implications. *Oxid Med Cell Longev.* 2017; 2017:1602074.
- Zhang L, Ovchinnikova O, Jönsson A, Lundberg AM, Berg M, Hansson GK, Ketelhuth DF. The tryptophan metabolite 3-hydroxyanthranilic acid lowers plasma lipids and decreases atherosclerosis in hypercholesterolaemic mice. *Eur Heart J.* 2012; 33:2025-2034.
- Wirleitner B, Rudzite V, Neurauter G, Murr C, Kalnins U, Erglis A, Trusinskis K, Fuchs D. Immune activation and degradation of tryptophan in coronary heart disease. *Eur J Clin Invest.* 2003; 33:550-554.
- Pertovaara M, Raitala A, Juonala M, Lehtimaki T, Huhtala H, Oja SS, Jokinen E, Viikari JS, Raitakari OT, Hurme M. Indoleamine 2,3-dioxygenase enzyme activity correlates with risk factors for atherosclerosis: the Cardiovascular Risk in Young Finns Study. *Clin Exp Immunol.* 2007; 148:106-111.
- Pedersen ER, Tuseth N, Eussen SJ, Ueland PM, Strand E, Svingen GF, Midttun O, Meyer K, Mellgren G, Ulvik A, Nordrehaug JE, Nilsen DW, Nygard O. Associations of plasma kynurenines with risk of acute myocardial infarction in patients with stable angina pectoris. *Arterioscler Thromb Vasc Biol.* 2015; 35:455-462.
- Chen J, Shao J, Cai R, Shen Y, Zhang R, Liu L, Qi T, Lu H. Anti-retroviral therapy decreases but does not normalize indoleamine 2,3-dioxygenase activity in HIV-infected patients. *PloS one.* 2014; 9:e100446.
- Planès R, Bahraoui E. HIV-1 Tat protein induces the production of IDO in human monocyte derived-dendritic cells through a direct mechanism: Effect on T cells proliferation. *PloS One.* 2013; 8:e74551.
- Chen J, Xun J, Yang J, Ji Y, Liu L, Qi T, Wang Z, Zhang R, Shen Y, Ponte R, Mehrraj V, Routy JP, Lu H. Plasma indoleamine 2,3-dioxygenase activity is associated with the size of the human immunodeficiency virus reservoir in patients receiving antiretroviral therapy. *Clin Infect Dis.* 2019; 68:1274-1281.
- Poredos P, Poredos AV, Gregoric I. Endothelial dysfunction and its clinical implications. *Angiology.* 2021; 72:604-615.
- Jenabian MA, El-Far M, Vyboh K, et al.

- Immunosuppressive tryptophan catabolism and gut mucosal dysfunction following early HIV infection. *J Infect Dis.* 2015; 212:355-366.
17. Ho JE, Scherzer R, Hecht FM, Maka K, Selby V, Martin JN, Ganz P, Deeks SG, Hsue PY. The association of CD4+ T-cell counts and cardiovascular risk in treated HIV disease. *Aids.* 2012; 26:1115-1120.
 18. Ala M, Eftekhar SP. The footprint of kynurenine pathway in cardiovascular diseases. *Int J Tryptophan Res.* 2022; 15:11786469221096643.
 19. Baumgartner R, Berg M, Matic L, Polyzos KP, Forteza MJ, Hjorth SA, Schwartz TW, Paulsson-Berne G, Hansson GK, Hedin U, Ketelhuth DFJ. Evidence that a deviation in the kynurenine pathway aggravates atherosclerotic disease in humans. *J Intern Med.* 2021; 289:53-68.
 20. Wang Q, Ding Y, Song P, Zhu H, Okon I, Ding YN, Chen HZ, Liu DP, Zou MH. Tryptophan-derived 3-hydroxyanthranilic acid contributes to angiotensin II-induced abdominal aortic aneurysm formation in mice *in vivo*. *Circulation.* 2017; 136:2271-2283.
 21. Jeong YI, Kim SW, Jung ID, et al. Curcumin suppresses the induction of indoleamine 2,3-dioxygenase by blocking the Janus-activated kinase-protein kinase Cdelta-STAT1 signaling pathway in interferon-gamma-stimulated murine dendritic cells. *J Biol Chem.* 2009; 284:3700-3708.
 22. Cuffy MC, Silverio AM, Qin L, Wang Y, Eid R, Brandacher G, Lakkis FG, Fuchs D, Pober JS, Tellides G. Induction of indoleamine 2,3-dioxygenase in vascular smooth muscle cells by interferon-gamma contributes to medial immunoprivilege. *J Immunol.* 2007; 179:5246-5254.
 23. Eussen SJ, Ueland PM, Vollset SE, Nygard O, Midttun O, Sulo G, Ulvik A, Meyer K, Pedersen ER, Tell GS. Kynurenes as predictors of acute coronary events in the Hordaland Health Study. *Int J Cardiol.* 2015; 189:18-24.
 24. Qi Q, Hua S, Clish CB, et al. Plasma tryptophan-kynurenine metabolites are altered in HIV infection and associated with progression of carotid artery atherosclerosis. *Clin Infect Dis.* 2018; 67:235-242.
 25. Cole JE, Astola N, Cribbs AP, Goddard ME, Park I, Green P, Davies AH, Williams RO, Feldmann M, Monaco C. Indoleamine 2,3-dioxygenase-1 is protective in atherosclerosis and its metabolites provide new opportunities for drug development. *Proc Natl Acad Sci U S A.* 2015; 112:13033-13038.
 26. Polyzos KA, Ovchinnikova O, Berg M, Baumgartner R, Agardh H, Pirault J, Gisterå A, Assinger A, Laguna-Fernandez A, Bäck M, Hansson GK, Ketelhuth DF. Inhibition of indoleamine 2,3-dioxygenase promotes vascular inflammation and increases atherosclerosis in Apoe/- mice. *Cardiovasc Res.* 2015; 106:295-302.
 27. Forteza MJ, Polyzos KA, Baumgartner R, Suur BE, Mussbacher M, Johansson DK, Hermansson A, Hansson GK, Ketelhuth DFJ. Activation of the regulatory T-cell/indoleamine 2,3-dioxygenase axis reduces vascular inflammation and atherosclerosis in hyperlipidemic mice. *Front Immunol.* 2018; 9:950.
 28. Kaiser H, Yu K, Pandya C, Mendhe B, Isales CM, McGee- Lawrence ME, Johnson M, Fulzele S, Hamrick MW. Kynurenone, a tryptophan metabolite that increases with age, induces muscle atrophy and lipid peroxidation. *Oxid Med Cell Longev.* 2019; 2019:9894238.
 29. Dubois-Deruy E, Peugnet V, Turkieh A, Pinet F. Oxidative stress in cardiovascular diseases. *Antioxidants (Basel).* 2020; 9:864.
 30. Lubrano V, Balzan S. LOX-1 and ROS, inseparable factors in the process of endothelial damage. *Free Radic Res.* 2014; 48:841-848.
 31. Yang J, Chen J, Ji Y, Tang Q, Zhang R, Liu L, Shen Y, Xun J, Song W, Tang Y, Wang Z, Qi T, Lu H. Lipid profile and renal safety of tenofovir disoproxil fumarate-based anti-retroviral therapy in HIV-infected Chinese patients. *Int J Infect Dis.* 2019; 83:64-71.
 32. Ji Y, Zhang F, Zhang R, et al. Changes in intestinal microbiota in HIV-1-infected subjects following cART initiation: Influence of CD4+ T cell count. *Emerg Microbes Infect.* 2018; 7:113.
 33. Karki P, Birukov KG. Lipid mediators in the regulation of endothelial barriers. *Tissue barriers.* 2018; 6:e1385573.
 34. Dadvar S, Ferreira DMS, Cervenka I, Ruas JL. The weight of nutrients: kynurenone metabolites in obesity and exercise. *Journal Intern Med.* 2018; 284:519-533.
 35. Huang T, Song J, Gao J, et al. Adipocyte-derived kynurenone promotes obesity and insulin resistance by activating the AhR/STAT3/IL-6 signaling. *Nat Commun.* 2022; 13:3489.
 36. Borghi M, Puccetti M, Pariano M, Renga G, Stincardini C, Ricci M, Giovagnoli S, Costantini C, Romani L. Tryptophan as a central hub for host/microbial symbiosis. *Int J Tryptophan Res.* 2020; 13:1178646920919755.
 37. Kazemian N, Mahmoudi M, Halperin F, Wu JC, Pakpour S. Gut microbiota and cardiovascular disease: Opportunities and challenges. *Microbiome.* 2020; 8:36.
 38. Mellor AL, Munn DH. IDO expression by dendritic cells: Tolerance and tryptophan catabolism. *Nat Rev Immunol.* 2004; 4:762-774.
 39. Melhem NJ, Taleb S. Tryptophan: From diet to cardiovascular diseases. *Int J Mol Sci.* 2021; 22:9904.

Received August 28, 2023; Revised October 13, 2023;
Accepted October 21, 2023.

[§]These authors contributed equally to this work.

*Address correspondence to:

Hongzhou Lu, Department of Infectious Diseases and Nursing Research Institution, The Third People's Hospital of Shenzhen, Shenzhen, China.
E-mail: luhongzhou@fudan.edu.cn

Dr. Jun Chen, Department of infection and immunology, Shanghai Public Health Clinical Center, No. 2901 Caolang Road, Shanghai, China.

E-mail: qtchenjun@163.com

Released online in J-STAGE as advance publication October 26, 2023.

Effects of plant-based copper nanoparticles on the elimination of ciprofloxacin

**Tanongsak Sassa-deepaeng¹, Wachira Yodthong², Nattakanwadee Khumpirapang³,
Songyot Anuchapreeda^{4,6}, Siriporn Okonogi^{5,6,*}**

¹ Agricultural Biochemistry Research Unit, Faculty of Sciences and Agricultural Technology, Rajamangala University of Technology Lanna Lampang, Lampang, Thailand;

² Lampang Inland Fisheries Research and Development Center, Lampang, Thailand;

³ Department of Pharmaceutical Chemistry and Pharmacognosy, Faculty of Pharmaceutical Sciences, Naresuan University, Phitsanulok, Thailand;

⁴ Department of Medical Technology, Faculty of Associated Medical Sciences, Chiang Mai University, Chiang Mai, Thailand;

⁵ Department of Pharmaceutical Sciences, Faculty of Pharmacy, Chiang Mai University, Chiang Mai, Thailand;

⁶ Center of Excellence in Pharmaceutical Nanotechnology, Faculty of Pharmacy, Chiang Mai University, Chiang Mai, Thailand.

SUMMARY Ciprofloxacin (CIP) is frequently detected in the environment and causes the emergence of drug-resistant bacteria. High levels of CIP in the environment are also harmful to humans and animals. Therefore, effective elimination of CIP is required. In this study, plant-based copper nanoparticles (CuNPs) have been fabricated for the purpose of eliminating CIP. Aqueous extracts of 6 plants were compared for their phytochemicals and reducing activity. Among all the extracts, *Garcinia mangostana* extract (GM) was the most potent with the highest total phenolic compounds, flavonoids, tannins, terpenoids, and reducing activity. CuNPs synthesized using GM (GM-CuNPs) were characterized using UV-VIS spectroscopy and dynamic light scattering. The results showed that the maximum absorption of GM-CuNPs was at 340 nm. The average size of GM-CuNPs is in the nanoscale range of 159.2 ± 61 nm, with a narrow size distribution and a negative zeta potential of -4.13 ± 6.97 mV. The stability of GM-CuNPs is not solely due to their zeta potential but also phytochemicals in the extract. GM-CuNPs at 25 mM showed the highest efficiency of 95% in removing CIP from aqueous medium pH 6-7 at 25-35°C within 20 min. The results indicated that the electrostatic attraction between the negative charge of GM-CuNPs and the positive charge of CIP controlled the drug adsorption on the nanoparticles. In conclusion, the developed GM-CuNPs have excellent CIP removal efficiency. These synthesized GM-CuNPs are expected to be environmentally friendly for the removal of antibiotics and other drugs.

Keywords *Garcinia mangostana*, eco-friendly, green synthesis, metal nanoparticles, plant extract

1. Introduction

It is known that many drugs in humans and animals are eliminated through urine and feces, and released into the wastewater system (1). Ciprofloxacin (CIP), one of the most widely used antibiotics for treatment of bacterial infections in both humans and animals, is secreted in the urine in its original form (2). Therefore, large amounts of CIP are found in wastewater systems. In addition, pharmaceutical manufacturers and hospitals are also the most important sources of contaminated wastewater. This leads to increase contamination in surface and groundwater, and is extremely harmful to the environment and human health (3,4). It has been reported that CIP contamination of daily drinking water can

cause mild nausea, vomiting, headaches, and diarrhea. Higher CIP contamination can cause more serious adverse effects, such as thrombocytopenia and acute renal failure. Additionally, the presence of CIP in water supplies has resulted in the development of antibiotic-resistant bacteria (5), resulting in an increase in health problems. This is because treating drug-resistant bacteria is difficult, high cost, and requires different drug or a higher dose. Therefore, the effective removal of CIP is required. Technology using metal nanoparticles appears to be a convenient alternative (6) and promising for the removal of CIP by an adsorption mechanism (7,8). Several metal-based techniques have been developed to synthesize metal nanoparticles, such as chemical laser ablation, chemical reduction, coprecipitation, and wave-

assisted processes (9,10). However, these methods are expensive and not environmentally friendly. This is because many harmful by-products are released into the environment. The limitations of these methods have given rise to new technologies of plant-based synthesis, by biomolecules are used instead. Plant-assisted synthesis is environmentally friendly, cost effective, and can help overcome all limitations. It has been proven to be an effective and highly reliable technique in preparing metal nanoparticles. However, to obtain the desired metal nanoparticles by plant-based synthesis, it is necessary to use biomaterial with high reducing power. Several reports indicate that certain plant-derived phenolic compounds such as flavonoids and tannins possess antioxidant activity and reducing power. In this study, the phytochemical contents of 6 potential plant extracts, *Ageratum conyzoides*, *Emilia sonchifolia*, *Garcinia mangostana*, *Sesbania grandiflora*, *Tridax procumbens*, and *Xanthium strumarium* were compare and the most effective plant extract was selected for synthesis of copper nanoparticles (CuNPs).

A. conyzoides, an allelopathic plant in the family Asteraceae, is a good source of antioxidants due to its high content of total phenolic compounds and flavonoids (11). Different parts of this plant have been used in folk medicine for decades. *E. sonchifolia*, *T. procumbens* and *X. strumarium* are members of the Asteraceae family. *E. sonchifolia* has previously been reported to inhibit the formation of hydroxyl radicals and superoxide radicals (12). Its major active ingredient is emiline, which is an alkaloid with antioxidant potential and neuroprotective effect against corticosterone-induced apoptosis in cancer cell lines (13). Up to date, there are no reports of using this compound as a reducing agent in the production of metal nanoparticles. Therefore, it remains a challenge as a primary plant in this experiment. *T. procumbens* contains alkaloids, carotenoids, flavonoids, fatty acids, steroids, phytosterols, tannins, and has high antioxidant activity (14). *X. strumarium* has been reported to have high antioxidant activity and reducing power (15). The antioxidant properties of this plant are related to the levels of alkaloids, phenolic acids, diterpenes, saponins, glycosides, essential oils and phytosterols (16,17). *G. mangostana* is a tropical perennial with edible fruits. It belongs to the Guttiferae family. This plant has been used in traditional and folk medicine systems in Southeast Asia to treat cystitis, dysentery, gonorrhea, inflammatory skin and abnormalities of urinary tract and to increase the efficiency of wound healing (18). It has been documented as a reducing agent for the fabrication of metal nanoparticles due to its phytochemical composition in the aqueous extract (19). *S. grandiflora*, which belongs to the family Leguminosae, is an important agroforestry as a food source for humans, cattle, and goats in Thailand. Its bark extract possesses strong antibacterial activity (20). Antioxidant activity and the use in the plant-based synthesis of silver nanoparticles

from this plant have also been reported (21). The main objective of this study was to synthesize CuNPs for the elimination of CIP. In this synthesis, a green biosynthesis method was used. The most effective plant extracts from these six potential plants were used as reducing agents. The synthesized CuNPs were studied for their physicochemical characterization and CIP removal efficiency in various water conditions.

2. Materials and Methods

2.1. Materials

Copper sulfate pentahydrate, ferric chloride, potassium ferricyanide, sodium nitrate and sodium nitrite were purchased from Ajax Finechem (New South Wales, Australia). CIP hydrochloride and gallic acid were from Bio Basic Inc. (Markham, Canada). Epigallocatechin gallate, quercetin, and 2,2-diphenyl-1-picrylhydrazyl hydrate (DPPH) were from Sigma-Aldrich (Steinheim, Germany). Hydrochloric acid (HCl) was from QRÖC (Auckland, New Zealand). Folin-Ciocalteu reagent was from Loba Chemie (Mumbai, India). Aluminum chloride hexahydrate, bromophenol blue, and calcium carbonate were from Kemaus (New South Wales, Australia). Trichloroacetic acid and vanillin were from Merck (Damstadt, Germany). Sodium hydroxide (NaOH) was from RCI Lab-scan (Bangkok, Thailand). All other solvents and chemicals were of analytical grade.

2.2. Plants and extract preparation

A. conyzoides, *E. sonchifolia*, *G. mangostana*, *S. grandiflora*, *T. procumbens* and *X. strumarium* were collected from northern Thailand during July-December 2021. The plants were authenticated by herbalists from Rajamangala University of Technology Lanna, Thailand. All specimens are preserved at the university's herbarium. Fresh leaves of each plant were detached from the stems and washed thoroughly with tap water and deionized water, respectively. After that, the whole leaf material was dried in a hot air oven at 50°C until a constant weight was achieved. Then pulverized with an electric blender. The plant powder sieved through a 20-mesh sieve was vacuum-wrapped in a plastic bag and stored in a deep freezer at -20°C for further use.

To prepare the aqueous extract of each plant, 100 mg of dried plant powder was boiled with 10 mL of distilled water at 85°C for 30 min. Afterwards, the mixture was cooled to room temperature. It was then filtered through a 0.22-micron nylon syringe filter. The obtained filtrate was used for further studies.

2.3. Phytochemical studies

Freshly prepared aqueous extracts of each plant were

examined for total phenolic content (TPC), flavonoids and tannins. TPC content was determined by mixing 20 μL of the extract with 100 μL Folin-Ciocalteu reagent in 1,980 μL deionized water. After 5 min of incubation, 300 μL of 7% sodium nitrate solution was added and mixed well. The resulting mixture was further incubated for 60 min in the dark at room temperature. It was then measured for the absorbance at 765 nm. TPC was determined using a calibration curve made from various concentrations of gallic acid and expressed as μg of gallic acid equivalent (GAE) per mg of extract.

The total flavonoid content (TFC) of the samples was determined by mixing 20 μL of extract with 380 μL deionized water, then 100 μL of 5% sodium nitrite solution was added. After 5 min of incubation, the mixture was added with 100 μL of 10% aluminum chloride solution and allowed to stand for 6 min at room temperature. Finally, 400 μL of 1M NaOH solution was added. After completion of 15 min of incubation in the dark, absorbance was measured at 415 nm. TFC was determined using a calibration curve generated from quercetin at various concentrations and expressed as μg quercetin equivalent (QE) per mg of extract.

For determination of total tannin content (TTC), 250 μL of extract was vigorously shaken with 450 μL of 1% vanillin reagent. After 5 min of incubation, the mixture was mixed with 300 μL of concentrated HCl and then was incubated for 30 min at ambient temperature. Finally, the color of the solution changed to red. The absorbance was measured at 500 nm. TTC was determined using a calibration curve generated from epigallocatechin gallate at various concentrations and expressed as μg of epigallocatechin gallate equivalent (EE) per mg of extract.

2.4. Determination of reducing power

High reducing power is an important factor in the production of metal nanoparticles. Measurement of the reducing potential of plant extracts was performed using an assay according to a previously described method (22) with some modifications. Briefly, the diluted concentration of each extract (12.5, 25, 50 and 100 $\mu\text{g}/\text{mL}$) and the standard antioxidant, gallic acid was mixed with 1.0 mL of 0.2 M sodium phosphate buffer (pH 6.6) and 1.0 mL of 1% potassium ferricyanide. After vigorously shaking, the mixture was incubated at 50°C in a dry bath for 20 min, then 1.0 mL of 10% trichloroacetic acid was mixed and centrifuged at 4,000 rpm for 10 min. An aliquot of 0.5 mL of supernatant was diluted with the same volume of distilled water. Finally, 50 μL of 0.1% ferric chloride was added. After incubation for 10 min, the absorbance was determined at 700 nm against a reagent blank. Distilled water was used as a blank. The reducing power was determined using a calibration curve made from gallic acid at various concentrations and expressed as μg of GAE per mg of extract.

2.5. Synthesis of CuNPs

The synthesis of CuNPs was conducted according to a previously described method (23) with some modification. Briefly, copper sulfate was dissolved in deionized water to obtain a final concentration of 50 mM. After that, 200 μL of extract and 300 μL of deionized water were vigorously mixed with 500 μL of copper sulphate solution prior to refluxing at 80°C for 30 min in a dry incubator to stimulate the reduction of metal salt. The color of the dispersion gradually changed from colorless to yellow and then to dark orange. This indicates the formation of particles in the nanoscale range (24). The solution was allowed to cool to ambient temperature and used for further studies.

2.6. Characterization of CuNPs

The formed CuNPs was characterized using a V-1200 spectrophotometer with UV-Professional analysis software (Dshing Instrument Co., Ltd., ZhuHai, China). The UV-visible spectrum of CuNPs enclosed in 1.5 mL disposable PMMA cuvettes (BRAND GmbH & Co. KG, Wertheim, Germany) was detected in the wavelength range 320 to 800 nm, operating at a resolution of 5 nm. The extracts and copper sulfate solution were also examined under the same conditions.

The lyophilized CuNPs were resuspended in 1 mL deionized water. The size and size distribution (PDI) as well as zeta potential of CuNPs were determined using a Nano-ZS zetasizer (DTS 1060, Malvern Instruments Ltd., Worcestershire, UK) based on the principle of dynamic light scattering (25,26). The results were automatically calculated by the software according to the instrument manufacturer's recommendations.

2.7. Removal efficiency of CuNPs

In this experiment, CuNPs synthesized using selected plant extracts were used. The CIP removal efficiency (CRE) of the synthesized CuNPs was examined using the CIP solutions. For the preparation of CIP solution, 25 mg of CIP hydrochloride was dissolved in 100 mL of distilled water. Factors that might affect CRE include: CuNPs concentration, contact time, pH, and temperature were monitored. To study the effects of pH, the pH of the tested solution was adjusted by adding 0.1 N HCl or 0.1 N NaOH to achieve a pH range of 3-10.

The selected CuNPs colloidal dispersion was mixed with freshly prepared CIP sample solution and kept at room temperature for 60 min. The samples were collected at different time intervals and centrifuged at 500 rpm for 10 min. An aliquot of 250 μL of the supernatant was mixed with 100 μL of 20 mM acetate buffer, pH 4.1, and 375 μL of 0.1% bromophenol blue. After incubation at room temperature for 10 min, 2.5 mL of chloroform was added and the mixture

was shaken vigorously for 30 s, which resulted in the separation between chloroform and water. The yellow layer was determined at 416 nm relative to the blank. Calibration curves were generated by diluting CIP to various concentrations ($R^2 = 0.99$). The CIP content was expressed in μg . The system without CuNPs was used as a control. CRE can be calculated using the following equation: $\text{CRE} (\%) = [(A_c - A_s)/A_c] \times 100$, where A_c is the absorbance of the control and A_s is the absorbance of the sample.

2.8. Statistical analysis

All experiments were carried out in triplicate. The obtained data were analyzed using Microsoft Excel 2016 for Windows and presented as mean \pm standard deviation (SD). The data were analyzed by one-way ANOVA and Duncan's mean comparison test at the 5% significance level.

3. Results

3.1. Phytochemicals and reducing power of extracts

The phytochemical content and reducing power of the extracts of the six plants are shown in Table 1. It can be clearly seen that the *G. Mangostana* extract had the highest TPC, TFC, and TTC with the GAE, QE, and EE values of $98.86 \pm 1.20 \text{ mg/g}$, $109.22 \pm 4.06 \text{ mg/g}$, and $209.67 \pm 7.29 \text{ mg/g}$, respectively. This extract was selected for further studies.

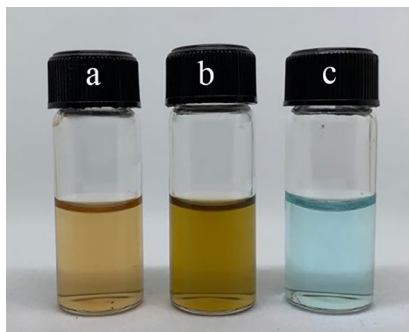


Figure 1. Appearance and color of *G. mangostana* extract solution (a), GM-CuNPs colloidal system (b), and copper sulfate solution (c).

3.2. CuNPs synthesis and particle characterization

G. mangostana extract was used as a reducing agent in the synthesis of CuNPs, and the obtained CuNPs were named as GM-CuNPs. The blue color of the copper sulfate solution changed to light brown after boiling the mixture at 80°C for 30 min. The different appearance and color of GM-CuNPs colloidal system are shown in Figure 1. After characterization, the results confirmed that the particle size of GM-CuNPs was in the nanoscale range with an average diameter of $159 \pm 61 \text{ nm}$ and a narrow PDI value of 0.280 ± 0.003 . GM-CuNPs were also found to have a negative surface charge with a zeta potential of $-4.13 \pm 6.97 \text{ mV}$.

3.3. Effect of GM-CuNPs concentration on CIP removal

In this study, aqueous medium, pH 7, containing CIP at a concentration 0.25 g/L was treated with GM-CuNPs at concentrations ranging from 0.20 to 100 mM for 60 min at room temperature. The results as shown in Figure 2, indicate that the removal efficiency increased with the increase in the concentration of the synthesized GM-CuNPs. An increase in CIP removal capacity was observed from a CRE value of 24.1% to 98.2% when the GM-CuNPs concentration increased from 0.20 mM to 100 mM. The removal efficiency was highest when the concentration of GM-CuNPs was 25 mM. From these results, GM-CuNPs at a concentration of 25 mM was considered the most effective concentration to remove CIP and was selected for further study.

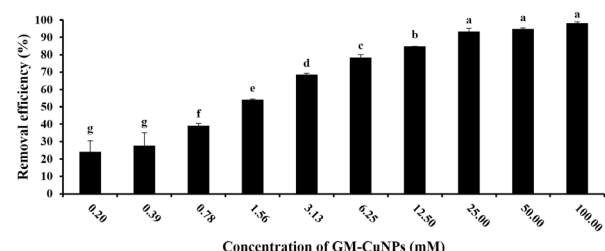


Figure 2. Effect of GM-CuNPs concentration on CIP removal efficiency. Different letters indicated statistically significant values ($p < 0.05$).

Table 1. Phytochemical properties and reducing power of the extracts

Plants	TPC	TFC	TTC	Reducing power
<i>A. conyzoides</i>	44.88 ± 0.37^b	42.19 ± 0.45^b	13.78 ± 0.85^b	234.61 ± 4.25^b
<i>E. sonchifolia</i>	24.05 ± 0.84^c	21.49 ± 0.61^c	2.87 ± 0.15^c	92.98 ± 3.92^d
<i>G. mangostana</i>	98.86 ± 1.20^a	109.22 ± 4.06^a	209.67 ± 7.29^a	358.82 ± 2.34^a
<i>S. grandiflora</i>	18.12 ± 1.20^e	21.78 ± 1.73^e	1.79 ± 0.60^e	41.61 ± 2.79^f
<i>T. procumbens</i>	15.73 ± 0.21^f	14.19 ± 0.60^d	6.84 ± 2.33^c	75.45 ± 3.21^e
<i>X. strumarium</i>	21.40 ± 0.16^d	23.63 ± 0.70^c	7.49 ± 0.26^c	121.82 ± 0.08^c

Data present mean \pm standard deviation of triplicate analysis. Different lowercase letters in the same column indicate statistically significant values ($p < 0.05$).

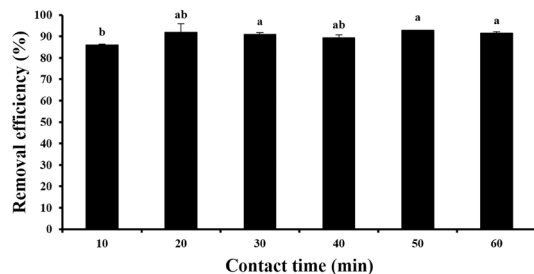


Figure 3. Effect of exposure time on CIP removal efficiency. Different letters indicate statistically significant values ($p < 0.05$).

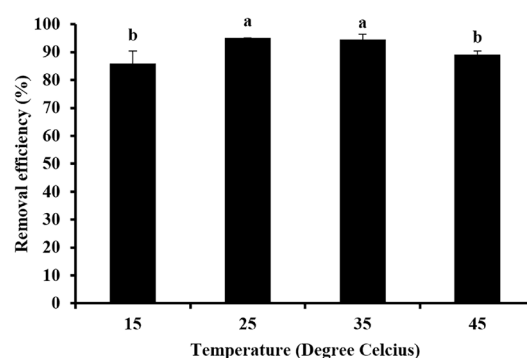


Figure 5. Effect of temperature on CIP removal efficiency. Different letters indicate statistically significant values ($p < 0.05$).

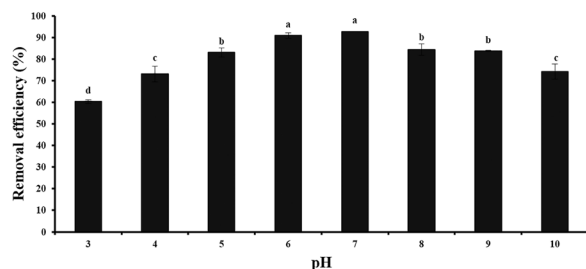


Figure 4. Effect of pH on CIP removal efficiency. Different letters indicate statistically significant values ($p < 0.05$).

3.4. Effect of exposure time

Exposure period between GM-CuNPs and CIP for different time intervals (10, 20, 30, 40, 50, and 60 min) was studied using GM-CuNPs at a concentration of 25 mM in medium at pH 7.0 and at room temperature. CRE values were found to increase with increasing exposure time. As shown in Figure 3, the CRE value at an exposure time of 10 min was $86.0 \pm 0.7\%$. Then, as the exposure time increased, the CRE value gradually increased to $91.8 \pm 1.1\%$ at an exposure time of 60 min. It is seen that CIP was rapidly removed by GM-CuNPs and achieved the highest removal efficiency in the first 20 min and then reached equilibrium.

3.5. Effect of pH

We hypothesized that pH might be another important factor for controlling the CIP removal process of GM-CuNPs. Therefore, the synthesized GM-CuNPs were added to the CIP aqueous solutions at various pH ranges of 3-10 to obtain a final concentration of 68 mM CIP and 25 mM GM-CuNPs. The results showed that the removal efficiency of GM-CuNPs at different pH was different as shown in Figure 4. It was found that increasing the pH value from 3.0 to 6.0 could increase the percentage of CRE from 60.4% to 92.8%, respectively. The highest CRE value in 20 min contact was obtained in the pH range of 6-7. However, when the pH was further increased, it was found that the efficiency of removal decreased.

3.6. Effect of temperature

CIP removal efficiency by GM-CuNPs at various temperatures are presented in Figure 5. The results showed that the CIP removal efficiency was highest at the temperature range of 25-35°C (with CRE of 95.1 and 94.5%) and slightly decreased at 15°C and 45°C (with CRE of 85.9 and 89.2%).

4. Discussion

Flavonoids and tannins are important phytochemical groups. The principle chemical structure of flavonoids consists of two phenyl rings connected by a linear three-carbon bond (27). Flavonoids are classified according to their substituents and the oxidation state of the heterocyclic ring into flavones, isoflavones, flavanones, flavanols, and anthocyanidin (28). Tannins are bitter nitrogen-free polyphenolic compounds that have a bitter taste. Their molecular weight ranges between 500 to 20,000. Tannins can be divided into two groups: condensed tannins or non-hydrolysable tannins such as proanthocyanidins and hydrolysable tannins such as catechin and gallic acid (29). Both flavonoids and tannins possess various pharmacological effects, such as antioxidant, antiviral, antibacterial, and anti-inflammatory properties (28,30). It has been reported that the antioxidant effects of these polyphenolic compounds are due to H-atom transfer or single-electron transfer mechanisms (31,32). Therefore, these phenolic compounds have significant impact on the reducing properties of the sample, and affect the redox reactions of metal nanoparticles formulation (33,34). The results confirm that among the six plant extracts, *G. Mangostana* extract possessed the highest TPC, TFC, and TTC, and the highest reducing power. Therefore, this extract was selected for nanometal preparation.

During synthesis, the color of copper sulfate solution transformed from blue to light brown, confirming that all Cu^{2+} were reduced to Cu^0 and GM-CuNPs were completely formed. The color of the obtained CuNPs colloidal systems is due to the fluctuation of the surface plasmon excitation in CuNPs. A wide range of colors was observed after the formation of CuNPs

was completed. This variation can be caused by several factors, including reaction time and temperature. In addition, one of the most important factors is the type of reducing agent. It has been reported that when ascorbic acid (35) and *Fortunella margarita* extract (36) were used as a reducing agent, the colors of the obtained CuNPs colloidal systems were yellow-brown and yellowish-green, respectively. The current study used *G. Mangostana* extract, which has a different color from the two reducing agents reported above. Therefore, the color of colloidal GM-CuNPs obtained was light brown. However, these color changes are useful in indicating the complete formation of CuNPs. The maximum absorbance of the synthesized CuNPs is in the range approximately 320–370 nm. High absorbance indicates a high conversion of Cu^{+2} to Cu^0 and results in a high concentration of CuNPs (37). Consistent with previously reported (38), they found that an absorption peak of 370 nm was observed when *Cissus vitiginea* extract was used. In the present study, the absorbance of the synthesized CuNPs was 340 nm, which is consistent with CuNPs synthesized using curry leaf extract (39). The particle size of GM-CuNPs was in the nanoscale range with a narrow size distribution similar to that synthesized using the aqueous extract of *Carica papaya* leaves as a reducing agent and copper sulfate as a precursor (40). The zeta potential is an important parameter for predicting the stability of particles in colloidal systems. In general, a zeta potential of ± 30 mV is sufficient to prevent particles from coalescing by electrostatic repulsion (41). Zeta potential values near zero indicate weak repulsive forces between particles. This results in the agglomeration of particles. Interestingly, although the zeta potential values of the synthesized CuNPs using various plant extracts were close to zero (42–44), the obtained metal nanoparticles still did not aggregate. It has been reported that some phytochemicals present in plant extracts play important roles not only as reducing agents but also particle stabilizing agents (45). Therefore, the nanoparticles can be prevented from agglomeration, and the obtained CuNPs are stable despite their low zeta potential.

Our results show that the concentration of GM-CuNPs affects the removal efficiency. It has been reported that the addition of the nanoparticles increases the number of available adsorption sites (46), thus resulting in an increase in CRE. The present study shows that CIP was rapidly eliminated by GM-CuNPs and the highest elimination with CRE of 91.8% was achieved in the first 20 min, and then equilibrium was reached. This result suggests that the increasing time leads to increased contact between the CIP molecules and the active sites of GM-CuNPs (47). After CIP molecules saturate on the active sites of the nanoparticles, the CRE value does not significantly increase because the particles have reached their full capacity. This result is in agreement with previous reports showing that the removal of antibiotics

by CuNPs depends on the adsorption mechanism (48).

CIP is a zwitterionic molecule with two pK_a s; pK_{a1} of 6.1 and pK_{a2} of 8.7 (49,50), which is due to the proton predominance of the amine and carboxylic groups, respectively. The removal of CIP from water using GM-CuNPs was a pH-dependent phenomenon. It was observed that the removal process occurred along with the charge interaction adsorption mechanism. The highest CRE values within 20 min were found in the pH range of approximately 6–7, where the CIP molecule was in its zwitterionic form. In this pH range, CIP molecules possess both negative and positive charges. As a result, the interaction between GM-CuNPs and CIP is maximized. At pH lower than 6 or lower than pK_{a1} of CIP, the solution contained a high amount of H^+ cation, which completely interacted with the anion of GM-CuNPs. This competition resulted in a decrease in the adsorption of CIP by the active site of GM-CuNPs. At pH greater than 7, the negative salt form of CIP at pK_{a2} was dominant (51,52) and was repelled by the negatively charged of GM-CuNPs. Therefore, the adsorption of CIP by GM-CuNPs decreased again in alkaline medium. From these results, it was concluded that the highest removal efficiency of CIP by GM-CuNPs could be obtained only in the optimum pH range of 6–7. In studies on the effects of temperature, it was found that the maximum removal efficiency could only be achieved at appropriate temperature. This can be considered that interaction between CIP molecules and GM-CuNPs is a specific reaction that occurs only at specific temperature. The decreased removal efficiency at temperatures above and below 25–35°C is confirmed to be due to the reduced attraction between the active sites of GM-CuNPs and CIP. In addition, the adsorption efficiency at higher temperatures decreased due to the high mobility of both the adsorbent, GM-CuNPs, and the adsorbate, CIP (53). It can be concluded that among the factors studied, pH plays an important role in the CRE of GM-CuNPs. Therefore, it is necessary to adjust the pH to 6–7 before the removal of CIP by this nanoparticle system.

Acknowledgements

The authors are grateful to the Department of Science, Faculty of Science and Agricultural Technology, Rajamangala University of Technology Lanna, Lampang province, Thailand for providing chemical materials. We also would like to thank the Center of Excellence in Pharmaceutical Nanotechnology, Chiang Mai University for the partial support.

Funding: This work was partially supported by Global and Frontier Research University Fund, Naresuan University; Grant number R2566C053 and Agricultural Biochemistry Research Unit, Faculty of Sciences and Agricultural Technology, Rajamangala University of Technology Lanna Lampang.

Conflict of Interest: The authors have no conflicts of interest to disclose.

References

1. Nadia O, Bamfo N, Hosey-Cojocari C, Benet L, Remsberg C. Examination of urinary excretion of unchanged drug in humans and preclinical animal models: Increasing the predictability of poor metabolism in humans. *Pharm Res.* 2021; 38:1139-1156.
2. Jakobsen L, Lundberg C, Frimodt-Møller N. Ciprofloxacin pharmacokinetics pharmacodynamics against susceptible and low-level resistant escherichia coli isolates in an experimental ascending urinary tract infection model in mice. *Antimicrob Agents Chemother.* 2020; 65:e01804-e018020.
3. Dewit B, Dewulf J, Demeestere K, Van De Vyvere V, De Wispelaere P, Van Langenhove H. Ozonation of ciprofloxacin in water: HRMS identification of reaction products and pathways. *Environ Sci Technol.* 2008; 42:4889-4895.
4. El-Shafey E, Al-Lawati H, Al-Sumri A. Ciprofloxacin adsorption from aqueous solution onto chemically prepared carbon from date palm leaflets. *J Environ Sci.* 2012; 24:1579-1586.
5. Fick J, Soderstrom H, Lindberg R, Chau Phan C, Tysklind M, Larsson D. Contamination of surface, ground, and drinking water from pharmaceutical production. *Environ Toxicol Chem.* 2009; 28:2522-2527.
6. Liu W, Sutton NB, Rijnaarts HHM, Langenhoff AAM. Pharmaceutical removal from water with iron- or manganese-based technologies: A review. *Crit Rev Environ Sci Technol.* 2016; 46:1584-1621.
7. Mohammed AA, Kareem SL. Enhancement of ciprofloxacin antibiotic removal from aqueous solution using zno nanoparticles coated on pistachio shell. *Desalin Water Treat.* 2021; 213:229-239.
8. He P, Mao T, Wang A, Yin Y, Shen J, Chen H, Zhang, P. Enhanced reductive removal of ciprofloxacin in pharmaceutical wastewater using biogenic palladium nanoparticles by bubbling H₂. *RSC Advan.* 2020; 10:26067-26077.
9. Reverberi AP, Kuznetsov NT, Meshalkin VP, Salerno M, Fabiano B. Systematical analysis of chemical methods in metal nanoparticles synthesis. *Theor Found Chem Eng.* 2016; 50:59-66.
10. Haddawi SF, Humud HR, Hamidi SM. Signature of plasmonic nanoparticles in multi-wavelength low power random lasing. *Opt Laser Technol.* 2020; 121:105770.
11. Adetuyi F, Karigidi K, Akintimehin E, Adeyemo O. Antioxidant properties of *Ageratum conyzoides* L. Asteraceae leaves. *Bangladesh J Sci Ind Res.* 2018; 53:265-276.
12. Shylesh BS, Padikkala J. Antioxidant and anti-inflammatory activity of *Emilia sonchifolia*. *Fitoterapia* 1999; 70:275-278.
13. Shen SM, Shen L, Zhang J, Li G, Li Z, Pan R, Si J. Emililine, a new alkaloid from the aerial parts of *Emilia sonchifolia*. *Phytochem Lett.* 2013; 6:467-470.
14. Gubbiveeranna V, Nagaraju S. Ethnomedicinal, phytochemical constituents and pharmacological activities of *Tridax procumbens*: A review. *Int J Pharm Pharm Sci.* 2016; 8:1-7.
15. Guemmaz T, Zerargui F, Boumerfeg S, Arrar L, Aouachria S, Khennouf S, Charef NE, Baghiani A. Anti-hemolytic, anti-lipid peroxidation, antioxidant properties and acute toxicity of *Xanthium strumarium* leaves extracts. *Annu Res Rev Biol.* 2018; 24:1-12.
16. Sharifi-Rad J, Hoseini-Alfatemi SM, Sharifi-Rad M, Sharifi-Rad M, Iriti M, Sharifi-Rad M, Sharifi-Rad R, Raeisi S. Phytochemical compositions and biological activities of essential oil from *Xanthium strumarium* L. *Molecules.* 2015; 20:7034-7047.
17. Srinivas P, Rajashekhar V, Upender Rao E, Venkateshwarlu L, Anil kumar CH. Phytochemical screening and *in vitro* antimicrobial investigation of the methanolic extract of *Xanthium strumarium* leaf. *Int J Drug Dev Res.* 2011; 3:286-293.
18. Mohamed G, Al-Abd A, El-Halawany A, Abdallah H, Ibrahim S. New xanthones and cytotoxic constituents from *Garcinia mangostana* fruit hulls against human hepatocellular, breast, and colorectal cancer cell lines. *J Ethnopharmacol.* 2017; 198:302-312.
19. Veerasamy R, Xin TZ, Gunasagaran S, Xiang TFW, Yang EFC, Jeyakumar N, Dhanaraj SA. Biosynthesis of silver nanoparticles using mangosteen leaf extract and evaluation of their antimicrobial activities. *J Saudi Chem Soc.* 2011; 15:113-120.
20. Anantaworasakul P, Okonogi S, Klayraung S. Antibacterial activities of *Sesbania grandiflora* extracts. *Drug Discov Ther.* 2016; 5:1256-1262.
21. Samuel P. Bioefficacy of *Sesbania grandiflora* leaves silver nanoparticles against *Aedes aegypti* larvae. *J Adv Sci Res.* 2021; 12:176-184.
22. Zhang A, Fang Y, Wang H, Li H, Zhang Z. Free-radical scavenging properties and reducing power of grape cane extracts from 11 selected grape cultivars widely grown in China. *Molecules.* 2011; 16:10104-10122.
23. Amaliyah S, Pangesti DP, Masruri M, Sabarudin A, Sumitro SB. Green synthesis and characterization of copper nanoparticles using *Piper retrofractum* Vahl extract as bioreductor and capping agent. *Heliyon.* 2020; 6:e04636.
24. Harshiny M, Iswarya CN, Matheswaran M. Biogenic synthesis of iron nanoparticles using *Amaranthus dubius* leaf extract as a reducing agent. *Powder Technol.* 2015; 286:744-749.
25. Khumpirapang N, Sassa-Deepaeng T, Suknuntha K, Anuchapreeda S, Okonogi S. Masculinizing effects of chrysin-loaded poloxamer micelles on siamese fighting fish. *Vet Sci.* 2021; 8:305.
26. Sassa-deepaeng T, Pikulkaew S, Okonogi S. Development of chrysin loaded poloxamer micelles and toxicity evaluation in fish embryos. *Drug Discov Ther.* 2016; 10:150-155.
27. Iwashina I. The Structure and distribution of the flavonoids in plants. *J Plant Res.* 2000; 113:287-299.
28. Panche AN, Diwan AD, Chandra S. Flavonoids: An overview. *J Nutr Sci.* 2016; 5:e47.
29. Khanbabae K, Ree T. Tannins: Classification and definition. *Nat Prod Rep.* 2001; 18:641-649.
30. Mutha RE, Tatiya AU, Surana SJ. Flavonoids as natural phenolic compounds and their role in therapeutics: an overview. *Futur J Pharm Sci.* 2021; 7:25.
31. Gourlay G, Constabel CP. Condensed tannins are inducible antioxidants and protect hybrid poplar against oxidative stress. *Tree Physiol.* 2019; 39:345-355.
32. Quideau S, Deffieux D, Douat-Casassus C, Pouységu L. Plant polyphenols: Chemical properties, biological

- activities, and synthesis. *Angew Chem Int Edit.* 2011; 50:586-621.
33. Gutiérrez-Grijalva EP, Ambriz-Pére DL, Leyva-López N, Castillo-López RI, Heredia JB. Dietary phenolic compounds, health benefits and bioaccessibility. *Arch Latinoam Nutr.* 2016; 66:87-100.
 34. Aryal S, Baniya MK, Danekhu K, Kunwar P, Gurung R, Koirala N. Total Phenolic content, flavonoid content and antioxidant potential of wild vegetables from western Nepal. *Plants (Basel).* 2019; 8:96.
 35. Suárez-Cerda J, Espinoza-Gómez H, Alonso-Núñez G, Rivero IA, Gochi-Ponce Y, Flores-López LZ. A green synthesis of copper nanoparticles using native cyclodextrins as stabilizing agents. *J Saudi Chem Soc.* 2017; 21:341-348.
 36. Amjad R, Mubeen B, Ali SS, Imam SS, Alshehri S, Ghoneim MM, Alzarea SI, Rasool R, Ullah I, Nadeem MS, Kazmi I. Green synthesis and characterization of copper nanoparticles using *Fortunella margarita* leaves. *Polymers (Basel).* 2021; 13:4364.
 37. Mathur A, Kushwaha A, Dalakoti V, Dalakoti G, Singh DD. Green synthesis of silver nanoparticles using medicinal plant and its characterization. *Der Pharm Lett.* 2014; 5:118-122.
 38. Wu S, Rajeshkumar S, Madasamy M, Mahendran V. Green synthesis of copper nanoparticles using *Cissus vitiginea* and its antioxidant and antibacterial activity against urinary tract infection pathogens. *Artif Cells Nanomed B.* 2020; 48:1153-1158.
 39. Ashtaputrey SD, Ashtaputrey PD, Yelane N. Green synthesis and characterization of copper nanoparticles derived from *Murraya koenigii* leaves extract. *J Chem Pharm Sci.* 2017; 10:1288-2291.
 40. Sankar R, Manikandan P, Malarvizhi V, Fathima T, Shivashangari KS, Ravikumar V. Green synthesis of colloidal copper oxide nanoparticles using *Carica papaya* and its application in photocatalytic dye degradation. *Spectrochim Acta A.* 2014; 121:746-750.
 41. Manikandan A, Sathyabama M. Green synthesis of copper-chitosan nanoparticles and study of its antibacterial activity. *J Nanomed Nanotechnol.* 2015; 6:1-5.
 42. Narayanan M, Jahier-Hussain FA, Srinivasan B, Sambantham MT, Al-Keridis LA, AL-Mekhlafi FA. Green syntheses and characterization of copper-oxide nanoparticles by *Thespesia populnea* against skin-infection causing microbes. *J King Saud Univ-Sci.* 2022; 34:101885.
 43. Alhalili Z. Green synthesis of copper oxide nanoparticles CuO NPs from *Eucalyptus globoulus* leaf extract: Adsorption and design of experiments. *Arab J Chem.* 2022; 15:103739.
 44. Ijaz F, Shahid S, Khan SA, Ahmad W, Zaman S. Green synthesis of copper oxide nanoparticles using *Abutilon indicum* leaf extract: Antimicrobial, antioxidant and photocatalytic dye degradation activities. *Trop J Pharm Res.* 2017; 16:743-753.
 45. Amaliyah S, Pangesti D, Masruri M, Sabarudin A, Sumitro S. Green synthesis and characterization of copper nanoparticles using *Piper retrofractum* Vahl extract as bioreductor and capping agent. *Heliyon* 2020; 6:e04636.
 46. Balarak D, Mahvi AH, Shim MJ, Lee SM. Adsorption of ciprofloxacin from aqueous solution onto synthesized NiO: Isotherm, kinetic and thermodynamic studies. *Desalin Water Treat.* 2021; 212:390-400.
 47. Abdel-Aziz HM, Farag RS, Abdel-Gawad SA. Carbamazepine removal from aqueous solution by green synthesis zero-valent iron/cu nanoparticles with *Ficus benjamina* leaves' extract. *Int J Environ Res.* 2019; 13:843-852.
 48. Oliveira LMF, Nascimento MA, Guimarães YM, Oliveira AF, Silva AA, Lopes RP. Removal of beta-lactams antibiotics through zero-valent copper nanoparticles. *J Braz Chem Soc.* 2018; 29:1630-1637.
 49. Moradi SE, Haji Shabani AM, Dadfarnia S, Emami S. Effective removal of ciprofloxacin from aqueous solutions using magnetic metal-organic framework sorbents: Mechanisms, isotherms and kinetics. *J Iran Chem Soc.* 2016; 13:1617-1627.
 50. ElShaer A, Ouyang D, Hanson P, Mohammed AR. Preparation and evaluation of amino acid based salt forms of model zwitterionic drug ciprofloxacin. *J Pharm Drug Deliv Res.* 2013; 2:1-10.
 51. Igwegbe CA, Oba SN, Aniagor CO, Adeniyi AG, Igahalo JO. Adsorption of ciprofloxacin from water: A comprehensive review. *J Ind Engin Chem.* 2021; 93:57-77.
 52. El-Bendary N, El-Etriby HK, Mahanna H. Reuse of adsorption residuals for enhancing removal of ciprofloxacin from wastewater. *Environ Technol.* 2022; 43:4438-4454.
 53. Altaf S, Zafar R, Zaman WQ, Ahmad S, Yaqoob K, Syed A, Khan AJ, Bilal M, Arshad M. Removal of levofloxacin from aqueous solution by green synthesized magnetite (Fe_3O_4) nanoparticles using *Moringa olifera*: Kinetics and reaction mechanism analysis. *Ecotoxicol Environ Saf.* 2021; 226:112826.

Received August 4, 2023; Revised October 3, 2023; Accepted October 8, 2023.

*Address correspondence to:

Siriporn Okonogi, Center of Excellence in Pharmaceutical Nanotechnology, Faculty of Pharmacy, Chiang Mai University, Chiang Mai, Thailand 50200.
E-mail: okng2000@gmail.com

Released online in J-STAGE as advance publication October 16, 2023.

FASN promotes gallbladder cancer progression and reduces cancer cell sensitivity to gemcitabine through PI3K/AKT signaling

Haihong Cheng^{1,§}, Yuxin Sun^{1,§}, Xiaopeng Yu², Di Zhou⁴, Jun Ding³, Shouhua Wang^{2,*}, Fei Ma^{1,2,*}

¹ Department of Oncology, Xinhua Hospital Affiliated to Shanghai Jiao Tong University School of Medicine, Shanghai, China;

² Department of General Surgery, Xinhua Hospital Affiliated to Shanghai Jiao Tong University School of Medicine, Shanghai, China;

³ Department of Biliary and Pancreatic Surgery, Shanghai Shuguang Hospital Affiliated with the Shanghai University of Traditional Chinese Medicine, Shanghai, China;

⁴ Department of Hepatobiliary Surgery, Tenth People's Hospital Affiliated to Tongji University, Shanghai, China.

SUMMARY Lipid metabolism plays an important role in the growth and development of tumors. However, the role of lipid metabolism in gallbladder cancer (GBC) has not been clearly clarified. Here, we demonstrated that fatty acid synthase (FASN), a key enzyme in *de novo* fatty acid biosynthesis, had upregulated expression in GBC samples both at protein and mRNA levels. Analysis of clinical data indicated the association between elevated FASN expression and poorer histology grades. Furthermore, FASN activity impairment through FASN knockdown or treatment with orlistat resulted in the inhibition of cell proliferation and migration, as well as increased sensitivity to gemcitabine. Both FASN knockdown and orlistat treatment induced cell apoptosis. Mechanistically, impairment of FASN activity suppressed the activation of the PI3K/AKT signaling pathway, which led to increased cell apoptosis and sensitivity to gemcitabine. These findings were also validated through nude mouse xenograft models, thus highlighting the potential of targeting FASN as a clinical treatment strategy. Collectively, the present study underscores the crucial role of FASN in the progression of gallbladder cancer *via* the PI3K/AKT pathway.

Keywords GBC, orlistat, drug combination

1. Introduction

Gallbladder cancer (GBC) represents the most frequent malignant tumor within the biliary system (1), with a poor prognosis and a median survival of only 4-7 months (2). It was estimated that there were 115,949 cases of GBC and 84,695 deaths in 2020 (3). Despite surgery being the principal treatment method for gallbladder cancer, most patients are typically diagnosed during advanced stages, and as a result, are not eligible for radical resection (4). As a consequence, chemotherapy-based comprehensive treatment represents the primary strategy for extending the survival time of patients suffering from advanced GBC. Currently, gemcitabine (GEM) constitutes one of the principal drugs employed in first-line chemotherapy regimens for gallbladder cancer. Nonetheless, its objective response rate is a mere 30%, largely due to its low sensitivity (5). It is therefore urgent to explore the molecular mechanisms that underlie tumor progression and chemotherapy resistance in GBC to pave the way for the development of novel therapeutic

approaches.

Fatty acid synthase (FASN) is the paramount lipogenic enzyme responsible for the terminal stages of *de novo* synthesis of fatty acids, specifically palmitate. In contrast to healthy cells, cancerous cells rely on the active production of fatty acids to construct membranes that promote cellular growth and proliferation. Additionally, palmitate can form covalent bonds with certain tumor-promoting growth factors, including Wnt, HRAS, and NRAS. These factors must undergo post-translational modification through palmitoylation to achieve correct localization and functional efficacy (6). While FASN is known to be overexpressed in a multitude of cancer types, its expression in healthy tissues is comparably meager. FASN activity seems to coincide with the advancement of numerous human malignancies. In human cancers, FASN is excessively upregulated and linked with unfavorable prognoses, as it sustains cancer cell growth and survival. Conversely, in the majority of normal cells, FASN is markedly repressed by adequate exogenous dietary fat supplementation (7). Additionally,

it has been demonstrated that overexpression of FASN contributes to cellular resistance against genotoxic drugs, including doxorubicin and cisplatin (8,9). Another study has indicated that FASN expression is markedly upregulated in pancreatic cancer. Furthermore, this study revealed that knockdown of FASN could reverse the cellular resistance to gemcitabine induced by overexpression of PKM2 (10). Although studies have identified FASN as a potential prognostic and therapeutic target in various cancers, its role in GBC remains unknown. In this study, we will examine the expression level of FASN through tissue microarray (TMA) and quantitative RT-PCR. Furthermore, we will elucidate the functional role of FASN in the progression of GBC and its impact on gemcitabine sensitivity.

Orlistat, a compound with reactive β -lactones, shows irreversible FASN inhibition ability. Currently, orlistat is registered as an obesity treatment drug in several countries. Its mechanism of action involves suppression of gastrointestinal lipases, which impairs the metabolism of lipids in the gastrointestinal lumen and prevents the absorption of up to 30% of the lipids in dietary fat (11). Studies indicate that orlistat shows therapeutic effects on a variety of cancers *in vivo* and *in vitro* (12,13). It has been reported that orlistat can reverse resistance to sorafenib in liver cancer (14) and cisplatin in ovarian cancer (15) by regulating the process of fatty acid metabolism. Given its favorable safety profile and affordability, the potential role of orlistat in cancer treatment is an area of significant clinical interest. Specifically, its role in GBC and the underlying mechanisms of action warrants further exploration.

In summary, our study affirms the significance of FASN in GBC through evaluating the correlation between FASN expression in GBC tissues and clinical features. *In vivo* and *in vitro* experiments were performed to ascertain the function of FASN in the progression of GBC and its impact on sensitivity to gemcitabine.

2. Materials and Methods

2.1. Cell lines and culture

NOZ, and the SGC-996 of human GBC cell lines, obtained from colleagues of Shanghai Key Laboratory of Biliary Tract Disease Research of Xinhua Hospital, Shanghai Jiao Tong University School of Medicine, China. These cells were routinely maintained in DMEM medium (Gibco, NY, USA) supplemented with 10% fetal bovine serum (Yeasen, Shanghai, China) and ampicillin/streptomycin (1%). All cells were cultured at 37°C, 5% CO₂. Cells were routinely verified and assured for free of mycoplasma contamination.

2.2. Patients and specimens

48 pairs of GBC tissues and adjacent normal tissues were

collected for this study to verify expression of FASN with TMA. The patients received surgery between 2018 and 2021 in Xinhua Hospital of Shanghai Jiao Tong University School of Medicine (Shanghai, China). The complete medical records of 38 cases of these patients were available and the clinicopathologic features were retrospectively analyzed. All procedures followed were in accordance with the Helsinki Declaration (as revised in 2013). Informed consent was obtained from all patients for being included in the study.

2.3. Tissue microarray (TMA)

Tissue microarrays were constructed with 2 mm cores to evaluate the expression of FASN. The tissue sections were soaked in xylene for 15 min and then rehydrated through three decreased concentrations of ethanol for 2 min, and boiled in a pH 6.0 antigen retrieval solution for 20 min at 95°C. To remove endogenous peroxidase, the tissue sections were blocked with 3% hydrogen peroxide after cooling for enough time. The slides were then incubated with 10% goat serum for 60 min at room temperature. After incubation with primary and second antibodies, labeling was detected.

FASN expresses cytoplasmically. A total score (IHC score) which is obtained by multiplying proportion score (< 5%, 0; 6 to 25%, 1; 26 to 50%, 2; 51 to 75%, 3; and > 75%, 4) and intensity score (0; no staining, 1; weak intensity, 2; moderate intensity, 3; strong intensity), which represent the average intensity and proportion of positively stained cancer cells relatively. Subsequently, the 48 pairs of samples were designated as absent/low FASN expressers (IHC scores 0 to 4) or high FASN expressers (IHC scores 6 to 12) (16). A ratio was calculated to define the relative FASN expression of cancer (IHC scores) to the adjacent tissue (IHC scores): R = IHC score (cancer)/IHC score (paired normal tissue). A ratio greater than 2 was defined as relatively high expression. The evaluation of the immunohistochemical staining was independently performed by two experienced pathologists without knowledge of clinical data.

2.4. Plasmids, lentivirus particles and regents

The sequences of Small Interfering RNA (siRNA) were purchased from Tsingke Biotechnology Co., Ltd. (Beijing, China). siRNAs were transfected using RFect Reagent (Changzhou Biogenerating Biotechnologies corporation, Jiangsu, China) according to provided manufactures. The sequence of the siRNA is as follows: 5'-GCCGAGTACAATGTCAACATT -3'. Cells were used for further experiments at 48 h after transfection.

Short hairpin RNAs (shRNAs) against FASN were cloned into a pLKO.1 vector. HEK293T cells were co-transfected with pLKO.1 shRNA, psPAX2 and pMD2.G plasmid (gifts from Jiaxue Wu, School of

Life Sciences Fudan University, Shanghai, China) at a ratio of 4:3:1. The lentiviral particles were harvested 48 h after transfection. GBC cells were infected with recombinant lentivirus transducing units in 4 µg/mL polybrene (Beyotime, Shanghai, China). Cells were selected with puromycin for 1 week 48 after infection. The forward sequence of shRNA1 and shRNA2 are 5'-CCGGAAGCCGAGTACAATGTCAACACTCGA GTGTTGACATTGTACTCGGCTTTTG -3'and 5'-CCGGAACTGCTAGGTATGGAGTTCTCTCGAG AGAACTCCATACCTAGCAGTT TTTTG-3'.

2.5. CCK-8 assay and colony formation assay

The cell counting kit-8 (CCK-8) (Yeasen, Shanghai, China) was used to assess cell proliferation and viability. The NOZ and SGC-996 cells were seeded at a concentration of 2,000 cells/well in 100 µL in 96-well plates. To measure the IC₅₀ of GEM, gradient concentrations of them were added to cells for 48 or 72 h after cells were seeded for 24 h. The concentration of DMSO in the medium was controlled below 0.1%. CCK-8 (10 µL) was added to each well, then the absorbance at 450 nm was measured after incubating at 37°C for 2 h. The IC₅₀ value was calculated using GraphPad Prism 9.0.

The NOZ and SGC-996 cells were seeded at 1,000 cells/well in 6-well culture plates and grew for about two weeks. 4% paraformaldehyde was then used to fix the cells for 30 min, and 0.5% crystal violet solution was used to stain. The colony numbers (> 50 cells/colony) were manually counted.

2.6. Apoptotic assay

GBC cells were plated in 6-well plates (2×10^5 cells/well) and incubated overnight. After incubation, cells were transfected with control, FASN siRNA or treated with orlistat or gemcitabine for 48 h. Then, the apoptotic state of GBC cells was assessed by the Annexin V-FITC and PI (BD, United States, Cat number: 556547) cell staining following manufacturer's protocol. The samples were detected using flow cytometry (Cytoflex, Beckman, United States) and the results were analyzed using the CytExpert Software.

2.7. Western blot analysis

GBC cells were plated in 6-well plates (2×10^5 cells/well) and incubated overnight. After incubation, cells were transfected with control, FASN siRNA or treated with Orlistat or gemcitabine for 48 h. Then, cells were harvested and protein was extracted with radioimmunoprecipitation assay buffer (Beyotime, Shanghai, China). Protein was separated on 7.5-12.5% sodium dodecyl sulfate (SDS)-polyacrylamide gels and transferred onto 0.22 µm PVDF membrane (Merck Millipore, Burlington, MA, USA). The membranes were

blocked with 5% milk (Yeast, Shanghai, China) for 1 h, incubated with the primary antibodies (1:1,000 dilution) at 4°C overnight, and incubated with the secondary antibody (1:1,000 dilution) at room temperature for 1h. Bands were visualized using ECL (Yeast, Shanghai, China). Antibody information: anti-β-actin (Abclonal, Wuhan, China, AC026); anti-FASN (Abclonal, A19050); anti-E-cadherin (Abclonal, A11509); anti-CDK-4 (Raybiotech, Georgia, USA, 144-00366); anti-cyclin-D1 (Cell Signaling, Massachusetts, Danvers, USA, #2978); anti-Bcl-2 (Proteintech, Wuhan, China, 60178-1-Ig); anti-Bax (Proteintech, 50599-2-Ig); anti-vimentin (Proteintech, 10366-1-AP); anti-PI3K (Proteintech, 20584-1-AP); anti-p-PI3K(Tyr458/Tyr199) (Cell Signaling, #4228); anti-AKT (Cell Signaling, 10176-2-AP); anti-p-AKT (Ser473) (Cell Signaling, #9271).

2.8. Xenografted animals

Four-week-old BALB/c nude mice were purchased from the Shanghai SLAC Laboratory Animal Co., Ltd. (Shanghai, China), and the study was approved by Laboratory Animal Ethical and Welfare Committee Xin Hua Hospital Affiliated to Shanghai Jiao Tong University School of Medicine. We subcutaneously administered 1×10^6 NOZ cells (NC, lv-shFASN) resuspended in 0.1 mL PBS to nude mice on the left armpit. The mice were randomly grouped into four groups ($n = 6$). Two groups (control and shFASN) received an intraperitoneal injection with vehicle (Phosphate buffered saline, PBS) and the others (control and shFASN) with gemcitabine (50 mg/kg, twice a week), and body weight was measured every 2 days. We sacrificed the mice using CO₂, removed the tumors and weighed them. The tumor volume was calculated (V) ($\text{length} \times \text{width}^2$)/2.

2.8. Statistical analyses

All *in vitro* experiments were conducted in triplicate, and data were presented as mean ± standard deviation (SD). Differences between the two groups were evaluated using the Student's *t*-test. Depending on the total sample size and expected frequencies, the chi-square test or Fisher's exact test were chosen to assess the significance of differences of clinicopathological figures between groups. Data analyses were carried out in the GraphPad Prism 9 and SPSS version 25. * $p < 0.05$, ** $p < 0.01$, *** $p < 0.001$, and **** $p < 0.0001$ indicated statistical significance.

3. Results

3.1. Enhanced FASN expression is detected in GBC and involved with unfavorable clinicopathology of GBC tissue

To evaluate FASN expression in GBC, we collected

a total of 48 human GBC paired tumors and adjacent normal tissues. Tissue microarray data showed that FASN was mainly localized on the cell membrane and the cytoplasm of GBC tissues (Figure 1A). We assessed and scored staining pattern of FASN in both GBC and adjacent paracancerous gland tissue. It revealed that expression levels of FASN protein in cancer and normal tissues are both high. Of note, FASN protein expression was significantly increased in cancers compared to the matched gallbladder tissues (Figure 1B). Specifically, 40 out of 48 cases exhibited high expression of FASN (score > 4) in cancer tissues, while 20 out of 48 cases showed high expression in paracancerous tissues. RT-PCR data from another collected cohort also suggested that FASN mRNA expression levels were notably higher in gallbladder cancer tissues (14 cases) than in the adjacent normal tissues (14 cases) (Figure 1C). To investigate the correlation between FASN protein expression and clinicopathological features, 38 cases of complete medical reports were obtained and analyzed (Table 1). FASN expression was not statistically associated with age, gender, histological types, resection method, and gallstone state, but high FASN expression was significantly correlated with advanced clinical stage and nevin stage (Table 1). These results indicate upregulated FASN expression in GBC tissues and this gene's oncogenic properties in GBC.

3.2. FASN knockdown promotes apoptosis and inhibits proliferation and migration of GBC cells

After evaluating the FASN expression in GBC cell lines by western blot (Figure 2A), we selected NOZ and SGC-996 for further experiments. To further elucidate the oncogenic function of FASN, we knocked down the FASN protein expression in GBC cells by siRNA. The

knockdown efficiency was confirmed by western blot (Figure 2B). The CCK8 assay and colony formation assay showed that the proliferative capacity of NOZ and SGC-996 cells were impaired following the knockdown

Table 1. Summary of patient characteristics according to FASN expression

Variable	Total number	FASN expression		<i>P</i> value
		Relatively low (R < 2)	Relatively high (R ≥ 2)	
Age (y)				1
> 65	19	9	10	
≤ 65	19	10	9	
Gender				1
Male	11	5	6	
Female	27	14	13	
Histological types				1
Adenocarcinoma	33	17	16	
Other ^a	5	2	3	
Clinical stage				0.003**
1-2	7	7	0	
3-4	31	12	19	
T classification				0.055
T1-T2	11	9	2	
T3-T4	27	10	17	
N classification				0.329
N0	18	10	8	
N1	10	3	7	
N2	10	6	4	
M classification				1
M0	26	13	13	
M1	12	6	6	
Nevin staging				0.008**
IV, V	31	12	19	
I, II, III	7	7	0	
Resection method				0.728
R1, R2	12	7	5	
R0	26	12	14	
Gallstone				1
(+)	18	9	9	
(-)	20	10	10	

^aadenosquamous carcinoma, large cell neuroendocrine carcinoma, sarcomatoid carcinoma; χ^2 test was performed.

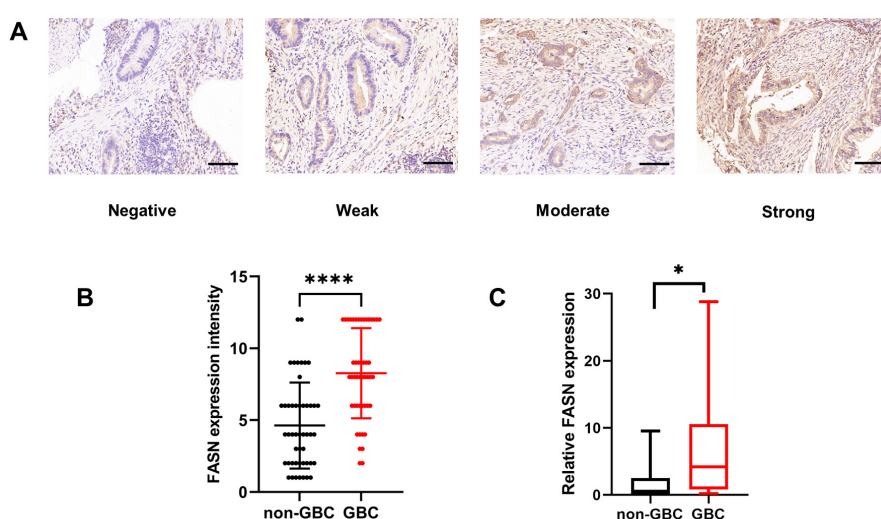


Figure 1. Enhanced FASN expression is detected in GBC and involved with unfavorable clinicopathology of GBC tissue. (A), Representative images of FASN expression in GBC tissues as visualized by TMA (Bar, 100 μm). (B), Expression of protein FASN in 48 paired GBC and adjacent normal tissues analyzed by TMA. (C), qPCR analysis of FASN mRNA expression. Data information: In (B), data are presented as mean ± SD. **p* < 0.05, *****p* < 0.0001 (Mann-Whitney U test for B, Student's-*t* test for C).

of FASN (Figures 2C and 2D). This was further proved by impaired protein levels of cyclin-D1 and CDK-4 in FASN knocking down cells (Figure 2G). Moreover, FASN knockdown significantly enhanced apoptosis in NOZ and SGC-996 cells (Figure 2E). Increased levels of apoptosis associated proteins Bax and decreased levels of Bcl-2 in FASN knockdown cells supported the results above (Figure 2G). Transwell assay and western blot assay were performed to evaluate the effect of FASN on the migration ability of GBC cells. The migrated cell numbers were significantly reduced after the knocking down of FASN (Figure 2F). Enhanced E-cadherin and reduced vimentin protein expression after knocking down FASN supported that FASN indeed promoted migration in GBC cells (Figure 2G). Taken together, these results demonstrate that FASN might promote proliferation and migration while impairing apoptosis of GBC cells.

3.3. Orlistat promotes apoptosis and inhibits proliferation and migration of GBC cells

Orlistat is a classical inhibitor of the thioesterase domain of FASN approved by the Food and Drug Administration for treating obesity, recently it has been proven to halt cell proliferation, and induce cancer cell apoptosis in various types of tumors (12,17). However, the role of orlistat in GBC remains unknown. To characterize the effects of orlistat on GBC and pave a way for clinical application, we first measure cell viability of NOZ/SGC-996 incubated with different concentrations of orlistat for 48 h via CCK-8 assay (supplementary Figure S1, <http://www.ddtjournal.com/action/getSupplementalData.php?ID=167>). Cell viability assay showed orlistat suppressed the growth of both two cell lines dose-dependently (supplementary Figure S1, <http://www.ddtjournal.com/action/getSupplementalData.php?ID=167>, Figure 3A). Also, the

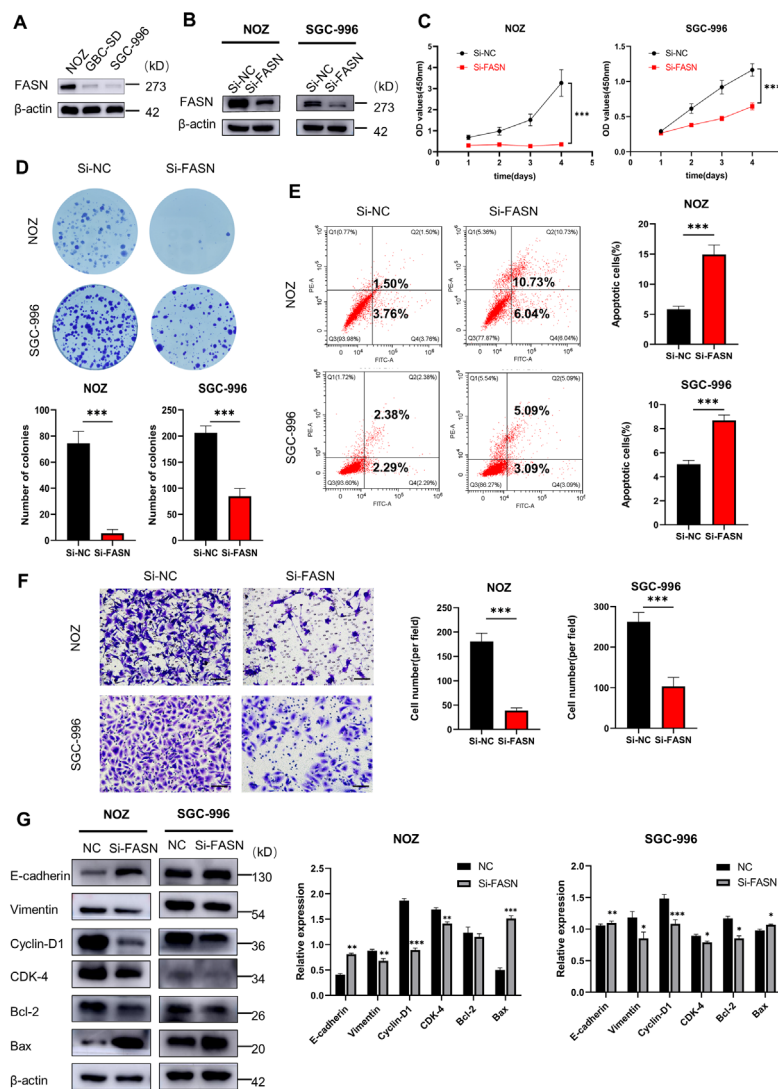


Figure 2. FASN knockdown promotes apoptosis and inhibits proliferation and migration of GBC cells. (A), Relative expression of FASN in three GBC cell lines. (B), Knockdown efficiency in NOZ and SGC-996. (C), Cell viability assay of FASN knockdown cell lines. (D), Colony formation assays and statistical analysis of two cell lines transfected with si-FASN. (E), Apoptosis assays and quantification of the apoptotic cell population. (F), Transwell assays and statistical results (Bar,100 μ m). (G), Western blotting of cell fractions in FASN knockdown cell lines of NOZ and SGC-996. Data are presented as mean \pm SD. * p < 0.05, ** p < 0.01, *** p < 0.001.

number of colonies formed by GBC cells was obviously reduced after treatment by different concentrations of orlistat for 48 h (Figure 3B). Orlistat also induced NOZ and SGC-996 cell apoptosis to a degree (Figure 3C). Besides, the transwell assay for cell migration showed that the number of migrated NOZ (0, 10, 100 μ M) and SGC-996 (0, 50, 100 μ M) cells treated with orlistat were decreased in a dose-dependent manner (Figure 3D). We observed an increase in protein expression of Bax and E-cadherin, and a decrease in the expression of Bcl-2, cyclin-D1, CDK-4, and vimentin in NOZ/SGC-996 cells (Figure 3E), which supported and verified that orlistat treatment could induce cell apoptosis, inhibit GBC cell proliferation and migration.

3.4. Impaired activity of FASN enhances gemcitabine sensitivity in GBC

FASN was reported to mediate chemoresistance of various drugs like gemcitabine (10), cisplatin, and doxorubicin (18). Considering that orlistat indeed showed anti-cancer activity in GBC cells without killing normal cells (18), we further wondered whether FASN inhibition by orlistat could show a positive effect on gemcitabine sensitivity *in vitro*. Then we evaluated sensitivity changes to gemcitabine in both NOZ and SGC-996 cells in the presence of 10 μ M orlistat. Compared to gemcitabine alone, combined treatment with orlistat for 72 h significantly lowered the IC₅₀ of gemcitabine in NOZ (from 56.14 nM to 15.18n M) and SGC-996 (from 1,206 nM to 406.6 nM) (Figures 4A and 4B).

We then examined the effect of the combined use of gemcitabine (1 μ M) and orlistat (10 μ M) on protein expression associated with cancer progression. Western

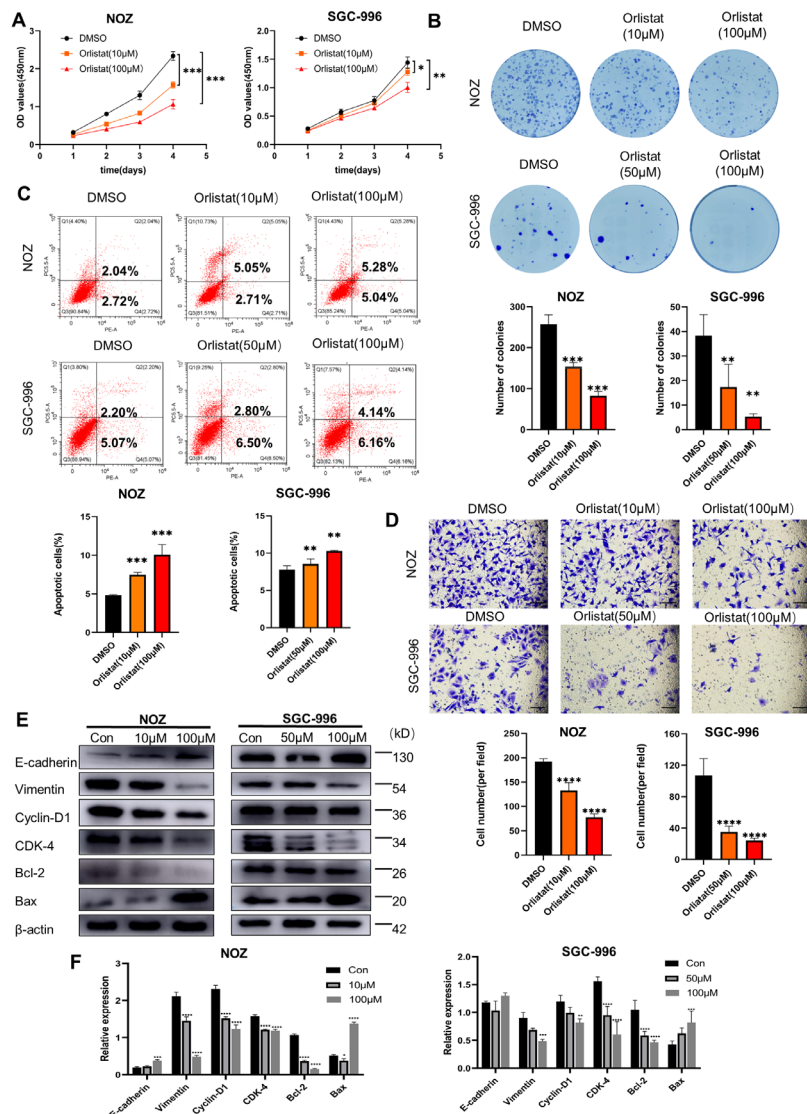


Figure 3. Orlistat promotes apoptosis and inhibits proliferation and migration of GBC cells. (A), Cell viability assay of cells pretreated with orlistat for 48h. (B), Colony formation assays and statistical analysis of two cell lines incubated with orlistat. (C), Apoptosis assays and quantification of the apoptotic cell population. (D), Transwell assays and statistical results (Bar,100 μ m). (E-F), Western blotting of cell fractions in cell lines of NOZ and SGC-996 treated with orlistat for 48h. Data are presented as mean \pm SD. * p < 0.05, ** p < 0.01, *** p < 0.001, **** p < 0.0001.

blot results demonstrate that the addition of orlistat could enhance the effect of gemcitabine on the expression of apoptosis-associated protein (Bax and Bcl-2), which indicated that orlistat could promote gemcitabine-induced cell death (Figures 4C-4E). Also, the combination of gemcitabine with orlistat showed synergistic decreasing expression of cyclin-D1 and CDK-4 (Figures 4C-4E). Additionally, the combination of the two agents enhanced the suppression of migration compared to treatment with gemcitabine alone (Figures 4C-4E).

Apart from that, flow cytometry apoptosis assays were conducted to evaluate the effects of FASN knockdown on gemcitabine sensitivity in GBC cells, revealing that FASN knockdown cells had a higher proportion of apoptosis (Figure 4F). Taken together, these results revealed that impairment of FASN activity could enhance the gemcitabine sensitivity in GBC cells.

3.5. FASN mediated PI3K/AKT activation involves in GBC cells sensitivity to gemcitabine

Accumulating evidence has revealed that PI3K/AKT activation participates in multi-drug resistance and neoplastic lipogenesis of various cancers. Therefore, we examined the phosphorylated forms of PI3K and AKT in NOZ and SGC-996 with downregulated FASN expression or orlistat treatment by western blot assay. It suggested that activation levels of PI3K/AKT pathway was significantly impaired by FASN activity repression, with relatively slight or no changes in the total protein expression levels (Figures 5A and 5B). Furthermore, treatment with gemcitabine or orlistat independently or in combination was conducted to assess the modulatory effect on PI3K/AKT cascade reaction. Compared to separately application or vehicle control (DMSO), the

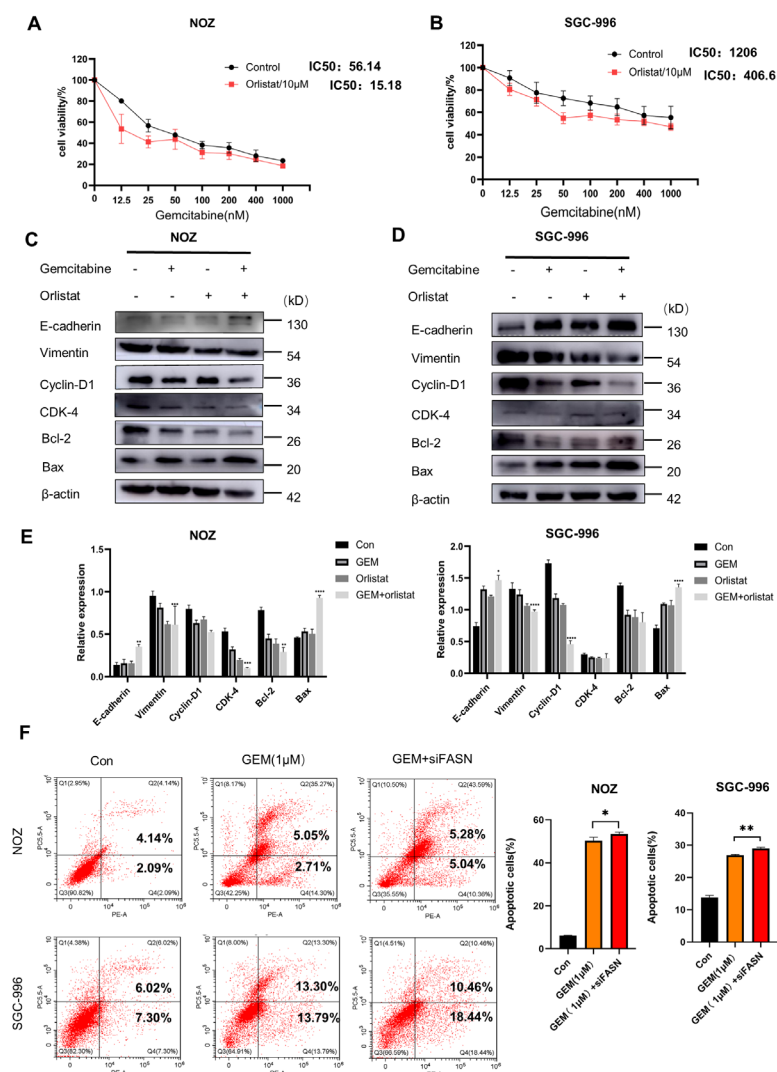


Figure 4. Impaired activity of FASN enhances gemcitabine sensitivity in GBC. (A-B), CCK8 assay showing the IC₅₀ of gemcitabine with or without orlistat (10 μM) addition in NOZ/SGC-996 cells. (C-E), Western blot analysis of bax, bcl-2, cyclin D1, CDK-4, vimentin and E-cadherin in cells treated with gemcitabine (1 μM) or orlistat (10 μM) alone or in combination. (F), Apoptosis assays and quantification of the apoptotic cell population in GBC cells treated with gemcitabine (1 μM), siFASN, or a combination of both. Data are presented as mean ± SD. The GEM + orlistat group was compared to the GEM group, and the other groups were compared to the control group. *p < 0.05, **p < 0.01, ***p < 0.001, ****p < 0.0001 . GEM: gemcitabine.

gemcitabine/orlistat simultaneous administration showed more efficiency on inhibition of PI3K/AKT signaling (Figure 5C). Taken together, FASN mediates GBC progression and gemcitabine resistance, at least, in part, through PI3K/AKT pathway.

To further validate the role of the PI3K/AKT pathway in GBC cells, a rescue experiment was conducted using SC79, an AKT agonist. The apoptotic proportions of NOZ and SGC-996 cells treated with gemcitabine or gemcitabine in combination with orlistat (100 μ M) were assessed. As depicted in Figure 5D, orlistat augmented the apoptotic effect induced by gemcitabine, and pre-treatment with SC79 for one hour partially reversed the trend.

3.6. FASN knockdown inhibits tumor growth and enhances gemcitabine sensitivity in mice

To further explore the role of FASN in GBC progression

and gemcitabine sensitivity *in vivo*, we developed nude mouse xenograft models to perform following experiments. FASN-silenced and matching control (lv-shFASN and lv-control) NOZ cells (Figure 6A) were subcutaneously injected into the right armpit of nude mice. These two kinds of mice were randomly divided into two groups separately and administered either gemcitabine (50 mg/kg) or PBS intraperitoneally. The tumor size and weight of mice were measured twice a week. The difference in the tumor volumes and weights between the lv-control and FASN-silenced, the lv-control treated with gemcitabine and the FASN-silenced treated with gemcitabine grouped mice were calculated. As exhibited by Figures 6B-6E, FASN knockdown could significantly abrogate tumor growth and the tumor abrogation effect of gemcitabine was significantly more evident in mice transfected with FASN-impaired cells. Immunohistochemical analyses of xenograft

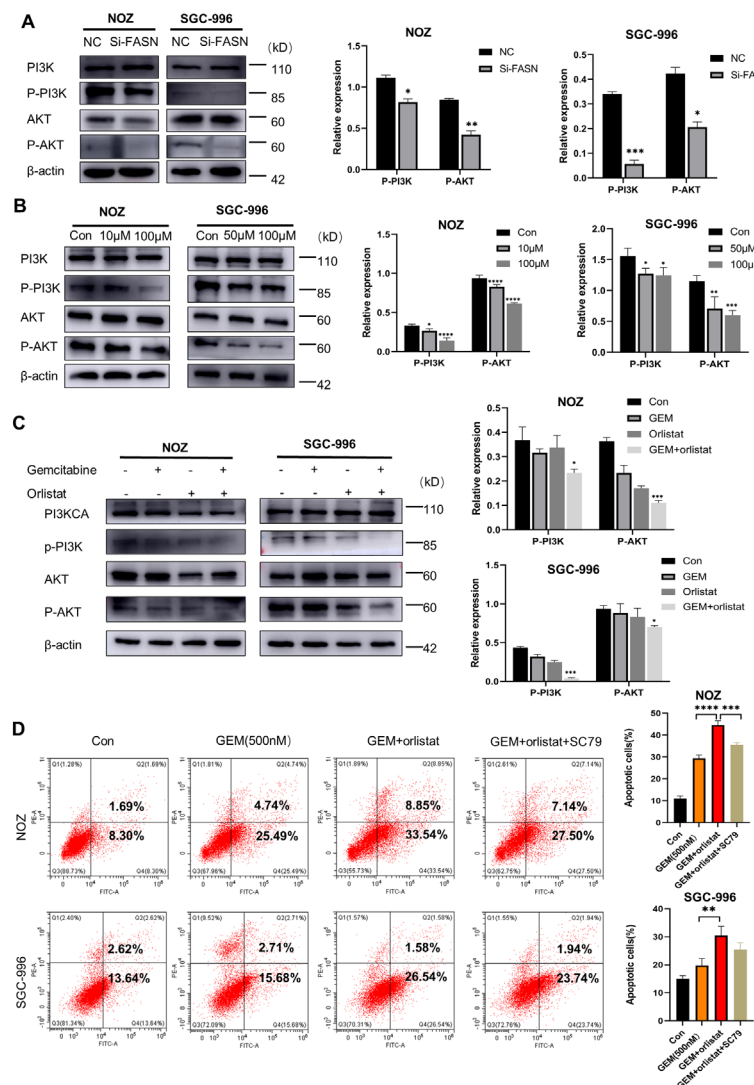


Figure 5. FASN mediated PI3K/AKT activation involves in GBC cells sensitivity to gemcitabine. (A-B), Western blot assay showing the expression levels of PI3K, p-PI3K, AKT, and p-AKT in FASN knockdown (A) and orlistat treatment (B) NOZ/SGC-996 cells. (C),Western blot analysis of PI3K, p-PI3K, AKT, and p-AKT in cells treated with gemcitabine (1 μ M)/orlistat (10 μ M) alone or in combination. (D), Apoptosis assays and quantification of the apoptotic cell population in cells treated with gemcitabine (500 nM) or gemcitabine in combination with orlistat (100 μ M). Pretreatment with 10 μ M SC79 was used to rescue the effect of orlistat. Data are presented as mean \pm SD. The GEM + orlistat group was compared to the GEM group, and the other groups were compared to the control group. * p < 0.05, ** p < 0.01, *** p < 0.001, **** p < 0.0001.

tumor tissues demonstrated that the expression level of apoptosis marker cleaved caspase 3 was elevated in the gemcitabine treatment group, and this was further enhanced by FASN knockdown (Figure 6F). Additionally, gemcitabine treatment, FASN knockdown, and their combination decreased the expression of Ki-67 (Figure 6F). Western blot analysis also showed that stable FASN knockdown downregulated p-AKT protein levels in xenograft tumor tissues (Figure 6G). Collectively, these results suggest that FASN knockdown can inhibit GBC tumor growth and improve gemcitabine sensitivity *in vivo* via the PI3K/AKT signaling pathway.

4. Discussion

Dysregulation of lipid metabolism is closely associated with the occurrence and progression of various tumors (19-21). Current clinical research indicates that lipid metabolism-targeted therapies exhibit promising anti-

cancer effects (19,22). Nevertheless, there is still a relatively limited amount of research regarding lipid metabolism in GBC. Epidemiological and clinical studies have demonstrated a positive correlation between obesity and overweight status with an elevated risk of GBC (23-25). Bile lipidomics experiments have revealed that the abnormal composition of lipids in the bile of GBC patients is correlated with disease severity (26), suggesting that lipid metabolism dysfunction may serve as a hallmark for early diagnosis of GBC (27). α -Mangostin, a dietary xanthone, has been shown to augment the susceptibility of gallbladder cancer to gemcitabine treatment by repressing lipid biosynthesis through the targeting of AMPK/SREBP1 signaling pathways (28). These findings suggest that aberrant lipid metabolism may also be involved in the tumorigenesis and malignant progression of GBC. To further clarify the relationship between lipid metabolism and GBC progression, we focused on a potential target, FASN, by

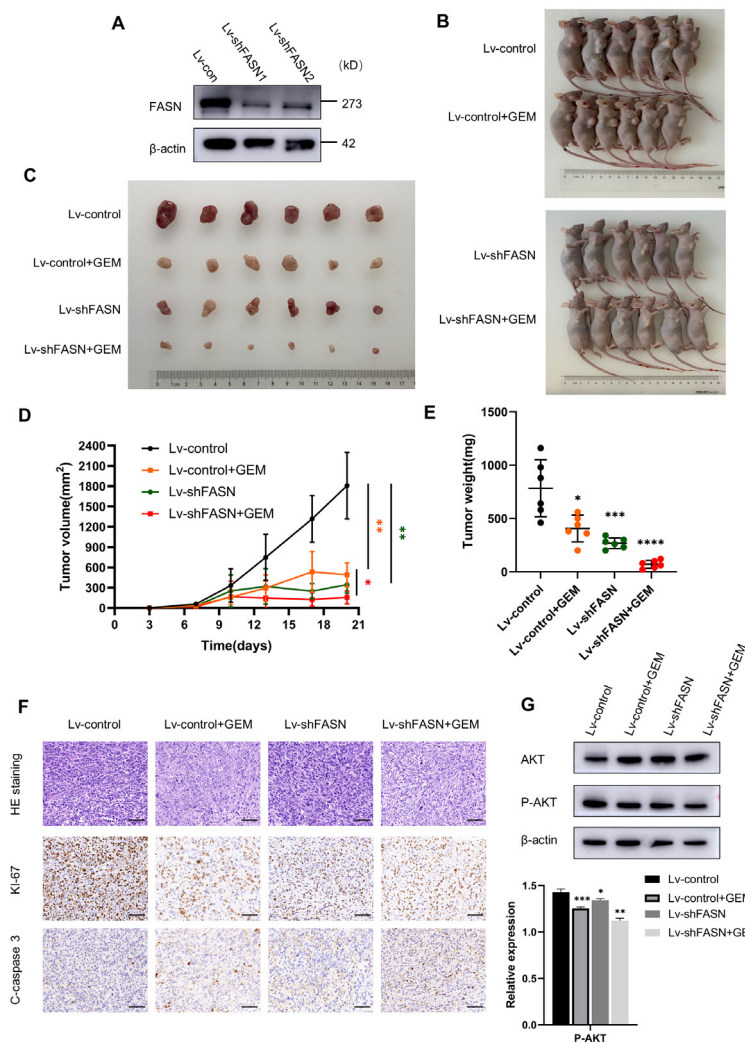


Figure 6. FASN knockdown inhibits tumor growth and enhances gemcitabine sensitivity in mice. (A), Validation of FASN knockdown efficiency. (B-C), Xenograft tumors in BALB/c nude mice. NOZ (Lv-control, Lv-shFASN) cells were inoculated into BALB/C nude mice. One week later, the mice were intraperitoneally injected with gemcitabine(50mg/kg) or PBS. The volumes (D) and weight (E) of tumors were measured. (F), IHC of Ki-67 and cleaved caspase 3 (c-caspase 3) in the tumors (Bar,100 μm). (G), Western blot analysis of AKT and p-AKT in four groups of xenograft tumor tissues. Data are presented as mean \pm SD. The Lv-shFASN + GEM group was compared to the Lv-control + GEM group, and the other groups were compared to the Lv-control group. * $p < 0.05$, ** $p < 0.01$, *** $p < 0.001$, **** $p < 0.0001$.

exploring its expression and function in GBC.

Fatty acids are a primary source of energy for rapidly dividing tumor cells and also serve as the fundamental building blocks for cell membrane synthesis. FASN is an essential enzyme in fatty acid synthesis and plays a pivotal role in this process. Extensive research has been conducted on the role of FASN in cancer progression and carcinogenesis (8,9,12), but its involvement in GBC has not been reported. In this study, we demonstrate that FASN is upregulated in GBC and facilitates malignant progression and gemcitabine insensitivity. Additionally, we show that inhibition of FASN leads to cell apoptosis by regulating the levels of PI3K and AKT phosphorylation, which are crucial for the oncogenic process. Further, we reveal that apoptosis induced by FASN inhibition can be rescued by the application of an AKT activator, SC79.

Studies have shown that various types of tumors, including prostate cancer, breast cancer, ovarian cancer, colon cancer, and gastric cancer, exhibit high FASN expression and elevated FASN activity (12). According to a previous study, ovarian cancer tissue overexpressed FASN protein by an average of 1.8 times relative to healthy fallopian tube tissue (29). The expression levels of FASN were found to be associated with different grades of ovarian cancer tissues (29). Additionally, FASN in serum was absent or present at lower levels in both normal and non-malignant conditions, suggesting that it may be useful as a marker for early cancer detection (30). In our results, both FASN protein and mRNA are overexpressed in GBC tissues compared to adjacent normal tissues. Moreover, increased FASN expression is positively correlated with more advanced GBC pathological stages, which are associated with poorer clinical outcomes for patients. Since some patients are lost to follow-up and the samples collected were from 2018 to 2020, the survival data is incomplete. Additional cohorts including more patients are needed to reaffirm these conclusions.

A previous study demonstrated that knockdown or knock-out of FASN inhibited esophageal squamous cell carcinoma cell proliferation (31). Exogenous expression of FASN enhanced the proliferation, migration, and cell motility of SK-UT-1 *via* promoting trimethylation of H3K9 (H3K9me3) and acetylation of H3K27 (H3K27ac) in uterine leiomyosarcomas cells (32). In addition, the reduction of palmitate synthesis by FASN inhibition contributed to cancer cell apoptosis by disrupting cell membranes formation, repressing signaling transduction such as PI3K-AKT-mTOR and lipid biosynthesis, and suppressing gene expression such as c-Myc (33). Interestingly, FASN is also dispensable for the function of Treg cells and FASN knock-out in Treg inhibits tumor growth (34). But no documentation uncovers the role of FASN playing in GBC. The results of our *in vitro* and *in vivo* experiments clearly demonstrate that inhibition of FASN by knockdown leads to a marked reduction in

GBC cell proliferation and migration while increasing apoptotic rates. Unfortunately, we encountered challenges in performing functional experiments by overexpressing FASN in GBC cells due to the large size of the protein, which can reach up to 273 kD, making it difficult to overexpress using current technologies. Therefore, we selected the FASN inhibitor orlistat to support our knockdown experiment. In the future, this part of the experiment could potentially be completed through supplementation with FASN catalytic products or the use of mutation techniques to enhance the enzyme activity of FASN (31).

Resistance is one of the key contributing factors to low response rate to chemotherapy in GBC. Lipid metabolism has been reported to be associated with drug resistance (20), FASN activity inhibition was also reported to reverse chemotherapy resistance in pancreatic cancer (10,35) and ovarian cancer (29). In our study, gemcitabine treated GBC cells show increased apoptotic rates after FASN knockdown. And in our xenograft animal experiment, gemcitabine shows more excellent therapeutic efficiency on tumor growth in mice transfected with FASN-knockdown NOZ cells. These findings suggest a possible target for GBC treatment and warrant further investigation to uncover the underlying mechanisms.

Orlistat irreversibly inhibits FASN through binding to the thioesterase domain of this enzyme. It is widely used for obesity treatment with considerable advantages in clinical safety over other inhibitors. Moreover, scores of studies have sought to verify the anticancer potential of this agent through *in vivo* and *in vitro* experiments aimed at evaluating its efficacy (12). Therefore, we conducted further investigations into the potential role of orlistat in GBC cells. Our findings reveal that orlistat effectively inhibits GBC cell progression, particularly in NOZ cells expressing higher levels of FASN. These results suggest that inhibitors may exhibit greater efficacy against tumors with elevated FASN activity. Thus, cancer patients exhibiting abnormally high FASN expression may represent appropriate targets for therapy. We further explored whether FASN inhibition by orlistat could enhance gemcitabine sensitivity. The CCK-8 assay demonstrates that administration of orlistat (10 μ M) can indeed reduce the IC₅₀ in GBC cell lines. Additionally, apoptotic assays indicate that orlistat can amplify gemcitabine-induced cell death. Nonetheless, we must acknowledge that the synergistic effect of orlistat and gemcitabine is not particularly pronounced, although we should not discount its modest effect. Considering that the side effects of orlistat are manageable, higher doses of the drug could be administered to enhance its effectiveness. In the future, a combination of orlistat and gemcitabine may improve the efficacy and safety of chemotherapy regimens for GBC. Further animal and clinical studies should be conducted to pave the way for GBC treatment.

PI3K/AKT signaling transduction is considered one of the causes of chemoresistance in various tumors. Aberrant activation of this pathway inhibits chemotherapy-induced apoptosis *via* multiple mechanisms (36). Phosphorylation activated AKT promotes cancer cells survival through mediating Bcl-2 and Bax expression (37). Cancer cells escape from apoptosis depending on Bcl-2 in a variety of tumors (38). In gastrointestinal stromal tumor cells, FASN knockdown resensitized drug-resistant cells to imatinib by inactivating the PI3K/AKT/mTOR signaling pathway (39). The present study validates that FASN knockdown and inhibition downregulate the phosphorylation level of PI3K and AKT protein without affecting expression levels of total protein. Both FASN downregulation and inhibition also induce apoptosis *via* enhancing Bax and suppressing Bcl-2 protein expression. Similarly, orlistat enhances gemcitabine-induced GBC cell death through boosting regulation of Bcl-2/Bax expression. Additionally, pretreatment with SC79, an AKT agonist, was shown to reverse the increased apoptosis of GBC cells caused by the combination treatment of orlistat and gemcitabine. Although we have conducted different experiments to confirm the role PI3K/AKT pathway plays in the function of FASN, we do not know how FASN interact with PI3K/AKT. Further mechanisms should be explored in following studies.

In conclusion, our study provides compelling evidence that FASN inactivation exerts inhibitory effects on GBC cell proliferation and migration, while promoting cell apoptosis and gemcitabine sensitivity through the PI3K/AKT pathway. This work not only identifies FASN as a promising therapeutic biomarker for GBC patients, but also highlights the potential clinical utility of orlistat, a lipid metabolism regulator, in improving the clinical outcomes of GBC patients through enhancing gemcitabine sensitivity. These findings open up a promising avenue for further research into targeting lipid metabolism in the treatment of GBC.

Acknowledgements

We thank colleagues from the Department of General Surgery and Laboratory of General Surgery, Xinhua Hospital Affiliated to Shanghai Jiao Tong University School of Medicine for help with all the experiments.

Funding: This work was supported by special project of clinical research of Shanghai Municipal Health Commission (No. 202040447).

Conflict of Interest: The authors have no conflicts of interest to disclose.

References

- Koppatz H, Takala S, Peltola K, But A, Makisalo H, Nordin A, Sallinen V. Gallbladder cancer epidemiology, treatment and survival in Southern Finland – a population-based study. *Scand J Gastroenterol.* 2021; 56:929-939.
- Lazcano-Ponce EC, Miquel JF, Munoz N, Herrero R, Ferrecio C, Wistuba, II, Alonso de Ruiz P, Aristi Uriza G, Nervi F. Epidemiology and molecular pathology of gallbladder cancer. *CA Cancer J Clin.* 2001; 51:349-364.
- Sung H, Ferlay J, Siegel RL, Laversanne M, Soerjomataram I, Jemal A, Bray F. Global cancer statistics 2020: GLOBOCAN estimates of incidence and mortality worldwide for 36 cancers in 185 countries. *CA Cancer J Clin.* 2021; 71:209-249.
- Rakic M, Patrlij L, Kopljari M, Klicek R, Kolovrat M, Loncar B, Basic Z. Gallbladder cancer. *Hepatobiliary Surg Nutr.* 2014; 3:221-226.
- Park K, Kim KP, Park S, Chang HM. Comparison of gemcitabine plus cisplatin versus capecitabine plus cisplatin as first-line chemotherapy for advanced biliary tract cancer. *Asia Pac J Clin Oncol.* 2017; 13:13-20.
- Buckley D, Duke G, Heuer TS, O'Farrell M, Wagman AS, McCulloch W, Kemble G. Fatty acid synthase – Modern tumor cell biology insights into a classical oncology target. *Pharmacol Ther.* 2017; 177:23-31.
- Menendez JA, Lupu R. Fatty acid synthase and the lipogenic phenotype in cancer pathogenesis. *Nat Rev Cancer.* 2007; 7:763-777.
- Wu X, Dong Z, Wang CJ, Barlow LJ, Fako V, Serrano MA, Zou Y, Liu JY, Zhang JT. FASN regulates cellular response to genotoxic treatments by increasing PARP-1 expression and DNA repair activity *via* NF-kappaB and SP1. *Proc Natl Acad Sci U S A.* 2016; 113:E6965-E6973.
- Liu H, Wu X, Dong Z, Luo Z, Zhao Z, Xu Y, Zhang JT. Fatty acid synthase causes drug resistance by inhibiting TNF-alpha and ceramide production. *J Lipid Res.* 2013; 54:776-785.
- Tian S, Li P, Sheng S, Jin X. Upregulation of pyruvate kinase M2 expression by fatty acid synthase contributes to gemcitabine resistance in pancreatic cancer. *Oncol Lett.* 2018; 15:2211-2217.
- Chandra P, Enespa, Singh R, Arora PK. Microbial lipases and their industrial applications: A comprehensive review. *Microb Cell Fact.* 2020; 19:169.
- Schcolnik-Cabrera A, Chavez-Blanco A, Dominguez-Gomez G, Taja-Chayeb L, Morales-Barcenas R, Trejo-Becerril C, Perez-Cardenas E, Gonzalez-Fierro A, Duenas-Gonzalez A. Orlistat as a FASN inhibitor and multitargeted agent for cancer therapy. *Expert Opin Investig Drugs.* 2018; 27:475-489.
- Jovankic JV, Nikodijevic DD, Milutinovic MG, Nikezic AG, Kojic VV, Cvetkovic AM, Cvetkovic DM. Potential of orlistat to induce apoptotic and antiangiogenic effects as well as inhibition of fatty acid synthesis in breast cancer cells. *Eur J Pharmacol.* 2023; 939:175456.
- Shueng PW, Chan HW, Lin WC, Kuo DY, Chuang HY. Orlistat resensitizes sorafenib-resistance in hepatocellular carcinoma cells through modulating metabolism. *Int J Mol Sci.* 2022; 23:6501.
- Papaevangelou E, Almeida GS, Box C, deSouza NM, Chung YL. The effect of FASN inhibition on the growth and metabolism of a cisplatin-resistant ovarian carcinoma model. *Int J Cancer.* 2018; 143:992-1002.
- Xie P, Zhang M, He S, et al. The covalent modifier Nedd8 is critical for the activation of Smurfl ubiquitin ligase in tumorigenesis. *Nat Commun.* 2014; 5:3733.
- Kridel SJ, Axelrod F, Rozenkrantz N, Smith JW. Orlistat

- is a novel inhibitor of fatty acid synthase with antitumor activity. *Cancer Res.* 2004; 64:2070-2075.
18. Wu X, Dong Z, Wang CJ, Barlow LJ, Fako V, Serrano MA, Zou Y, Liu JY, Zhang JT. FASN regulates cellular response to genotoxic treatments by increasing PARP-1 expression and DNA repair activity via NF-κB and SP1. *Proc Natl Acad Sci U S A.* 2016; 113:E6965-e6973.
 19. Snaebjornsson MT, Janaki-Raman S, Schulze A. Greasing the wheels of the cancer machine: The role of lipid metabolism in cancer. *Cell Metab.* 2020; 31:62-76.
 20. Cao Y. Adipocyte and lipid metabolism in cancer drug resistance. *J Clin Invest.* 2019; 129:3006-3017.
 21. Bian X, Liu R, Meng Y, Xing D, Xu D, Lu Z. Lipid metabolism and cancer. *J Exp Med.* 2021; 218.
 22. Cheng C, Geng F, Cheng X, Guo D. Lipid metabolism reprogramming and its potential targets in cancer. *Cancer Commun (Lond).* 2018; 38:27.
 23. Wang F, Wang B, Qiao L. Association between obesity and gallbladder cancer. *Front Biosci (Landmark Ed).* 2012; 17:2550-2558.
 24. Sharma A, Sharma KL, Gupta A, Yadav A, Kumar A. Gallbladder cancer epidemiology, pathogenesis and molecular genetics: Recent update. *World J Gastroenterol.* 2017; 23:3978-3998.
 25. Pati S, Irfan W, Jameel A, Ahmed S, Shahid RK. Obesity and cancer: A current overview of epidemiology, pathogenesis, outcomes, and management. *Cancers (Basel).* 2023; 15:485.
 26. Sharma N, Yadav M, Tripathi G, Mathew B, Bindal V, Falari S, Pamecha V, Maras JS. Bile multi-omics analysis classifies lipid species and microbial peptides predictive of carcinoma of gallbladder. *Hepatology.* 2022; 76:920-935.
 27. Yuan B, Fu J, Yu WL, Fu XH, Qiu YH, Yin L, Zhu B, Zhang YJ. Prognostic value of serum high-density lipoprotein cholesterol in patients with gallbladder cancer. *Rev Esp Enferm Dig.* 2019; 111:839-845.
 28. Shi Y, Fan Y, Hu Y, Jing J, Wang C, Wu Y, Geng Q, Dong X, Li E, Dong D. alpha-Mangostin suppresses the de novo lipogenesis and enhances the chemotherapeutic response to gemcitabine in gallbladder carcinoma cells via targeting the AMPK/SREBP1 cascades. *J Cell Mol Med.* 2020; 24:760-771.
 29. Bauerschlag DO, Maass N, Leonhardt P, Verburg FA, Pecks U, Zeppernick F, Morgenroth A, Mottaghay FM, Tolba R, Meinhold-Heerlein I, Brautigam K. Fatty acid synthase overexpression: target for therapy and reversal of chemoresistance in ovarian cancer. *J Transl Med.* 2015; 13:146.
 30. Ito T, Sato K, Maekawa H, Sakurada M, Orita H, Shimada K, Daida H, Wada R, Abe M, Hino O, Kajiyama Y. Elevated levels of serum fatty acid synthase in patients with gastric carcinoma. *Oncol Lett.* 2014; 7:616-620.
 31. Wang X, Tian J, Zhao Q, Yang N, Ying P, Peng X, Zou D, Zhu Y, Zhong R, Gao Y, Chang J, Miao X. Functional characterization of a low-frequency V1937I variant in FASN associated with susceptibility to esophageal squamous cell carcinoma. *Arch Toxicol.* 2020; 94:2039-2046.
 32. Guan M, Wu X, Chu P, Chow WA. Fatty acid synthase reprograms the epigenome in uterine leiomyosarcomas. *PLoS One.* 2017; 12:e0179692.
 33. Ventura R, Mordec K, Waszcuk J, Wang Z, Lai J, Fridlib M, Buckley D, Kemble G, Heuer TS. Inhibition of *de novo* palmitate synthesis by fatty acid synthase induces apoptosis in tumor cells by remodeling cell membranes, inhibiting signaling pathways, and reprogramming gene expression. *EBioMedicine.* 2015; 2:808-824.
 34. Lim SA, Wei J, Nguyen TM, Shi H, Su W, Palacios G, Dhungana Y, Chapman NM, Long L, Saravia J, Vogel P, Chi H. Lipid signalling enforces functional specialization of T(reg) cells in tumours. *Nature.* 2021; 591:306-311.
 35. Tadros S, Shukla SK, King RJ, Gunda V, Vernucci E, Abrego J, Chaika NV, Yu F, Lazenby AJ, Berim L, Grem J, Sasson AR, Singh PK. *De novo* lipid synthesis facilitates gemcitabine resistance through endoplasmic reticulum stress in pancreatic cancer. *Cancer Res.* 2017; 77:5503-5517.
 36. Wu D-m, Zhang T, Liu Y-b, Deng S-h, Han R, Liu T, Li J, Xu Y. The PAX6-ZEB2 axis promotes metastasis and cisplatin resistance in non-small cell lung cancer through PI3K/AKT signaling. *Cell Death Dis.* 2019; 10:349.
 37. Choi E, Kim E, Kim JH, Yoon K, Kim S, Lee J, Cho JY. AKT1-targeted proapoptotic activity of compound K in human breast cancer cells. *J Ginseng Res.* 2019; 43:692-698.
 38. Garcia-Aranda M, Perez-Ruiz E, Redondo M. Bcl-2 Inhibition to overcome resistance to chemo- and immunotherapy. *Int J Mol Sci.* 2018; 19:3950.
 39. Li CF, Fang FM, Chen YY, Liu TT, Chan TC, Yu SC, Chen LT, Huang HY. Overexpressed fatty acid synthase in gastrointestinal stromal tumors: Targeting a progression-associated metabolic driver enhances the antitumor effect of imatinib. *Clin Cancer Res.* 2017; 23:4908-4918.

Received June 7, 2023; Revised August 23, 2023; Accepted September 13, 2023.

[§]These authors contributed equally to this work.

*Address correspondence to:

Fei Ma, Department of Oncology, Xinhua Hospital Affiliated to Shanghai Jiao Tong University School of Medicine, No. 1665 Kongjiang Road, Shanghai 200092, China.
E-mail: mafei@xinhuamed.com.cn

Shouhua Wang, Department of General Surgery, Xinhua Hospital Affiliated to Shanghai Jiao Tong University School of Medicine, No. 1665 Kongjiang Road, Shanghai 200092, China.
E-mail: wshlife1987@126.com

Released online in J-STAGE as advance publication September 22, 2023.

Efficacy of *Andrographis paniculata* spray in acute pharyngitis: A randomized controlled trial

Risa Okonogi¹, Vich Thampanya², Siriporn Okonogi^{3,4,*}

¹ Department of Otorhinolaryngology, Chiang Rai Prachanukroh Hospital, Chiang Rai, Thailand;

² Department of Internal Medicine, Chiang Rai Prachanukroh Hospital, Chiang Rai, Thailand;

³ Department of Pharmaceutical Sciences, Faculty of Pharmacy, Chiang Mai University, Chiang Mai, Thailand;

⁴ Center of Excellence in Pharmaceutical Nanotechnology, Chiang Mai University, Chiang Mai, Thailand.

SUMMARY Acute viral pharyngitis is a self-limited disease but the symptoms, a sore throat in particular, can affect one's quality of life. Medicine for symptom relief is the main treatment. Recently, many studies have shown that *Andrographis paniculata* was efficacious in treating many diseases, including upper respiratory infections. However, adverse reactions to systemic intake are a concern. Therefore, *A. paniculata* spray is intended to reduce systemic adverse reactions and provide patients with more comfort as its local use. This randomized, double-blind study enrolled 60 adult patients with acute viral pharyngitis. All patients were asked to score the severity of symptoms including a sore throat, difficulty swallowing, and coughing using an 11-point numeric rating scale from 0 to 10. A physical examination was performed to score the severity of erythematous and swollen mucosa using a 0-3 score (0 = no, 1 = mild, 2 = moderate, and 3 = severe). The patients were randomized to receive treatment with either an *A. paniculata* spray or a positive control chamomile spray. Results revealed a significant reduction in the severity of all signs and symptoms in both groups ($p < 0.05$). The duration of treatment response in the *A. paniculata* spray group was 1.9 ± 0.7 days compared to 2.5 ± 1.2 days in the chamomile spray group ($p = 0.049$). No adverse events were noted in either group. *A. paniculata* spray is safe and highly efficacious in treating acute viral pharyngitis and can reduce symptoms more rapidly than a positive control spray.

Keywords *Andrographis paniculata*, acute viral pharyngitis, sore throat, plant extract, spray

1. Introduction

Acute pharyngitis is the inflammation of the mucous membrane of the oropharynx located in the upper part of the respiratory system. It is mostly caused by viruses and bacteria (1). Other less common causes of pharyngitis are allergies, trauma, cancer, reflux, and certain toxins (2). Patients with acute pharyngitis have a sore throat, cough, and difficulty swallowing. The disease can progress rapidly and may cause severe throat edema leading to dyspnea and suffocation. In adults, approximately 80%-90% of pharyngitis cases are caused by viruses (3) and in children, up to about 95% of cases of an acute sore throat are associated with viral infection (4). This indicates that the primary cause of acute pharyngitis is viruses. Even though viral pharyngitis can self-resolve in less than a week (5), many patients suffer from a severe sore throat that affects their quality of life. Thus far, there are no specific drugs for the treatment of viral pharyngitis. However, antibiotics are sometimes

prescribed without being indicated. A point that must be emphasized is that excessive and inappropriate use of antibiotics can lead to the development of new resistant strains of microorganisms (6). Therefore, treatment or medication to relieve symptoms and avoid unnecessary use of antibiotics might be the best alternative. Many herbs have been used for centuries as remedies for human diseases. Recently, interest in searching for high efficacious and safe, new bioactive components from plants has increased. Many types of plants have been reported to have various pharmacological activities (7-9).

Andrographis paniculata, known as Fah Talay Jone (in Thai), is an annual herb in the family Acanthaceae. The plant is commonly found in many countries in Asia, and particularly India, China, and Thailand. It is one of the principal herbs in traditional medicinal remedies for the treatment of acute upper respiratory tract infection and diarrhea in India, China, and Thailand (10). It has been reported to have medicinal and pharmacological properties and to be effective for the treatment of various

diseases such as cancer, diabetes, high blood pressure, ulcer, leprosy, bronchitis, skin diseases, flatulence, colic, influenza, dysentery, dyspepsia, and malaria (11). The anti-inflammatory and antimicrobial activities of this plant have been reported (12,13). Its extract was prescribed in oral form to treat upper respiratory infections, including acute pharyngitis, during the coronavirus disease 2019 (COVID-19) pandemic (14). However, adverse reactions have been reported after systemic administration (15). Therefore, local administration using throat spray containing *A. paniculata* extract has been considered.

In many countries including Thailand, the herbal sprays that are commercially available are those containing chamomile extract. Due to its anti-inflammatory action, chamomile extract has been reported to relieve symptoms in patients with acute nasopharyngitis (16). Since the COVID-19 outbreak, the sprays have been used more widely and are in short supply. *A. paniculata* extract has therefore been put forward as a local herb that can help to relieve COVID-19 symptoms. To the extent known, no study has reported on *A. paniculata* extract spray to treat pharyngitis. Therefore, this pilot study was conducted with the aim of highlighting the first ever report on the efficacy of *A. paniculata* spray in acute pharyngitis. The clinical effectiveness and safety of *A. paniculata* spray in relieving symptoms of acute pharyngitis were investigated in comparison to chamomile spray.

2. Materials and Methods

2.1. Materials

A. paniculata extract was kindly provided by the Chao Phya Abhaibhubejhr Hospital Foundation, Prachinburi Province, Thailand. All chemicals and solvents used were of the highest pharmaceutical grade available. A commercial herbal spray containing mainly 37% chamomile extract, namely chamomile spray, was used as a positive control and purchased from a drug store in Thailand.

2.2. Preparation of *A. paniculata* spray

A. paniculata spray was prepared by the Chao Phraya Abhaibhubejhr Hospital Foundation using a cosolvent method. The formula contains 0.3% of *A. paniculata* extract, glycerine, ethanol, and flavoring agents. The mixture was gently mixed until a homogeneous solution formed. The resulting solution was adjusted to volume with sterile water and gently shaken to avoid air bubbles. The final solution was transferred into a light-protected container with a spray nozzle.

2.3. Study design and sample size

This study was approved by Chiang Rai Prachanukroh

Hospital's Ethics Committee in Human Research (No. CR 0033.102/EC.66-025). All study procedures were in accordance with the provisions of the Declaration of Helsinki. The study protocol was registered with the Thai Clinical Trials Registry (TCTR 20230915005).

A randomized, double-blind study was conducted by the Department of Otolaryngology at Chiang Rai Prachanukroh Hospital in Thailand from February 1 to April 30, 2023. Sample sizes were calculated using the ANCOVA method and based on a previous study (17). The estimated sample sizes for two groups with repeated measures were used. From this calculation, the sample size (*n*) with an alpha error of 5% and a power of 80% is 28 patients/group. To compensate for unexpected loss during follow-up, 30 patients were included in each group. Therefore, a total of 60 patients were recruited.

2.4. Participant selection and eligibility criteria

Adult patients (aged from 18 years old) treated at Chiang Rai Hospital with an acute sore throat for less than 4 days were enrolled. Patients with a pain score greater than 5 out of 10 and a diagnosis of acute pharyngitis confirmed by an otolaryngologist were included in this study. The exclusion criteria were a positive COVID-19 test, a history of allergies, intolerance or sensitivity to any of the study medications, pregnant or lactating women, and patients who had taken antibiotics or corticosteroids less than 14 days prior.

2.5. Randomization and blinding

The patients in each group were randomized using a computer-generated blocked randomization schedule. Both groups received throat spray bottles and were blinded to treatment. Both sprays were packaged in bottles with the same appearance labeled as either A or B. Codes A and B were announced as either *A. paniculata* spray or chamomile spray after the end of the study analysis.

2.6. Study assessment

On the first day of study participation (day 0), the patients were asked to rate the severity of their symptoms, including a sore throat, difficulty swallowing, and coughing using an 11-point numeric rating scale from 0 to 10 (0 = no symptoms and 10 = the worst symptom that you can imagine). An otolaryngologist then performed a physical examination to assess the throat mucosa and score the severity of erythema of the pharyngeal mucosa (0 = no, 1 = mild, 2 = moderate, and 3 = severe erythema) and swelling of the pharyngeal mucosa (0 = no, 1 = mild, 2 = moderate and 3 = severe swelling). After the history was taken and a physical examination was performed, the patients were advised to spray the throat 2 spritzes/time and 3 times a day for

5 days. Symptoms were assessed for another 5 days (day 1 to day 5 = 1 to 5 days after using the sprays). The patients were asked to record the severity of their daily symptoms. These included a sore throat, difficulty swallowing, and coughing on an 11-point numeric rating scale from 0 to 10. A 20% or greater reduction in symptoms from the pretreatment score was considered acceptable (18). In addition, the patients were examined twice by an otolaryngologist on day 3 and day 5 of the study. All patients were asked to score their satisfaction with the received spray at the end of day 5.

2.7. Safety assessment

Adverse events were monitored throughout the study. All participants were asked to promptly report any severe adverse events or adverse reactions that occurred. They would then be asked to discontinue the study and receive immediate medical treatment from an expert physician.

2.8. Statistical analysis

Baseline demographic characteristics were described using descriptive statistics. Scores from the numeric rating scale and evaluations of the pharyngeal mucosa

were expressed as the mean \pm S.D. Differences between groups were assessed using the Chi-squared test for categorical variables and the Mann-Whitney *U* test for continuous variables. The level of statistical significance was set at $p < 0.05$.

3. Results and Discussion

The aim of the current study was to investigate the efficacy of the developed throat spray containing an extract of *A. paniculata* in patients with acute viral pharyngitis. A commercial herbal spray, namely chamomile spray, was used as a positive control. Although acute viral pharyngitis can resolve by itself, supportive treatment is also an important option for relieving a sore throat (5). Many studies have proven that *A. paniculata* extract has the potential to inhibit inflammation of the upper respiratory tract (URI) including pharyngitis (19,20). However, some systemic adverse effects, e.g., induction of acute renal injury (15) and gastrointestinal disorders (21) after parenteral and oral administration, have been reported. In the current study, local administration of the developed *A. paniculata* spray was used to reduce systemic adverse reactions. A total of 60 patients were enrolled and remained in the

Table 1. Patient demographics and clinical characteristics

Items	<i>A. paniculata</i> spray		Chamomile spray		<i>p</i> -value
	n	%	n	%	
Gender					0.596
Female	17	56.67	20	66.67	
Male	13	43.33	10	33.33	
Age (years)		42.6 \pm 13.9*		44.1 \pm 15.2*	0.685
Occupation					0.638
None	2	6.67	0	0.00	
Government employee	5	16.67	6	20.00	
Office worker	3	10.00	4	13.33	
Company employee	2	6.67	2	6.67	
Farmer	1	3.33	4	13.33	
Nurse	2	6.67	2	6.67	
Housewife	3	10.00	6	20.00	
Freelance	8	26.67	4	13.33	
Other	4	13.33	2	6.67	
Underlying illness	16	53.33	3	36.67	0.299
Currently using medication	12	40.00	9	30.00	0.589
Duration of sore throat (days)		2.4 \pm 1.1*		2.6 \pm 0.9*	0.508
Difficulty swallowing	21	70.00	25	83.33	0.360
Cough	22	73.33	26	86.67	0.333
Fever	1	3.33	3	10.00	0.612
Headache	3	10.00	3	10.00	1.000
Hoarseness	6	20.00	7	23.33	1.000
Dyspnea	1	3.33	0	0.00	1.000
Nasal congestion/rhinorrhea	13	43.33	17	56.67	0.439
Otalgia	1	3.33	1	3.33	1.000
Throat soreness score (0-10)		5.7 \pm 0.9*		6.5 \pm 1.7*	0.148
Difficulty swallowing scale (0-10)		4.6 \pm 1.9*		5.5 \pm 2.1*	0.202
Cough severity (VAS 0-10)		4.0 \pm 3.0*		5.1 \pm 2.7*	0.065
Body temperature (°C)		36.41 \pm 0.17*		36.42 \pm 0.24*	0.759
Erythematous of the pharynx (0-3)		2.4 \pm 0.7*		2.3 \pm 0.7*	0.469
Swollen mucosa of the pharynx (0-3)		2.0 \pm 0.5*		2.1 \pm 0.6*	0.812

* Data express the mean \pm S.D.

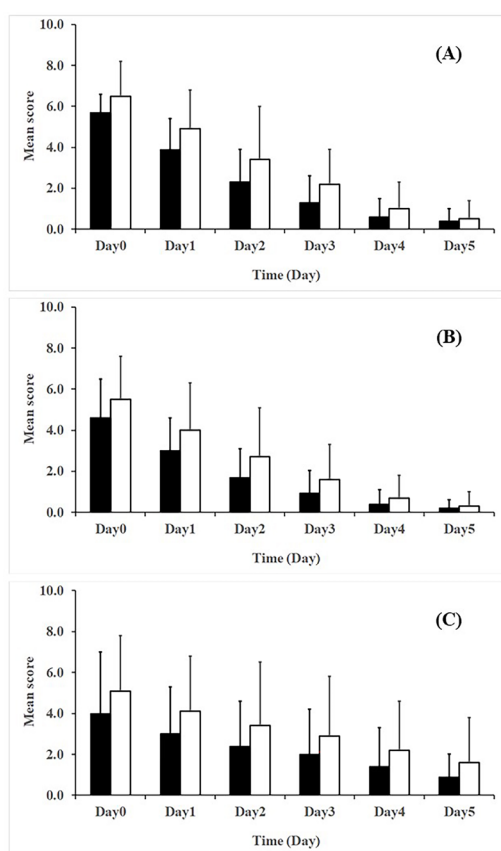


Figure 1. Mean score for the severity, as determined by patients using an 11-point numeric rating scale from 0 to 10, of throat pain (A), difficulty swallowing (B), and coughing (C) after using *A. paniculata* spray (black column) and chamomile spray (white column).

final analysis (*A. paniculata* spray: $n = 30$, chamomile spray: $n = 30$). The two groups did not differ in baseline demographics and clinical characteristics as shown in Table 1. The mean duration of the clinical sore throat was 2.4 days in the *A. paniculata* spray group and 2.6 days in chamomile spray group. Common comorbid symptoms for each group were difficulty swallowing and coughing. The baseline signs and symptoms of pharyngeal inflammation did not differ significantly between the two groups.

Results indicated that the severity of a sore throat, difficulty swallowing, and coughing decreased significantly from day 1 after use of the spray in both groups and the score continued to decrease to nearly 0 at the end of the assessment as shown in Figure 1. The percentage of responders on day 1 was 80% in the *A. paniculata* spray group and 66.7% in the chamomile spray group. The mean (\pm SD) of the response duration was 1.9 (\pm 0.7) days and 2.5 (\pm 1.2) days in the *A. paniculata* spray group and chamomile spray groups, respectively ($p = 0.049$). Twenty-two patients in each group (73.3%) had no sore throat (score = 0) at the end of the study. The mean (\pm SD) duration to absence of pain was 3.4 (\pm 1.1) days and 3.7 (\pm 1.1) days in the *A. paniculata* spray and chamomile spray groups,

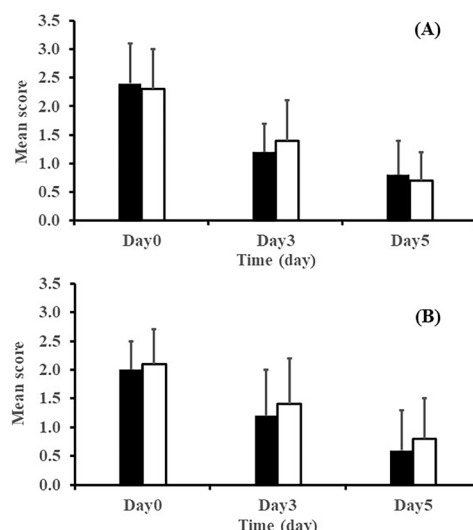


Figure 2. Mean score for the severity, as determined by otolaryngologists, of erythema (A) and swelling (B) of the pharyngeal mucosa after using *A. paniculata* spray (black column) and chamomile spray (white column).

respectively ($p = 0.468$). There was no difference in the overall satisfaction of using sprays between the two groups. In addition, there were no adverse events during this study. Other assessments scored by an otolaryngologist including erythema and swelling of the pharyngeal mucosa also decreased significantly in both groups as shown in Figure 2. Daily symptom scores between the two groups were compared, revealing no statistical difference.

The current results indicate that the sprays significantly alleviated clinical symptoms. Most patients were pain-free after less than 5 days of using the sprays, while the disease resolved on its own within 10 days. The duration to becoming pain-free did not differ between groups, but the duration of a clinical response differed. The *A. paniculata* group had a slightly faster recovery than the chamomile group. The current results on the effectiveness of an *A. paniculata* spray in reducing the severity of a sore throat are consistent with those reported by other studies involving *A. paniculata* in tablet form (22-24). However, the use of tablets results in significantly more adverse reactions than a topical spray. Adverse effects from an *A. paniculata* extract as reported earlier were mostly mild gastrointestinal symptoms such as constipation, nausea, vomiting, diarrhea, or dyspeptic symptoms (25). In contrast, there were no adverse events during the current study. This confirms that that topical application of an *A. paniculata* spray can be highly efficacious without causing systemic adverse reactions and that the study objective was achieved. The *A. paniculata* spray had anti-inflammatory action in terms of reducing pain without causing adverse reactions in this study, but the medicine should only be recommended when appropriate as determined by a physician.

Most patients were similarly satisfied with each

spray, but some participants mentioned the intense taste of the *A. paniculata* spray. Patients complaining about the taste of pharmaceutical products is one of the most important problems. *A. paniculata* is known as the king of bitters (11), so a challenge for further development is to use pharmaceutical technology to mask or minimize the bitter taste of an *A. paniculata* spray while maintaining its powerful anti-inflammatory action. In addition, the current work is a pilot study. The sample size for this study was calculated based on previous studies, assuming similar efficiency of the spray. Further studies with larger populations will help with the use of an *A. paniculata* spray in the future.

4. Conclusion

The current study yielded positive results with an *A. paniculata* spray that can be used as an alternative treatment to relieve the symptoms of pharyngitis while causing fewer systemic adverse reactions. It is a safe and convenient form of administration that capitalizes on the beneficial properties of Asian herbs. It has anti-inflammatory action in patients with acute viral pharyngitis. It can effectively relieve symptoms faster than a chamomile extract spray.

Acknowledgements

The authors wish to thank Chao Phraya Abhaibhubejhr Hospital for its financial support. The authors would also like to thank Dr. Patchara Ruangwongroj from the Department of Rehabilitation Medicine in Chiang Rai Prachanukroh Hospital for her advice on statistical analysis. The authors would also like to thank the Center of Excellence in Pharmaceutical Nanotechnology, Chiang Mai University, for the extent of its support.

Funding: None.

Conflict of Interest: The authors have no conflicts of interest to disclose.

References

- McMillan JA, Sandstrom C, Weiner LB, Forbes BA, Woods M, Howard T, Poe L, Keller K, Corwin RM, Winkelman JW. Viral and bacterial organisms associated with acute pharyngitis in a school-aged population. *J Pediatr.* 1986; 109:747-752.
- Alzahrani M, Maneno M, Daftary M, Wingate L, Ettienne E. Factors associated with prescribing broad-spectrum antibiotics for children with upper respiratory tract infections in ambulatory care settings. *Clin Med Insights Pediatr.* 2018; 12:1-8.
- Bisno AL. Primary care: Acute pharyngitis. *N Engl J Med.* 2001; 344:205-211.
- Brook I. Microbiology of common infections in the upper respiratory tract. *Prim Care.* 1998; 25:633-648.
- Wilson A. Pharyngitis. In: *Essential Infectious Disease Topics for Primary Care* (Skolnik NS, Albert RH, eds.). Humana Press, Totowa, NJ, 2008. pp. 15-24.
- Goossens H, Ferech M, Stichele R, Ellseviers M. Outpatient antibiotic use in Europe and association with resistance: A cross-national database study. *Lancet.* 2005; 365:579-587.
- Okonogi S, Kheawfu K, Holzer W, Unger FM, Viernstein H, Mueller M. Anti-inflammatory effects of compounds from *Polygonum odoratum*. *Nat Prod Commun.* 2016; 11:1651-1654.
- Suwant Wanachantararak P, Khongkhunthian S, Okonogi S. Antioxidant activity and potential of *Caesalpinia sappan* aqueous extract on synthesis of silver nanoparticles. *Drug Discov Ther.* 2018; 12:259-266.
- Okonogi S, Prakatthagomol W, Ampasavate C, Klayraung S. Killing kinetics and bactericidal mechanism of action of *Alpinia galanga* on food borne bacteria. *African J Microbiol Res.* 2011; 5:2847-2854.
- Banerjee S, Kar A, Mukherjee PK, Haldar PK, Sharma N, Katiyar CK. Immunoprotective potential of Ayurvedic herb Kalmegh (*Andrographis paniculata*) against respiratory viral infections – LC-MS/MS and network pharmacology analysis. *Phytochem Anal.* 2021; 32:629-639.
- Okhuaro A, Ehizogie Falodun J, Erharuyi O, Imieje V, Falodun A, Langer P. Harnessing the medicinal properties of *Andrographis paniculata* for diseases and beyond: A review of its phytochemistry and pharmacology. *Asian Pacific J Trop Dis.* 2014; 4:213-222.
- Zou W, Xiao Z, Wen X, Luo J, Chen S, Cheng Z, Xiang D, Hu J, He J. The anti-inflammatory effect of *Andrographis paniculata* (Burm. f.) Nees on pelvic inflammatory disease in rats through down-regulation of the NF-KB pathway. *BMC Complement Altern Med.* 2016; 16:483.
- Mishra PK, Singh RK, Gupta A, Chaturvedi A, Pandey R, Tiwari SP, Mohapatra TM. Antibacterial activity of *Andrographis paniculata* (Burm. f.) Wall ex Nees leaves against clinical pathogens. *J Pharm Res* 2013; 7:459-462.
- Chuthaputti A, Pornpatkul V, Suwankiri U. The efficacy of *Andrographis paniculata* (Burm. f.) Wall. ex Nees for the relief of the symptoms of influenza. *J Thai Tradit Altern Med.* 2007; 5:257-266.
- Zhang W, Zhang Z, Zhang Z, Wang Y, Zhou W. Andrographolide induced acute kidney injury: Analysis of 26 cases reported in Chinese literature. *Nephrol.* 2014; 19:21-26.
- Srivastava JK, Shankar E, Gupta S. Chamomile: A herbal medicine of the past with a bright future (review). *Mol Med Rep.* 2010; 3:895-901.
- Russo M, Bloch M, Looze F De, Morris C, Shephard A. Flurbiprofen microgranules for relief of sore throat: A randomised, double-blind trial. *Br J Gen Pract.* 2013; 63:149-155.
- Schachtel B, Aspley S, Shephard A, Shea T, Smith G, Schachtel E. Utility of the sore throat pain model in a multiple-dose assessment of the acute analgesic flurbiprofen: A randomized controlled study. *Trials.* 2014; 15:20-21.
- Coon JT, Ernst E. *Andrographis paniculata* in the treatment of upper respiratory tract infections: A systematic review of safety and efficacy. *Planta Med.* 2004; 70:293-298.
- Hu XY, Wu RH, Logue M, Blondel C, Lai LYW, Stuart B, Flower A, Fei YT, Moore M, Sheherd J, Liu JP, Lewith GT. Correction: *Andrographis paniculata* (Chuān Xīn Lián) for symptomatic relief of acute respiratory tract

- infections in adults and children: A systematic review and metaanalysis. PLoS ONE. 2018; 13:e0207713.
21. Saxena RC, Singh R, Kumar P, Yadav SC, Negi MPS, Saxena VS, Joshua AJ, Vijayabalaji V, Goudar KS, Venkateshwarlu K, Agarwal A. A randomized double blind placebo controlled clinical evaluation of extract of *Andrographis paniculata* (KalmColdTM) in patients with uncomplicated upper respiratory tract infection. Phytomedicine. 2010; 17:178-185.
22. Melchior J, Spasov AA, Ostrovskij OV, Bulanov AE, Wikman G. Double-blind, placebo-controlled pilot and phase III study of activity of standardized *Andrographis paniculata* Herba Nees extract fixed combination (Kan jang) in the treatment of uncomplicated upper-respiratory tract infection. Phytomedicine. 2000; 7:341-350.
23. Gabrielian ES, Shukarian AK, Goukasova GI, Chandanian GL, Panossian AG, Wikman G, Wagner H. A double blind, placebo-controlled study of *Andrographis paniculata* fixed combination Kan Jang in the treatment of acute upper respiratory tract infections including sinusitis. Phytomedicine. 2002; 9:589-597.
24. Melchior J, Palm S, Wikman G. Controlled clinical study of standardized *Andrographis paniculata* extract in common cold — A pilot trial. Phytomedicine. 1997; 3:315-318.
25. Leelarasamee A, Suankratay C, Hunnangkul S, Udompunturak S, Krittayaphong R, Poonsrisawat J, Wongsakorn N, Ittipanitphong C, Sirimai S. The efficacy and safety of *Andrographis paniculata* extract for the treatment of acute nonspecific upper respiratory tract infections: A randomized double blind placebo controlled trial. J Med Assoc Thail. 2021; 104:1204-1213.

Received July 27, 2023; Revised September 16, 2023; Accepted September 21, 2023.

*Address correspondence to:

Siriporn Okonogi, Department of Pharmaceutical Sciences, Faculty of Pharmacy, Chiang Mai University, Chiang Mai, Thailand 50200.
E-mail: okng2000@gmail.com

Released online in J-STAGE as advance publication October 11, 2023.

Hypofibrinolytic phenotype in Tsumura Suzuki Obese Diabetes (TSOD) mice unrelated to hyperglycemia

Naoki Ohkura^{1,*}, Ryo Morimoto-Kamata¹, Yuichi Kamikubo², Yoshihisa Takahashi³, Katsutaka Oishi^{4,5,6}

¹ Laboratory of Host Defence, School of Pharma-Sciences, Teikyo University, Tokyo, Japan;

² Thrombo Translational Research Lab Inc., Kumamoto University Cooperation Incubator, Minami-Kumamoto, Kumamoto, Japan;

³ Department of Pathology, School of Medicine, International University of Health and Welfare, Narita, Japan;

⁴ Healthy Food Science Research Group, Cellular and Molecular Biotechnology Research Institute, National Institute of Advanced Industrial Science and Technology (AIST), Ibaraki, Japan;

⁵ Department of Applied Biological Science, Graduate School of Science and Technology, Tokyo University of Science, Noda, Chiba, Japan;

⁶ Department of Computational Biology and Medical Sciences, Graduate School of Frontier Sciences, The University of Tokyo, Kashiwa, Chiba, Japan.

SUMMARY Obesity and diabetes mellitus are associated with increased risk of arterial thrombosis and venous thromboembolism. Tsumura Suzuki Obese Diabetes (TSOD) mice are useful models for elucidating the molecular mechanisms of these diseases. We investigated normoglycemic [Ng]-TSOD mice with a metabolic abnormality that was accompanied by a coagulative and fibrinolytic state with a phenotype that distinctly differed from that of standard TSOD mice. As in TSOD mice, plasminogen activation inhibitor-1 (PAI-1) that inhibits fibrinolysis was substantially augmented in Ng-TSOD mice, suggesting that they are hypofibrinolytic. However, blood clotting parameters were within the normal range in Ng-TSOD mice. These findings indicated that Ng-TSOD mice are novel models with a hypofibrinolytic phenotype that is not associated with hyperglycemia.

Keywords type 2 diabetes, plasma, obesity, coagulation, hypofibrinolytic state

1. Introduction

Obesity and diabetes are significant risk factors for the development of cardiac diseases, arterial thrombosis and venous thromboembolism. The status of these illnesses can be determined as altered levels of blood lipids, adipocytokines, coagulative, and fibrinolytic factors in plasma (1). Various mouse models of type 2 diabetes have contributed to current understanding of metabolic syndrome and its related diseases (2). The Tsumura Suzuki Obese Diabetes (TSOD) polygenic mouse model of spontaneous obese Type 2 diabetes mellitus (DM) is an inbred line in which males are obese and have urinary glucose, hyperglycemia, hyperinsulinemia, increased food intake, body and fat weight (3). Obesity and DM are associated with increased risk of arterial thrombosis and venous thromboembolism. Effectively preventing thrombotic complications requires better understanding of how prothrombotic states develop in patients with metabolic disorders. Significantly higher plasminogen activation inhibitor-1 (PAI-1) levels in prediabetic patients than in healthy persons might

function as predictors of progressive diabetes (4). Although animal models are useful for investigating mechanisms, detailed studies of pro-thrombotic and hypofibrinolytic states are hampered by a lack of appropriate prediabetic mouse models.

Here we evaluated metabolic, coagulative and fibrinolytic parameters in normoglycemic [Ng]-TSOD mice with a metabolic abnormality as well as coagulative and fibrinolytic states to determine whether they could function as prediabetic models.

2. Materials and Methods

2.1. Animals

Sixteen-week-old Male TSOD, TSOD with undetectable urinary sugar and normoglycemia (Ng-TSOD) and non-diabetic Tsumura Suzuki Non-Obesity (TSNO) mice (Institute of Animal Reproduction, Kasumigaura, Japan) were housed at $24 \pm 2^\circ\text{C}$ and provided with food and water *ad libitum* for one week. Casual blood glucose levels were measured using a StatStrip Express 900

(Siemens Healthineers, Munich, Germany). Urinary sugar was evaluated using Uropaper IIIG (Eiken Chemical Co., Ltd., Tokyo, Japan). Table 1 shows renal and blood glucose levels in 16-week-old TSOD and Ng-TSOD mice. Blood specimens were collected from the inferior vena cava of 17-week-old mice as described (5). The Animal Care and Use Committee at Teikyo University approved all experiments involving mice (Approval No: 15-046).

2.2. Measurements of biochemical parameters and blood coagulation and fibrinolytic factors

Levels of glucose, triglyceride, and total cholesterol, free fatty acid, total protein, albumin, phospholipids, aspartate aminotransferase (AST) and alanine aminotransferase (ALT), were determined using Biochemical Test Kits (Fujifilm Wako Chemicals, Osaka, Japan). Insulin,

adiponectin and leptin were measured using ELISA kits from their respective suppliers (Mercodia, Uppsala, Sweden, Otsuka Pharmaceutical Co., Ltd., Tokyo, Japan, and Morinaga Institute of Biological Science, Inc. Kanagawa, Japan). We analyzed tumor necrosis factor- α (TNF- α) and C-reactive protein (CRP) using the respective ELISA kits (Chondrex Inc., Woodinville, WA, USA and Assaypro, St. Charles, MO, USA).

Levels of PAI-1 antigen and active PAI-1 were measured using Total and Active Murine PAI-1 ELISA kits (Molecular Innovations Inc., Novi, MI, USA) with slight modification. Fibrinogen and antithrombin levels were measured using ELISA kits (Assaypro). Prothrombin and activated partial thrombin (APTT) times were measured using Thromborel S (Dade Behring, Liederbach, Germany) and APTT reagent (Sysmex, Kobe, Japan), respectively, as described with slight modification (5).

2.3. Statistics

Values are expressed as means \pm standard deviations (SD). Differences among the three groups were analyzed using one-way ANOVA followed by Tukey post-hoc multiple comparison tests.

3. Results and Discussion

Glucose levels were significantly lower in Ng-TSOD, than in TSOD ($p < 0.001$), but the same as those in TSNO mice (Figure 1A). Mean body weight was slightly, but significantly lower in Ng-TSOD, than in TSOD mice ($p < 0.01$; Figure 1B). Insulin levels were significantly elevated in TSOD and Ng-TSOD, compared with TSNO ($p < 0.005$; $p < 0.01$), and those of Ng-TSOD and TSNO were indistinguishable (Figure 1C).

Figure 2 shows the plasma biochemical parameters in TSOD, Ng-TSOD and TSNO mice. Triglyceride levels were significantly lower in Ng-TSOD, than in TSOD mice ($p < 0.05$). Total cholesterol levels did not significantly differ between the Ng-TSOD and TSOD

Table 1. Body weight, blood and urinary glucose levels in TSOD and Ng-TSOD mice ($n = 6$ each)

Mouse no.	Body weight (g)	Blood glucose (mg/dL)	Urinary glucose
TSOD			
1	63.2	525	+
2	62.0	470	++
3	65.6	458	+
4	64.5	501	++
5	60.3	451	+
6	64.0	477	++
Average \pm SD	63.1 \pm 1.9	480 \pm 21	
Ng-TSOD			
1	58.1	203	-
2	56.1	183	-
3	55.8	188	-
4	58.2	175	-
5	48.7	168	-
6	57.6	172	-
Average \pm SD	55.8 \pm 3.6	182 \pm 13	

Glucose in blood from tail veins was measured using StatStrip Express 900 blood glucose meter (Nova Biochemical Corp., Waltham, MA, USA). Urinary glucose was measured using Uropaper III (Eiken Chemical Co., Ltd., Tokyo, Japan). -, undetectable; +, 500 mg/dL; ++, 2,000 mg/dL.

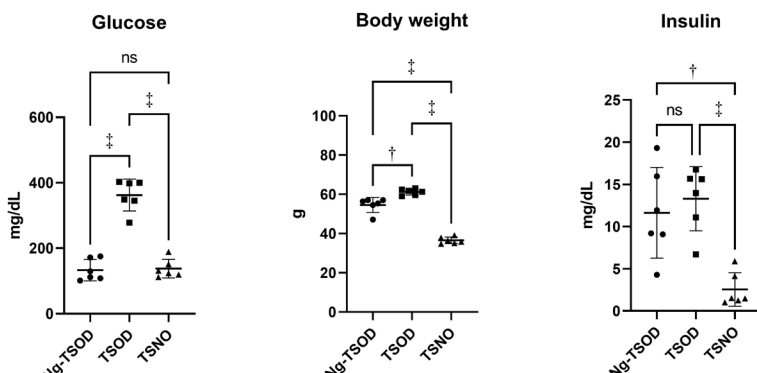


Figure 1. Body weight, glucose and insulin levels in Ng-TSOD, TSOD and TSNO mice ($n = 6$ each). Data are shown as means \pm standard deviation (SD). Significantly different at * $p < 0.01$, † $p < 0.005$, ‡ $p < 0.001$.

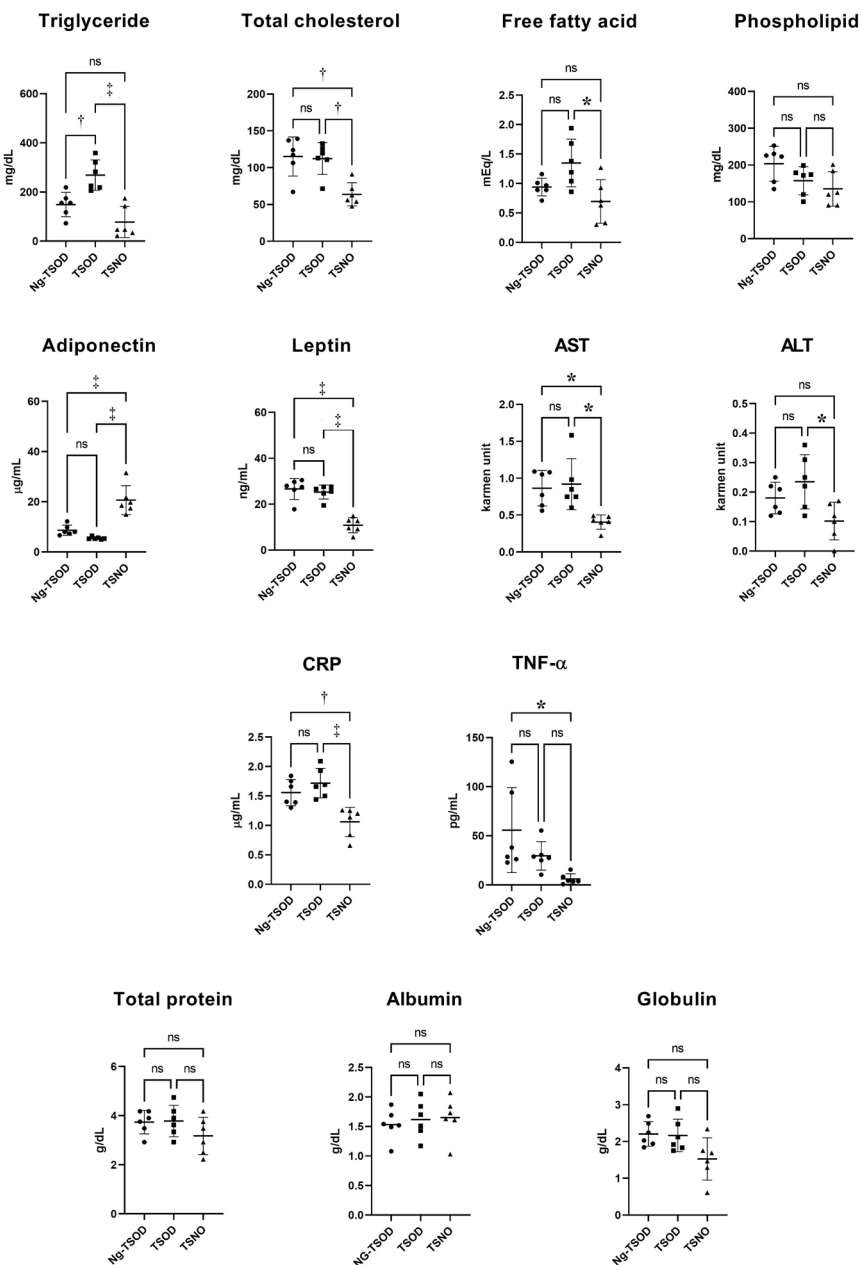


Figure 2. Plasma biochemical parameters in TSOD, Ng-TSOD and TSNO mice ($n = 6$ each). Data are shown as means \pm standard deviation (SD). Significant differences at $*p < 0.05$, $†p < 0.005$, $‡p < 0.001$.

mice, but both were significantly higher than in TSNO mice ($p < 0.01$ for both). Levels of free fatty acids did not significantly differ between Ng-TSOD and TSOD mice, and neither did adiponectin levels, both of which were significantly lower than in TSNO mice ($p < 0.001$ for both). Leptin levels did not significantly differ between Ng-TSOD and TSOD mice, but both were significantly higher than that in TSNO mice ($p < 0.001$ for both). Levels of AST did not significantly differ between Ng-TSOD and TSOD mice, but both were significantly higher than in TSNO mice ($p < 0.01$; $p < 0.01$). Levels of ALT did not significantly differ between Ng-TSOD and TSOD mice, but were significantly higher in TSOD, than in TSNO mice ($p < 0.05$) and similar between Ng-TSOD and TSNO mice. Levels of

CRP did not significantly differ between Ng-TSOD and TSOD mice, but both were significantly higher than in TSNO mice ($p < 0.01$ for both). Values for TNF- α did not significantly differ between Ng-TSOD and TSOD mice, but both were significantly higher than in TSNO mice. Total protein, albumin, globulin and PL did not significantly differ among all three groups.

Figure 3 shows values for coagulation parameters that are usually measured in humans at clinical laboratories and PAI-1 in TSOD, Ng-TSOD, and TSNO mice. Levels of PAI-1 and active PAI-1 were significantly higher in Ng-TSOD and TSOD, than in TSNO mice ($p < 0.005$ and $p < 0.05$, respectively), but the difference between Ng-TSOD and TSOD mice did not reach significance. Plasminogen levels

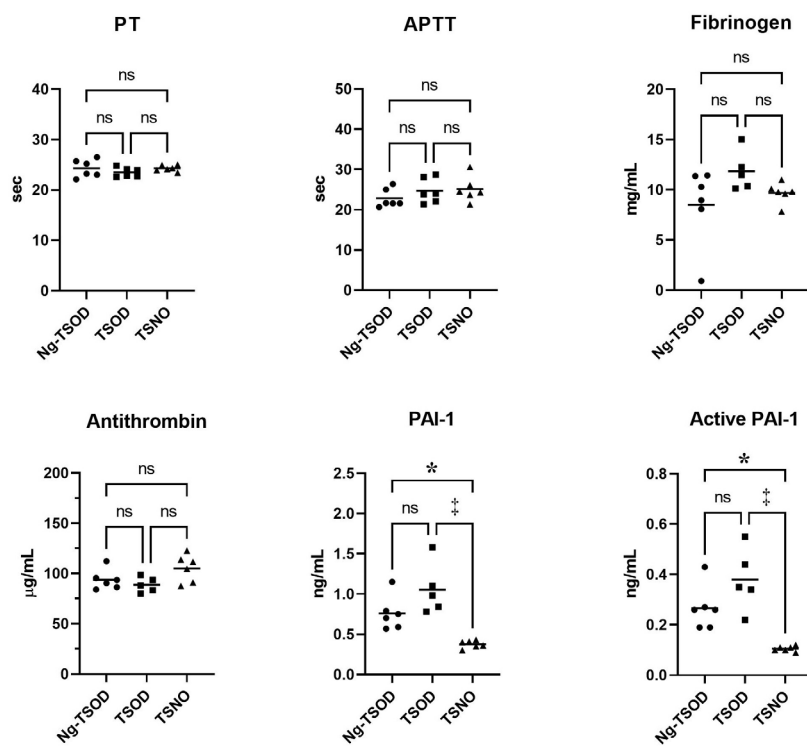


Figure 3. Plasma coagulation and fibrinolytic parameters in TSOD, Ng-TSOD and TSNO mice ($n = 6$ each). Data are shown as means \pm standard deviation (SD). Significantly different at $*p < 0.05$, $^{\dagger}p < 0.005$, $^{\ddagger}p < 0.001$.

were significantly lower and higher in Ng-TSOD, than in TSOD ($p < 0.01$) and TSNO mice ($p < 0.05$), respectively. None of prothrombin, APTT, fibrinogen and antithrombin significantly differed among the three groups.

We found that levels of insulin and body weight were significantly increased in Ng-TSOD, compared with TSNO mice, but were the same between Ng-TSOD and TSOD mice. In contrast, glucose levels were the same between Ng-TSOD and TSNO mice. We also identified levels of adiponectin, leptin and CRP in Ng-TSOD and TSOD mice, which are abnormal in nascent metabolic syndrome in humans (6). The genetics of Ng-TSOD and normal TSOD mice might differ because TSOD mouse models of multifactorial genetic diseases spontaneously develop various metabolic diseases (3,7).

Patients with diabetes are likely to develop thrombophilia due to abnormal blood coagulation and fibrinolytic factors (8). The primary inhibitor of tissue-type plasminogen activator (tPA) in plasma is PAI-1, which plays a key role in fibrinolysis (9). Increased PAI-1 is one of the main coagulation abnormalities associated with obesity and diabetes (9). Many factors such as insulin, glucose, lipids affect increases in blood PAI-1 activities in patients with diabetes (10). The present study found the same levels of total PAI-1 and active plasma PAI-1 that reflect PAI-1 activity in Ng-TSOD and TSOD mice. Nonetheless, blood clotting parameters in Ng-TSOD mice were within the normal range. Although blood glucose levels might increase

with advancing age in this phenotype, these mice could serve as models of hypofibrinolysis unrelated to hyperglycemia at least until they reach the age of ~ 17 weeks.

In conclusion, we found that PAI-1 was substantially augmented in Ng-TSOD, as in TSOD mice. This finding suggested that Ng-TSOD mice are hypofibrinolytic and that Ng-TSOD mice might be novel models that could provide insight into the association of prediabetes with hypofibrinolytic states. We believe that Ng-TSOD mice have potential applications for investigating the diagnosis and treatment of prediabetes.

Acknowledgements

This study was supported in part by a Grant-in-aid from the Ministry of Education, Culture, Sports, Science and Technology of Japan (MEXT) 19K02339 (to N Ohkura).

Funding: None.

Conflict of Interest: The authors have no conflicts of interest to disclose.

References

- Samad F, Ruf W. Inflammation, obesity, and thrombosis. *Blood*. 2013; 122:3415-3422.
- Katsuda Y, Ohta T, Shinohara M, Bin T, Yamada T. Diabetic mouse models. *Open J Anim. Sci.* 2013; 3:334-342.

3. Suzuki W, Iizuka S, Tabuchi M, Funo S, Yanagisawa T, Kimura M, Sato T, Endo T, Kawamura H. A new mouse model of spontaneous diabetes derived from ddY strain. *Exp Anim.* 1999; 48:181-189.
4. Haffner SM. Insulin resistance, inflammation, and the prediabetic state. *Am J Cardiol.* 2003; 92:18J-26J.
5. Ohkura N, Oishi K, Fukushima N, Kasamatsu M, Atsumi GI, Ishida N, Horie S, Matsuda J. Circadian clock molecules CLOCK and CRYs modulate fibrinolytic activity by regulating the PAI-1 gene expression. *J Thromb Haemost.* 2006; 4:2478-2485.
6. Bremer AA, Jialal I. Adipose tissue dysfunction in nascent metabolic syndrome. *J Obes.* 2013; 2013:393192.
7. Hirayama I, Yi Z, Izumi S, Arai I, Suzuki W, Nagamachi Y, Kuwano H, Takeuchi T, Izumi T. Genetic analysis of obese diabetes in the TSOD mouse. *Diabetes.* 1999; 48:1183-1191.
8. Sobczak AI, Stewart AJ. Coagulatory defects in type-1 and type-2 diabetes. *Int J Mol Sci.* 2019; 20:6345.
9. Taeye BD, Smith LH, Vaughan DE. Plasminogen activator inhibitor-1: A common denominator in obesity, diabetes and cardiovascular disease. *Curr Opin Pharmacol.* 2005; 5: 149-154.
10. Van De Craen B, Declerck PJ, Gils A. The biochemistry, physiology and pathological roles of PAI-1 and the requirements for PAI-1 inhibition *in vivo*. *Thromb Res.* 2012; 130:576-585.

Received August 22, 2023; Revised October 7, 2023;
Accepted October 8, 2023.

*Address correspondence to:

Naoki Ohkura, Laboratory of Host Defence, School of Pharma-Sciences, Teikyo University, 2-11-1 Kaga, Itabashi, Tokyo 173-8605, Japan.
E-mail: n-ohkura@pharm.teikyo-u.ac.jp

Released online in J-STAGE as advance publication October 14, 2023.

Effectiveness of an artificial intelligence-based training and monitoring system in prevention of nosocomial infections: A pilot study of hospital-based data

Ting Huang^{1,§}, Yue Ma^{1,§}, Shaxi Li^{1,§}, Jianchao Ran¹, Yifan Xu¹, Tetsuya Asakawa^{2,*}, Hongzhou Lu^{2,3,*}

¹ Department of Healthcare-associated Infection Management, National Clinical Research Center for Infectious Diseases, the Third People's Hospital of Shenzhen, Shenzhen, Guangdong, China;

² Institute of Neurology, National Clinical Research Center for Infectious Diseases, the Third People's Hospital of Shenzhen, Shenzhen, Guangdong, China;

³ Department of Infectious Diseases, National Clinical Research Center for Infectious Diseases, the Third People's Hospital of Shenzhen, Shenzhen, Guangdong, China.

SUMMARY This work describes a novel artificial intelligence-based training and monitoring system (AITMS) that was used to control and prevent nosocomial infections (NIs) by improving the skills of donning/removing personal protective equipment (PPE). The AITMS has two working modes, namely an AI-based protective equipment surveillance mode and an AI-based training mode, that were used for routine surveillance and training, respectively. Data revealed that the accuracy rate of donning/removing PPE improved as a result of the AITMS. Interestingly, the frequency of NIs decreased with the use of the AITMS. This study suggested the key role of using PPE in controlling and preventing NIs. Data preliminarily proved that appropriate donning/removing PPE may help to reduce the risk of NIs. In addition, the newest computerized technologies, such as AI, have proven to be useful in controlling and preventing NIs. These findings should helpful to formulate a better strategy against NIs in the future.

Keywords artificial intelligence, nosocomial infection, surveillance, training, artificial intelligence-based training and monitoring system (AITMS)

1. Introduction

The term "nosocomial infections (NIs)" is used to describe all infections acquired in a hospital. NIs have several characteristics that differ from community-acquired infections: *i*) NIs are healthcare-associated infections that are acquired after hospitalization and that manifest 48 hours after admission (1). Due to their considerable impact on clinical outcomes, some authors have proposed that the period for NIs should be extended to within 30 days of hospital discharge or 90 days after undergoing surgery (2). *ii*) NIs can be systemic; common NIs are pneumonia (hospital-acquired or ventilator-associated), urinary tract infections (catheter-associated), surgical site infections, central line-associated bloodstream infections, and *Clostridium difficile* infections (3). *iii*) Patients, relatives of the patient, caregivers, and medical personnel may be involved. *iv*) NIs are often associated with medical interventions, such as surgery, medication,

or invasive examinations. *v*) NIs readily occur in departments dealing with critical illnesses, such as the transplantation unit, chemotherapy unit, burn unit, or intensive care unit. *vi*) NIs can often be monitored and dealt with. NIs have been the sixth leading cause of death in United States (2). As a notable but intervenable cause of death in the hospital, NIs are of great concerned to clinicians and governments around the world. Indeed, NIs are commonly problematic because most NI-related pathogens, be they bacteria (4) or fungi (5), have natural resistance to empirical antibiotics and thus cannot be treated with commonly used antibiotics. Moreover, most people who contract an NI are older, neonates, those who are immunocompromised, or those who are suffering from chronic diseases. The clinical outcomes and quality of life (QOL) of patients markedly worsen once they develop an NI. Fortunately, however, NIs can be dealt with and prevented since they are hospital-related infections. In line with World Health Organization guidelines, the incidence of NIs

can be reduced approximately 70% by satisfactory infection prevention and control programs (6). The vast majority of countries have set up surveillance and information sharing systems to fight against NIs (7). To the extent known, however, merely creating such systems without specifying their detailed operation in clinical practice might yield limited achievements in terms of reducing the frequency of NIs. Hence, many practical measures are taken to reduce the risk of NIs in routine clinical tasks, such as using personal protective equipment (PPE). PPE is used to reduce the exposure risk of medical personnel when they are treating infected patients or making contact with contaminated surfaces. Typical PPE commonly consists of gloves, goggles, a gown, a head cover, a face mask and respirator, shoe covers, and a face shield, which are regarded as a general safety precaution for infection prevention. The effectiveness of PPE is influenced by proper selection of PPE (selection of the type of mask, for example), appropriate usage of PPE (donning/removal), and proper disposal of PPE (8). Although recommendations regarding PPE are sometimes controversial, PPE is undoubtedly emphasized and recommended during pandemics involving infectious respiratory diseases. During the COVID-19 pandemic, all frontline medical personnel were required to know appropriate methods of using PPE in clinical settings. Nonetheless, appropriately donning/removing PPE is quite complex and is poorly understood by most new medical personnel. John *et al.* reported that only 39% of untrained medical students can select the correct sequence of donning/removing PPE (9). Wilder-Smith *et al.* reported only 34% of medical personnel could correctly use PPE (10). Mitchell *et al.* reported that inappropriate donning/removing PPE is a significant risk factor for development of NIs (11). Conversely, proper use of PPE may help to reduce NIs (12). A point worth noting is that during an infectious respiratory disease pandemic, and especially in the early stages of the pandemic, inappropriate use of PPE might be dangerous, or even life-threatening. Flaws in donning/removing PPE can cause pathogen transmission and lead to NIs (13). Accordingly, effective and evaluable training in using PPE is indispensable for medical personnel. The conventional centralized training model has many limitations, such as the time and effort it takes and limited efficiency, so it cannot ensure all trainees learn/understand proper skills of donning/removing PPE. In this regard, many optimized training models have been proposed, such as the information-motivation-behavioral skills (IMB) model. Recently, Song *et al.* used the IMB model to improve the skills of donning/removing PPE. They found that a group receiving an IMB model-based intervention had better performance in terms of self-efficacy and qualified usage of PPE among medical personnel during the COVID-19 pandemic (12). However, this model

also has limitations. Noticeably, the entire process of donning/removing PPE cannot be monitored and supervised in real time. Flaws in the process could not be identified and corrected in a timely manner. This might serve as a Trojan horse for NIs. To ensure all personnel can properly don/remove PPE both in training and also in clinical practice, the current authors developed a novel artificial intelligence-based training and monitoring system (AITMS). The aim was to develop a newer system that would help to improve the donning/removing of PPE and reduce the frequency of NIs, ultimately helping to improve the clinical outcomes and QOL of inpatients. The current pilot study was designed to verify the effectiveness of the AITMS in preventing NIs.

2. Materials and Methods

2.1. Components of the AITMS

The AITMS consists of a camera with a voice broadcasting feature, a backend administration system on the cloud, a smartphone app, and an AI-based surveillance/training terminal for donning/removing PPE and hand hygiene (these are denoted as "behaviors" in the following sections). The terminal consists of an AI on a local computer, along with a large screen (for displaying correct "behaviors" or serving as a human-computer interface) with voice packets (for voice guidance and error prompts) (Figure 1). The AITMS has two working modes, namely, AI-based protective equipment surveillance mode (AIPESM) and AI-based training mode (AITM), which can be simply selected via the smartphone app or the terminal (Figure 1). The AIPESM is used to monitor a member of medical staff's "behaviors" and detect flaws in practice, whereas the AITM is used to train personnel if they need training. The AITM can certainly be used to solely train new personnel.

2.2. Definition of "standardized target behaviors (STBs)"

STBs were defined as per China's Technical Guidelines on Prevention and Control of Novel Coronavirus Infection in Medical Institutions (third edition) (14), including 7 steps of donning and 15 steps of removing protective equipment.

2.3. Generation of a dataset

Data collection sites were established where medical personnel don/remove PPE. All the normative "behaviors" performed by a group of skilled personnel were recorded by a camera based on the Kinect technology. Every frame of the video was recorded and preprocessed. The size of the video frame was

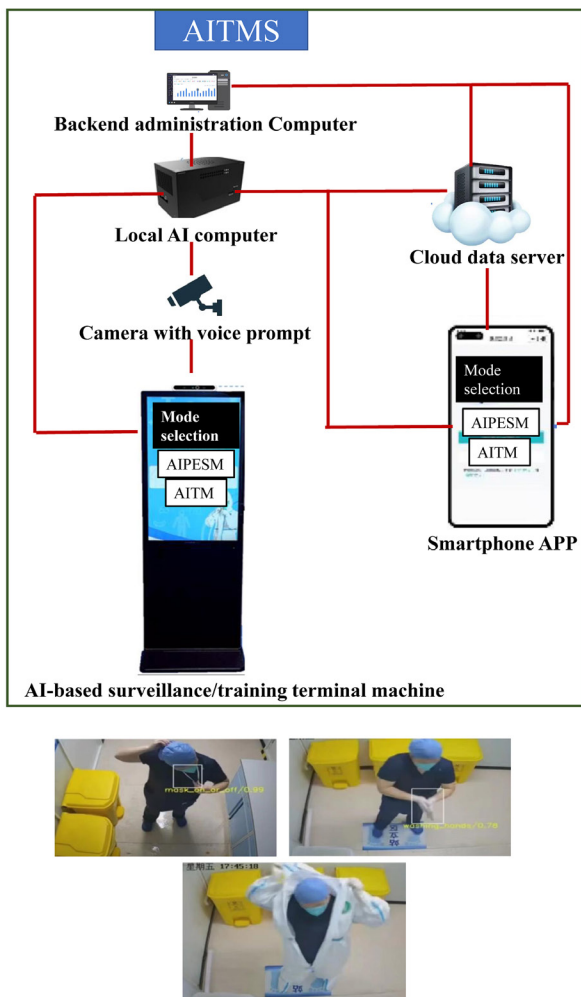


Figure 1. A diagram of the artificial intelligence-based training and monitoring system (AITMS). AI: Artificial intelligence; AITMS: artificial intelligence-based training and monitoring system; AIPESM: AI-based protective equipment surveillance mode; AITS: AI-based training mode (AITM); APP: application; PPE: personal protective equipment.

normalized. Then, the types of behaviors involved in donning/removing PPE and hand hygiene that need to be marked (target behaviors) and the marking rules were determined. Behaviors in all frames of preprocessed images were subsequently marked. The marked data were approved both by the AI and manually to avoid missing or wrong marks.

2.4. Training and creating an AI model to evaluate STBs in images with machine learning

After all of the images were marked, the system automatically identified marked images and label files, which were subsequently divided into a training set and a test set at a ratio of 9:1. The AI used the training set to train the model, and the model performance was checked using the test set. The models were continuously optimized by adjusting the parameters and tests. On the basis of the results of model testing,

samples were added when target behaviors or backgrounds were readily misdetected. These processes helped to improve the accuracy to reach the anticipated standard. Ultimately, an AI model to evaluate STBs in images was successfully created.

2.5. Application to actual processes

Once the data accuracy reached the standard, the AI model was applied to actual processes to make precise adjustments and to facilitate optimization. The system was used in locations where PPE is donned/removed. We ensured that all the "behaviors" of the testees (hand washing, donning/removing one's mask and protective suit, etc.) could be clearly detected. The current AI model to evaluate STBs in images had satisfactory accuracy, particularly at detecting the behaviors of donning/removing one's protective suit. In addition, this system enabled the AI model to improve its accuracy by continuous self-learning during actual use.

2.6. Scenarios for application

The AIPESM is activated to monitor clinical routine tasks of medical personnel. When medical personnel step into the designated area, he or she should don/ remove PPE and perform hand hygiene following the guidance of the voice prompt. The surveillance camera is activated and it performs real-time surveillance while the "behaviors" are performed. All the human postures and limb motion trajectories are captured and analyzed based on Kinect technology. All the "behaviors" of the testees are compared to the STBs in images evaluated by the AI model, including the sequence of behaviors, range, and angle. A "correct/incorrect" behavior is defined by the AI model according to its conformance to the STBs. Once an "incorrect behavior" occurs during the process, the camera captures this flaw and then submits it to the AI on the local computer. The AI system will judge whether this behavior is "incorrect". Once a flaw is confirmed, the system will remind the person to correct his or her behavior *via* the voice prompt. Only when a behavior is in line with the "STB" is it deemed to be a "correct behavior", and the person can continue with the process. If needed, experienced backend staff can also help personnel. Once a person is identified as needing training, he or she may choose to use the AITM. The required training course (donning a gown, for example) can be selected *via* the smartphone app. The theoretical knowledge and a video of the STB video will be displayed *via* the large screen to guide the person so that he or she can perform the "correct" behavior. The camera captures the person's movements during training, the system corrects his or her mistakes *via* the voice prompt, and it evaluates the person's performance during training. Other than in a clinical setting, the AITM can also

be used to train new personnel. Training, real-time evaluation/corrections, and administration of a final examination can be performed. Certificates will be issued along with the complete training files after the trainee passes the theoretical and practical exams. The files can be synchronized in the main computer and mobile terminal. Analysis of the obtained data will help to continuously optimize the training programs as well as the algorithms.

2.7. Data acquisition and analysis

The AITMS was introduced at this Hospital starting in February 2020. When surveillance started (from February 7, 2020 to February 13, 2022), none of the personnel had ever been trained by the AITMS. The accuracy rate automatically recorded by the system was recorded as the non-AITMS rate. From November 20 to 26, 2022, almost all of the personnel were trained with the AITHM. The accuracy rate at that time was recorded as the AITMS rate. Data on the frequency of NIs from 2019 to 2022 at this Hospital are available on the National Medical Institution Infection Surveillance System of China (<https://cniss.yygr.cn/>). The software SPSS (v24.0.0, IBM, USA) was used for statistical analysis. A chi-square test was used to compare rates. $p < 0.05$ was considered to be a statistically significant difference.

3. Results and Discussion

Figure 2A shows the accuracy rate before and after training with the AITMS. From February 7, 2020 to February 13, 2022, a total of 163 personnel had finished the evaluation, and their accuracy rate was 52.15% (85/163, non-AITMS rate). From November 20 to 26, 2022, the accuracy rate was 98.14% (3,159/3,219, AITMS rate). These data indicate that the accuracy rate of donning/removing PPE significantly increased as a result of using the AITMS (98.14% vs. 52.15%, $\chi^2 = 834.35$, $p < 0.001$). Indeed, after training with the AITMS, most of the medical personnel could properly don/remove PPE (Figure 2A). Interestingly, the frequency of NIs also decreased accordingly. As shown in Figure 2B, the frequency of NIs was 1.31% in 2019 and 1.39% in 2020 before use of the AITMS; after use of the AITMS, the frequency decreased sharply to 0.58% in 2021 and 0.38% in 2022. Hence, use of the AITMS helped to reduce the frequency of NIs even though the COVID-19 pandemic struck in 2021 and 2022.

This pilot study preliminarily verified the effectiveness of the AITMS. Use of the AITMS eventually reduced the frequency of NIs as the accuracy rate of donning/removing PPE improved. This study suggested the key role of using PPE in controlling and preventing NIs. Data preliminarily proved that appropriate donning/removing PPE may help to prevent the development of

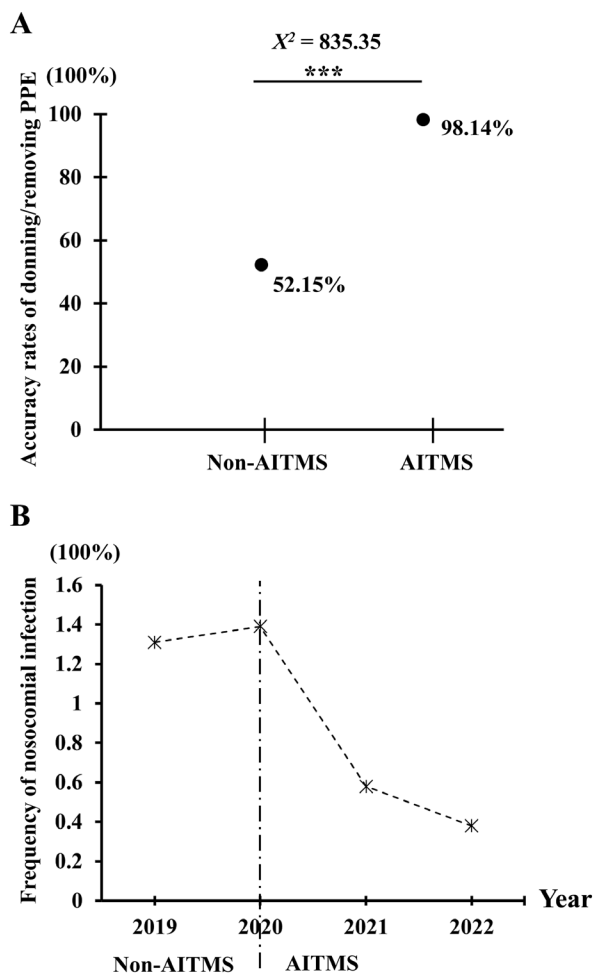


Figure 2. Effectiveness of using the AITMS. (A) Using the AITMS significantly improved the accuracy rate of donning/removing PPE. (B) Using the AITMS markedly reduced the frequency of NIs. The AITMS was not used during the two years on the left while it was used during the two years on the right. The decline in nosocomial infections is evident despite the COVID-19 pandemic in 2021 and 2022. AITMS: artificial intelligence-based training and monitoring system; PPE: personal protective equipment. *** means $p < 0.001$

NIs. In addition, the newest computerized technologies, such as AI, machine learning, big data, and mobile Internet (15), have proven to be useful in controlling and preventing NIs. The current results are in line with those of previous analogous studies (16,17). These findings should help to formulate a strategy against NIs in the future. In the future, more rigorous verification will be performed to provide robust evidence regarding use of the AITMS to reduce NIs.

Using AI-based technology to control and prevent NIs is a novel idea. Here, this novel AITMS has proven to be effective in both routine clinical practice and training. The two-mode design allows this system to be applied in multiple scenarios, such as routine surveillance, real-time correction of inappropriate "behaviors", timely training on demand, systematic training for new personnel, and evaluation and examination of trainees. Using this AI-based system

markedly improved the efficiency of surveillance and training. This system can ensure that medical personnel and trainees actually understand the skills of donning/removing PPE. Compared to conventional methods, the SITMS can save manpower and time, so it is particularly good in scenarios involving the outbreak of a certain infectious disease when numerous new personnel need to be rigorously trained in a short amount of time. It can also serve as a routine surveillance system in a hospital or department when PPE is often used. However, AI technology is far from flawless. There are still technological limitations so far: The recognition accuracy is affected by many factors, such as the camera angle, speed of human movement, and the degree to which movement is standardized (18), and this is particularly true for the recognition of fine movements (19). The efficiency of self-learning is still too limited (20). These limitations might potentially cause errors in the recognition of movements, so they should be addressed in future research and development. Even though AI cannot completely take the place of clinicians right now, the value of AI technology cannot be ignored. It can help to continuously optimize the strategies against NIs, including devising more reasonable "STBs", simpler but efficient training processes, and a more friendly human-computer interface. The current finding should help to achieve medical care with "no harm and no infections" in an era of constantly emerging infectious diseases (21).

Funding: This work was supported by a grant from Science and Technology Research Projects of Shenzhen (JSGG20220301090005007) and the Shenzhen High-level Hospital Construction Fund (No.23274G1001).

Conflict of Interest: The authors have no conflicts of interest to disclose.

References

- Kouchak F, Askarian M. Nosocomial infections: The definition criteria. *Iran J Med Sci*. 2012; 37:72-73.
- Liu JY, Dickter JK. Nosocomial infections: A history of hospital-acquired infections. *Gastrointest Endosc Clin N Am*. 2020; 30:637-652.
- Boev C, Kiss E. Hospital-acquired infections: Current trends and prevention. *Crit Care Nurs Clin North Am*. 2017; 29:51-65.
- Dai Z, Chen LY, Cai MJ, Yao YH, Zhu JH, Fang LL, Tang R, Liang XM. Clinical characteristics and microbiology of nosocomial enterococcal bloodstream infections in a tertiary-level hospital: A retrospective study, 2007-2019. *J Hosp Infect*. 2022; 122:203-210.
- Suleyman G, Alangaden GJ. Nosocomial fungal infections: Epidemiology, infection control, and prevention. *Infect Dis Clin North Am*. 2021; 35:1027-1053.
- World Health Organization. Guidelines on Core Components of Infection Prevention and Control Programmes at the National and Acute Health Care Facility Level. Geneva, 2016.
- Karako K, Song P, Chen Y, Tang W. New possibilities for medical support systems utilizing artificial intelligence (AI) and data platforms. *Biosci Trends*. 2023; 17:186-189.
- Mahmood SU, Crimbley F, Khan S, Choudry E, Mehwish S. Strategies for rational use of personal protective equipment (PPE) among healthcare providers during the COVID-19 crisis. *Cureus*. 2020; 12:e8248.
- John A, Tomas ME, Hari A, Wilson BM, Donskey CJ. Do medical students receive training in correct use of personal protective equipment? *Med Educ Online*. 2017; 22:1264125.
- Wilder-Smith A, Chiew CJ, Lee VJ. Can we contain the COVID-19 outbreak with the same measures as for SARS? *Lancet Infect Dis*. 2020; 20:e102-e107.
- Mitchell R, Roth V, Gravel D, Astrakianakis G, Bryce E, Forgie S, Johnston L, Taylor G, Vearncombe M, Canadian Nosocomial Infection Surveillance P. Are health care workers protected? An observational study of selection and removal of personal protective equipment in Canadian acute care hospitals. *Am J Infect Control*. 2013; 41:240-244.
- Song Y, Zhang L, Wang W. An analysis of the effect of personal protective equipment (PPE) training based on the information-motivation-behavior skills model in the practice of COVID-19 PPE application. *Infect Drug Resist*. 2022; 15:4829-4835.
- Fan J, Jiang Y, Hu K, Chen X, Xu Q, Qi Y, Yin H, Gou X, Liang S. Barriers to using personal protective equipment by healthcare staff during the COVID-19 outbreak in China. *Medicine (Baltimore)*. 2020; 99:e23310.
- China NHCoPsRo. Technical guidelines on prevention and control of novel coronavirus infection in medical institutions (third edition). https://www.gov.cn/xinwen/2021-09/14/content_5637141.htm (accessed Aug 26th 2023). (in Chinese).
- Asakawa T, Sugiyama K, Nozaki T, Sameshima T, Kobayashi S, Wang L, Hong Z, Chen S, Li C, Namba H. Can the latest computerized technologies revolutionize conventional assessment tools and therapies for a neurological disease? The example of Parkinson's disease. *Neurol Med Chir (Tokyo)*. 2019; 59:69-78.
- Soltan AAS, Yang J, Pattanshetty R, Novak A, Yang Y, Rohanian O, Beer S, Soltan MA, Thickett DR, Fairhead R, Zhu T, Eyre DW, Clifton DA, Collaborative CT. Real-world evaluation of rapid and laboratory-free COVID-19 triage for emergency care: External validation and pilot deployment of artificial intelligence driven screening. *Lancet Digit Health*. 2022; 4:e266-e278.
- Chen WS, Zhang WH, Li ZJ, et al. Evaluation of manual and electronic healthcare-associated infections surveillance: A multi-center study with 21 tertiary general hospitals in China. *Ann Transl Med*. 2019; 7:444.
- Chan HP, Samala RK, Hadjisiiki LM, Zhou C. Deep learning in medical image analysis. *Adv Exp Med Biol*. 2020; 1213:3-21.
- Sapinski T, Kaminska D, Pelikant A, Anbarjafari G. Emotion recognition from skeletal movements. *Entropy (Basel)*. 2019; 21.
- Duong MT, Rauschecker AM, Rudie JD, Chen PH, Cook TS, Bryan RN, Mohan S. Artificial intelligence for precision education in radiology. *Br J Radiol*. 2019;

- 92:20190389.
21. Yang Y, Guo L, Lu H. Emerging infectious diseases never end: The fight continues. *Biosci Trends*. 2023; 17:245-248.

Received August 22, 2023; Revised August 27, 2023; Accepted August 30, 2023.

[§]These authors contributed equally to this work.

*Address correspondence to:

Hongzhou Lu, Department of Infectious Diseases, National Clinical Research Center for Infectious Diseases, the Third

People's Hospital of Shenzhen, 29 Bulan Road, Shenzhen, Guangdong 518112, China.
E-mail: luhongzhou@szsy.sustech.edu.cn

Tetsuya Asakawa, Institute of Neurology, National Clinical Research Center for Infectious Diseases, the Third People's Hospital of Shenzhen, 29 Bulan Road, Shenzhen, Guangdong 518112, China.

E-mail: asakawat1971@gmail.com

Released online in J-STAGE as advance publication September 7, 2023.

A pilot study comparing the disinfecting effects of commercialized stable ClO₂ solution (free of activation) with conventional H₂O₂ on dental unit waterlines in the dental practice setting

Xiaolei Zhang^{1,§}, Jingjing Sha^{2,§}, Zefan Huang³, Sisi Chen², Xufei Luo¹, Ruijun Liu⁴, Tetsuya Asakawa^{5,*}, Qiang Zhang^{6,*}

¹ Department of Hospital Infection, Shenzhen Stomatolgy Hospital, Shenzhen, China;

² Department of Endodontics, Shenzhen Stomatolgy Hospital, Shenzhen, China;

³ Department of Nursing, Shenzhen Stomatolgy Hospital, Shenzhen, China;

⁴ Department of Periodontology, Shenzhen Stomatolgy Hospital, Shenzhen, China;

⁵ Institute of Neurology, National Clinical Research Center for Infectious Diseases, the Third People's Hospital of Shenzhen, Shenzhen, China;

⁶ Department of Orthodontics, Shenzhen Stomatolgy Hospital, Shenzhen, China.

SUMMARY Disinfection of dental unit waterlines (DUWLs) plays a key role in control and prevention of nosocomial infection in a dental clinic. The most conventional disinfectant is hydrogen peroxide (H₂O₂), while chlorine dioxide (ClO₂) has been considered however was limited by the "activation" procedures. With the availability of commercialized stable ClO₂ solution (free of activation), direct application of ClO₂ in the dental practice became possible. This study was designed to compare the disinfecting effects of stable 5 ppm of ClO₂ solution with conventional 0.24% of H₂O₂ on DUWLs in dental practice. Studies of colony-forming units (CFUs), confocal laser scanning microscopy (CLSM) and scanning electron microscope (SEM) were employed for evaluation. In CFUs studies, we found that the efficiency of ClO₂ was no less than those of H₂O₂. In the morphological studies, the stronger disinfecting effects of ClO₂ was verified by both CLSM and SEM studies for removal and prevention of biofilm. Importantly, ClO₂ solution achieved a better disinfecting efficiency not only at the surface of bacterial biofilm, but also, it has penetrating effects, presented disinfecting effects from the surface to the bottom of the biofilm. This pilot study provided evidence regarding the efficiency of stable ClO₂ solution on disinfection of DUWLs in the dental practice setting. Application of stable ClO₂ solution in dental practice is therefore become possible.

Keywords dental unit waterlines, hydrogen peroxide (H₂O₂), chlorine dioxide (ClO₂), disinfection, biofilm

1. Introduction

Dental unit waterlines (DUWLs) are a piping system providing pure water for dental treatment. This system is comprised of several narrow, long pipelines, which is often intermittent used with unbalanced and slow flows. Accordingly, DUWLs are easily contaminated by bacteria and then induced bacterial biofilm formation. Frequently used positions, such as air/water syringe, dental hand piece, and cuspidor faucet usually have more chance to be contaminated, potentially conduct bacteria to the waterline, and promote biofilm formation (1). It has been documented that bacterial biofilm on DUWLs is widely distributed, with the approximately 30-50 μm thickness, which is believed to potentially cause serious waterline contamination (2). If such contamination is neglected, the floating microorganisms or dissociative

biofilms might be transferred to the patient, or come to the air through a handpiece, thereby increasing the infectious risks to patients and dental staffs (3). Hence, surveillance and prevention of DUWLs-related contamination are routine works of a dental clinic. A battery of disinfectants and disinfecting methods, such as hydrogen peroxide (H₂O₂) (4), chlorine dioxide (ClO₂) (5), chlorhexidine gluconate (6), sodium hypochlorite (7), peracetic acid (8), intermittent sterilization with peracetic acid/H₂O₂ (9), continuous disinfection with hydrogen peroxide/silver ions (6) were investigated for use in DUWLs. Nonetheless, only few of them are actually used in a dental clinical setting for various reasons. An ideal disinfectant for using in the dental practice setting should have several characteristics, such as effective, safe, appropriate priced, convenient, and easily available. Accordingly, H₂O₂ is the most

commonly used disinfectant for DUWLs clinically.

ClO_2 is an effective, safe high-level disinfectant, which is widely used for disinfection of environments, surface of articles, and human. It has been reported using ClO_2 for oral cleaning (10-12) and wound cleaning (13). However, ClO_2 is not commonly used for dental clinical setting because it is difficult to obtain a stable ClO_2 solution, and store it for a long time. Hence, the ClO_2 solution usually has to be prepared before using by a chemical reaction of precursors, which is termed as "activation", that is inconvenient and unsafe for DUWLs in the actual clinical setting (14) because the reaction concentration is not easily controlled. Our previous studies mentioned availability of a commercialized stable ClO_2 solution that was free of activation (14,15), that make it possible for convenient use of ClO_2 in clinical setting since we can purchase the stable solution with a certain concentration. On the other hand, colony-forming units (CFUs) have been used as a standard index for evaluating the efficiency of disinfection in DUWLs scenario. Conversely, remove/control of bacterial biofilm during the disinfection in DUWLs has never been a standard index, even though it plays a key role in prevention and intervention of the DUWLs contamination.

Based on the aforementioned contexts, we designed this pilot study to compare the efficiency of disinfection in DUWLs between the conventional H_2O_2 and the commercialized stable ClO_2 solution (free of activation) in the clinical practice. Meanwhile, we also attempted to observe the changes of bacterial biofilm along with the CFUs affected by ClO_2 solution and H_2O_2 . We believe that the findings of this study will be useful for better understanding the efficiency of the commercialized stable ClO_2 solution (free of activation) as well as changes of bacterial biofilm affected by ClO_2 and H_2O_2 , that is useful for selection of an appropriate disinfectant for DUWLs in the dental practice setting.

2. Materials and Methods

2.1. Preparation of DUWLs and collection of the water samples

Experimental DUWLs in the present study were derived from the dental chair units (DCUs, UTTG27959, Planmeca, Helsinki, Finland), which had been normally used for the routine clinical practice for three years. Total 18 DCUs were involved in this study, where 12 DCUs were allocated to the ClO_2 group and 6 were allocated to the H_2O_2 group using a simple coin toss randomized method. Two sorts of disinfectants were prepared in the present study, namely 5 ppm of commercialized stable ClO_2 solution (free of activation) which was purchased from the manufacturer (Shenzhen Caseche Biotech Co., Ltd., Shenzhen, Guangdong, China) and 0.24% H_2O_2 (4). Concentrations of the agents were determined according

to the previous studies using ClO_2 (16,17) and H_2O_2 (4) for disinfection.

Once the investigation initiated, 500 mL ClO_2 and H_2O_2 solutions were put into the sterilizing bottle of DCUs respectively after the daily dental clinical work was finished. The disinfection procedures were opened for 4 min (wash with disinfectant for 2 min and then wash with pure water for 2 min); then the power switch was turned off overnight. Water samples were collected before the clinic work at the next morning. Sampling was performed as per the 2023 Guidelines for Infection Control and Management in Dental Unit Waterlines (18). Sampling was implemented at three positions, namely air/water syringe, dental hand piece, and cuspidor faucet following the principles of aseptic operation. Experiments were performed for 45 weeks, except the previous day for the baseline test. Water samples were measured once per week for the first 29 weeks, and once per two weeks for the last 16 weeks.

2.2. Detection of the CFUs in water samples

In terms of CFUs test, 200 μL sample water was put into a sterile petri dish, and mixed with medium, subsequently cultured at 37°C for 48 hours. CFUs were calculated as the numbers of bacterial colonies divided by the volume of diluent. Less than 100 CFUs/mL is considered as negative.

2.3. Confocal laser scanning microscopy (CLSM) study

After 12 weeks of disinfection (ClO_2 or H_2O_2), Waterline samples of DUWLs were cut into rings (0.2-0.5 mm length), which were immediately exposed to a LIVE/DEAD BacLight Bacterial Viability Kit (Cat. No. L7012, Thermo Fisher Scientific Inc., Waltham, MA, America) for 10 min, washed with PBS for 1 min, and then rinsed twice. Non-invasive CLSM images were acquired on the complete biofilm at the inner wall of DUWLs using a CLSM (FV3000, Olympus, Tokyo, Japan) (excitation light wavelength = 510/480 nm). Vital fluorescence staining (VFS) was performed as per the manufacturer's manual. Bright green staining displays live bacteria, red staining shows dead bacteria, and the yellow staining is the overlap (coexistence) of dead and live bacteria.

Image analysis was performed using an ImageJ 1.34p software (National Institutes of Health, Bethesda, MD, USA; <http://rsb.info.nih.gov/ij/>). Images of each color channel were assembled into stacked images, and the areas occupied by live bacteria and dead bacteria were calculated respectively. The ratio of live bacteria to dead bacteria was calculated and submitted to statistical analysis.

2.4. Scanning electron microscope (SEM)

Remaining waterline samples of DUWLs undergone

a 12-week sterilization were cut into a 1 cm section, then cut vertically from the middle line. All samples were placed into 2.5% glutaraldehyde for overnight fixation. After being dehydrated by ethanol gradient (30%, 50%, 70%, 80%, 85%, 90%, 95%, and anhydrous ethanol for 0.5 h at each concentration), the tubes were fixed on a special aluminum base. After spraying gold nanoparticles, they were observed and photographed using a scanning electron microscope (Su8220, Hitachi, Tokyo, Japan).

2.5. Statistics

A SPSS soft (V26.0.0, IBM, Armonk, NY, USA) was used for statistical analyzes. Comparisons of proportion were performed with a Chi-square test. The quantitative VFS data were compared using a Mann-Whitney *U* test. $p < 0.05$ was considered as the statistical significance.

3. Results and Discussion

In the present study, we compared the disinfecting effects of commercialized stable ClO_2 solution (free of activation) with conventional H_2O_2 for DUWLs by observing the states of biofilm. Our data suggest a better disinfecting efficiency of this ClO_2 solution than that of conventional H_2O_2 in terms of DUWLs disinfection. To the best of our knowledge, this study is the first study to evaluate the efficiency of commercialized stable ClO_2 solution (free of activation) using in disinfection of DUWLs. We believe that the findings of this study are helpful to select an appropriate disinfectant for DUWLs in the routine dental practice.

3.1. Analysis of the CFUs in the DUWLs

As shown as in Table 1, total 1,998 water samples were tested, of those, 1,332 were in ClO_2 group, and 666 were in H_2O_2 group. In the ClO_2 group, total 1,312 samples were identified as "-" once their detection values $< 100 \text{ CFU/mL}$, the pass rate was 98.48%. In the H_2O_2 group, total 648 samples were identified as "-", the pass rate was 97.30%. No significant difference was found between groups in total ($\chi^2 = 3.434$, $p = 0.064$). In terms of different positions, no signification difference was found between two groups (Table 1). These data indicated that the disinfecting efficiency of this stable

Table 1. Analysis of the colony-forming units in the dental unit waterlines

Positions	ClO_2 -/+	H_2O_2 -/+	X^2	p value
Air/water syringe	440/4	220/2	0	1.000
Dental hand piece	440/4	216/6	3.249	0.071
Cuspidor faucet	432/12	212/10	1.504	0.220
Total	1312/20	648/18	3.434	0.064

"-" means the detection value $< 100 \text{ CFUs/mL}$; "+" means the detection value $\geq 100 \text{ CFUs/mL}$, CFUs = colony-forming units.

ClO_2 solution was no weaker than those of conventional H_2O_2 .

3.2. Comparison of the disinfecting effects between ClO_2 and H_2O_2 by observing the changes of the biofilms

As shown as in Figure 1, the disinfecting effects between ClO_2 and H_2O_2 were compared with a CLSM along with a SEM. Biofilm is a thin layer at the surface of waterline. The results of the CLSM displayed that multitudes bacteria in the biofilm were

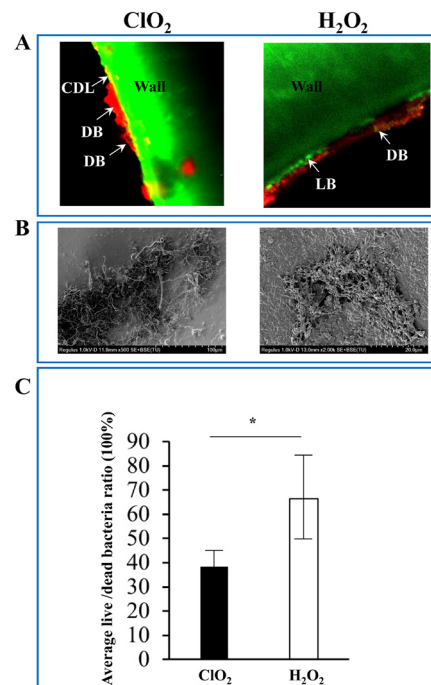


Figure 1. Comparison of the disinfecting effects between ClO_2 and H_2O_2 by observation of the changes of biofilms. **A.** Representative images of CLSM displaying the disinfecting effects on the biofilm (ClO_2 vs. H_2O_2). Green background is the wall of the waterline ("Wall" in the figure). Biofilm is a thin layer at the surface of waterline, where bright green patches represent live bacteria ("LB" in the figure); red patches represent dead bacteria ("DB" in the figure); yellow patches represent coexistence dead and living bacteria ("CDL" in the figure). In the ClO_2 group (left column), bright green patches could not be observed, the intermittent biofilm included large red patches and underneath linear yellow stripes indicating bacteria in the biofilm were disinfected. Moreover, ClO_2 had effects of infiltrating into the biofilm (penetrating effects). Whereas in the H_2O_2 group (right column), bright green patches were still visible indicating the survival of numerous live bacteria indicating the disinfecting effects were not satisfactory. No more penetrating effects were found here, hence, H_2O_2 exhibited a modest effect on killing the bacteria at the bottom of the biofilm. These data suggested a better efficacy of ClO_2 in removal of biofilm. **B.** Representative images of SEM. In the ClO_2 group (left column), the matrix of biofilm disappeared, indicating its integrity was destroyed. Whereas in the H_2O_2 group (right column), the biofilm structure was partially damaged. The damaged matrix structure along with the undamaged matrix structure were observed attaching to the surface of waterline. **C.** Quantitative results of VFS. The ratio of average live/dead ration of the ClO_2 group was significantly lower than that of H_2O_2 group. Data were presented as mean \pm standard error, * means $p < 0.05$. CLSM: confocal laser scanning microscopy, SEM: scanning electron microscope, VFS: vital fluorescence staining.

killed (red patches representing dead bacteria, and/or the underneath linear yellow stripes representation coexistence of live and dead bacteria) in the ClO₂ group, whereas they were partially killed as uneven red patches (dead bacteria) over the bright green stripes (representing alive bacteria) in the H₂O₂ group. Active bacteria (bright green patches) almost could not be observed in the ClO₂ group, whereas could be still found in the H₂O₂ group. These findings demonstrated a better disinfecting efficiency of ClO₂ than H₂O₂ (Figure 1A). Meanwhile, the results of the SEM showed that the matrix structure of biofilms was disrupted from surface to deep layers, thereby the matrix could not be found till the bottom of the biofilm (close to the basal layer), and the bacterial body were exposed in the ClO₂ group. Whereas in the H₂O₂ group, the damage of the matrix structure was slighter, only partial surface layer and matrix were damaged (Figure 1B). Findings of CLSM were in agreements with those of SEM, indicating ClO₂, in comparison to H₂O₂, can markedly damage the surface (including the matrix) structures and infiltrate into the biofilm, thereby achieves better disinfecting effects (referred to as "penetrating effects"). Quantitative data of VFS also verified the better efficiency of ClO₂. The average live/dead bacteria ratio in ClO₂ group were significantly lower than that of H₂O₂ group (38.41% vs. 66.36%, U = 19/00, p = 0.032) (Figure 1C).

3.3. What is special issue of the ClO₂ solution used in this study?

Disinfection of DUWLs plays a key role in control and prevention of nosocomial infection in a dental clinic. It has been documented that contaminated DUWLs are risky for the patients' health (19), even life-threatening in some extreme cases (20,21). Removal and control biofilm and planktonic microbes developed in DUWLs are undoubtedly the most important tasks in terms of prevention of DUWLs contamination-related nosocomial infections (22). In this regard, many disinfectants were evaluated. But only several disinfectants were actually applied in the clinical setting. H₂O₂, as a high-level disinfectant, acts as the most conventional disinfectant using in the DUWLs scenario (23), that is recommended by the manufacturer's manual of many DUWLs makers. However, H₂O₂ is far from a faultless disinfectant in the context of a dental practice. Its unstable and irritant nature limits its further application for dental practice setting. ClO₂ is another high-level disinfectant which has been considered for using in the dental practice due to its nontoxicity and nonirritant. The limitation of ClO₂ lies in difficulties of availability of a stable and storable ClO₂ solution (14). The aforementioned "activation" processes are quite inconvenient and inoperable in a dental scenario because the activation concentration sometimes is difficult to control. Fortunately, a novel stable ClO₂ solution (free of activation) recently became

available. Hence, using ClO₂ solution in the dental practice setting, even directly using it in human body (14) are becoming possible. Here, first, our CFUs study found that the disinfecting efficiency of 5 ppm of stable ClO₂ solution (free of activation) was no weaker than those of conventional 0.24% of H₂O₂ on DUWLs in actual dental practice (Table 1). During the subsequent morphological studies, we found that the 5 ppm of stable ClO₂ solution exhibited stronger disinfecting effects to biofilm at the surface of the waterline. Results of CLSM indicated that almost all patches representing live bacteria (bright green) were disappeared. Only patches representing dead bacteria (red) and coexistence of live/dead bacteria (yellow) were residual. By contrast, patches of live bacteria remained visible after disinfection with 0.24% of H₂O₂ (Figure 1A). Importantly, our CLSM data implied that ClO₂ may infiltrate into the biofilm (penetrating effects) and exhibit a better disinfection. The SEM data were in line with the CLSM data, namely 5 ppm of ClO₂ solution could completely destroy the integrity of biofilm, whereas 0.24% of H₂O₂ could only achieve a partial destroy (Figure 1B). Our data suggested that 5 ppm of ClO₂ solution displayed a stronger effect than 0.24% H₂O₂ in terms of removal/control of biofilm. The quantitative results of VFS also confirmed this finding (Figure 1C). Accordingly, the disinfecting efficiency of this stable ClO₂ solution (free of activation) was verified.

Another important issue is regarding the safety. In terms of the application scenarios of ClO₂, 5 ppm is indeed a very low dose, which is commonly used for disinfection of the fresh fruits and vegetables (24). As early in 1984, a human study by Lubbers *et al.* documented that no toxic reactions were found after oral intake of 5 ppm of ClO₂ (containing in the tap water) for 12 weeks (25). A later animal study found that no toxic effects were observed in the main organs in mice after oral administration of ClO₂ at 0-40 ppm for 90 days (26). By contrast, the doses of application of ClO₂ for the other scenarios commonly larger, for example, 300 ppm for disinfection of wounds with deep venous thrombosis or diabetic foot (13), 1,000 ppm for dental disinfection (12). These doses of ClO₂ directly used in human body are much greater than 5 ppm, however, are still safe. In this regard, 5 ppm of ClO₂ for DUWLs disinfection is undoubtedly safe.

3.4. Limitations and future prospects

Because the present study was designed in the scenario of dental practice setting, that means all the DUWLs were in practice every day, which required to be disinfected every day. Thus, we could not set up a "blank" control. This might be a limitation of this study. In addition, gradient experiments in different concentrations of ClO₂ and H₂O₂ are also indispensable to elucidate their destroying effects on biofilm, which

should be addressed in our future investigation.

Taken together, this pilot study conducted a comparison of the disinfecting effects on DUWLs between a commercialized stable ClO₂ solution (free of activation) and conventional H₂O₂. The present study verified the satisfactory efficiency of this stable ClO₂ solution in a low dose (5 ppm). The safe and effective nature of stable ClO₂ solution (free of activation) to biofilm indicates that it is suitable for disinfection and sterilization of DUWLs in actual dental practice.

Funding: This work was supported by a grant from Shenzhen Stomatolgy Hospital Program (grant No. SSK-2022-01).

Conflict of Interest: The authors have no conflicts of interest to disclose.

References

1. Pankhurst CL, Scully C, Samaranayake L. Dental unit water lines and their disinfection and management: A review. *Dent Update*. 2017; 44:284-285, 289-292.
2. Williams JF, Johnston AM, Johnson B, Huntington MK, Mackenzie CD. Microbial contamination of dental unit waterlines: prevalence, intensity and microbiological characteristics. *J Am Dent Assoc*. 1993; 124:59-65.
3. Umer F, Khan M, Khan FR, Tejani K. Managing dental unit waterlines: A quality improvement programme. *BMJ Open Qual*. 2022; 11:e001685.
4. Linger JB, Molinari JA, Forbes WC, Farthing CF, Winget WJ. Evaluation of a hydrogen peroxide disinfectant for dental unit waterlines. *J Am Dent Assoc*. 2001; 132:1287-1291.
5. Bansal R, Puttaiah R, Harris R, Reddy A. Evaluation of two methods in controlling dental treatment water contamination. *J Contemp Dent Pract*. 2011; 12:73-83.
6. Schel AJ, Marsh PD, Bradshaw DJ, et al. Comparison of the efficacies of disinfectants to control microbial contamination in dental unit water systems in general dental practices across the European Union. *Appl Environ Microbiol*. 2006; 72:1380-1387.
7. Liaqat I, Sabri AN. Effect of biocides on biofilm bacteria from dental unit water lines. *Curr Microbiol*. 2008; 56:619-624.
8. Montebugnoli L, Chersoni S, Prati C, Dolci G. A between-patient disinfection method to control water line contamination and biofilm inside dental units. *J Hosp Infect*. 2004; 56:297-304.
9. Dallolio L, Scuderi A, Rini MS, Valente S, Farruggia P, Sabattini MA, Pasquinelli G, Acacci A, Roncarati G, Leoni E. Effect of different disinfection protocols on microbial and biofilm contamination of dental unit waterlines in community dental practices. *Int J Environ Res Public Health*. 2014; 11:2064-2076.
10. Shinada K, Ueno M, Konishi C, Takehara S, Yokoyama S, Zaitsu T, Ohnuki M, Wright FA, Kawaguchi Y. Effects of a mouthwash with chlorine dioxide on oral malodor and salivary bacteria: A randomized placebo-controlled 7-day trial. *Trials*. 2010; 11:14.
11. Shinada K, Ueno M, Konishi C, Takehara S, Yokoyama S, Kawaguchi Y. A randomized double blind crossover placebo-controlled clinical trial to assess the effects of a mouthwash containing chlorine dioxide on oral malodor. *Trials*. 2008; 9:71.
12. Kale A, Mahale S, Sethi K, Karde P. Clinical and microbial comparative evaluation of 0.1% chlorine dioxide mouthwash versus 0.2% chlorhexidine mouthwash after periodontal surgery: A randomized clinical trial. *Int J Innov Res Sci Eng Techno*. 2020; 6:935-939.
13. Noszticzius Z, Wittmann M, Kály-Kullai K, Beregvári Z, Kiss I, Rosivall L, Szegedi J. Demonstrating that chlorine dioxide is a size-selective antimicrobial agent and high purity ClO₂ can be used as a local antiseptic. *arXiv*. 2013; 1304.5163.
14. Cao J, Shi Y, Wen M, Peng Y, Miao Q, Liu X, Zheng M, Asakawa T, Lu H. Can nasal irrigation with chlorine dioxide be considered as a potential alternative therapy for respiratory infectious diseases? The example of COVID-19. *Biosci Trends*. 2022; 16:447-450.
15. Asakawa T. Focusing on development of novel sampling approaches and alternative therapies for COVID-19: Are they still useful in an era after the pandemic? *Biosci Trends*. 2022; 16:386-388.
16. Bredács M, Frank A, Bastero A, Stolarz A, Pinter G. Accelerated aging of polyethylene pipe grades in aqueous chlorine dioxide at constant concentration. *Polymer Degradation and Stability*. 2018; 157:80-89.
17. Castagnetti D, Mammano GS, Dragoni E. Effect of chlorinated water on the oxidative resistance and the mechanical strength of polyethylene pipes. *Polymer testing*. 2011; 30:277-285.
18. Association CS. Guidelines for infection control and management in dental unit waterlines. <https://www.qiluhospital.com/show-294-32090-1.html> (accessed Sep 16 2023) (in Chinese).
19. Laheij AM, Kistler JO, Belibasakis GN, Valimaa H, de Soet JJ; European Oral Microbiology Workshop (EOMW) 2011. Healthcare-associated viral and bacterial infections in dentistry. *J Oral Microbiol*. 2012; 4.
20. Ricci ML, Fontana S, Pinci F, Fiumana E, Pedna MF, Farolfi P, Sabattini MA, Scaturro M. Pneumonia associated with a dental unit waterline. *Lancet*. 2012; 379:684.
21. Barbot V, Robert A, Rodier MH, Imbert C. Update on infectious risks associated with dental unit waterlines. *FEMS Immunol Med Microbiol*. 2012; 65:196-204.
22. Lin SM, Svoboda KK, Giletto A, Seibert J, Puttaiah R. Effects of hydrogen peroxide on dental unit biofilms and treatment water contamination. *Eur J Dent*. 2011; 5:47-59.
23. Zanetti F, De Luca G, Tarlazzi P, Stampi S. Decontamination of dental unit water systems with hydrogen peroxide. *Lett Appl Microbiol*. 2003; 37:201-206.
24. Praeger U, Herppich WB, Hassenberg K. Aqueous chlorine dioxide treatment of horticultural produce: Effects on microbial safety and produce quality-A review. *Crit Rev Food Sci Nutr*. 2018; 58:318-333.
25. Lubbers JR, Chauhan S, Miller JK, Bianchine JR. The effects of chronic administration of chlorine dioxide, chlorite and chloride to normal healthy adult male volunteers. *J Environ Pathol Toxicol Oncol*. 1984; 5:229-238.
26. Ma JW, Huang BS, Hsu CW, Peng CW, Cheng ML, Kao JY, Way TD, Yin HC, Wang SS. Efficacy and safety evaluation of a chlorine dioxide solution. *Int J Environ*

Res Public Health. 2017; 14:329.

E-mail: 13500052738@163.com

Received September 26, 2023; Revised October 15, 2023;
Accepted October 21, 2023.

Tetsuya Asakawa, Institute of Neurology, National Clinical Research Center for Infectious Diseases, the Third People's Hospital of Shenzhen, 29 Bulan Road, Shenzhen, Guangdong, China 518112.

E-mail: asakawat1971@gmail.com

[§]These authors contributed equally to this work.

*Address correspondence to:

Qiang Zhang, Department of Orthodontics, Shenzhen Stomatology Hospital, 70 Guiyuan North Street, Shenzhen, Guangdong, China 518001.

Released online in J-STAGE as advance publication October 26, 2023.

EQUIBIND: A geometric deep learning-based protein-ligand binding prediction method

Yuze Li¹, Li Li¹, Shuang Wang^{1,2,*}, Xiaowen Tang^{1,*}

¹ Department of Medical Chemistry, School of Pharmacy, Qingdao University, Qingdao, Shandong, China;

² Department of Stomatology, Huangdao District Central Hospital, Qingdao, Shandong, China.

SUMMARY Structure-based virtual screening plays a critical role in drug discovery. However, numerous docking programs, such as AutoDock Vina and Glide, are time-consuming due to the necessity of generating numerous molecular conformations and executing steps like scoring, ranking, and refinement for the ligand-receptor complexes. Consequently, achieving rapid and reliable virtual screening remains a noteworthy challenge. Recently, a team of researchers from Massachusetts Institute of Technology, led by Stärk et al., developed an SE(3)-equivariant geometric deep learning based protein-ligand binding prediction approach, EQUIBIND. In comparison to conventional docking methods, EQUIBIND has the capacity to predict the binding modes of small molecules with target proteins rapidly and precisely. It presents an innovative resolution for high-throughput screening of drug-like compounds.

Keywords EQUIBIND, deep learning, virtual screening, protein-ligand binding prediction

Drug discovery is a highly costly and time-intensive process, requiring several years and billions of dollars to discover new drugs that target either newly identified or well-established receptors. Throughout this protracted timeline, issues like drug-induced side effects and adverse reactions can lead to the failure of drug development endeavors (1). The central challenge in drug discovery revolves around deciphering the complex binding interactions between drug-like compounds and proteins. As a result, the accurate and efficient identification of binding sites within proteins for compounds, the characterization of binding conformations, and the evaluation of ligand-protein interactions have become critical aspects of the drug discovery process. In recent decades, computational methodologies have gained significant traction in predicting drug binding sites and conducting virtual screenings to identify potential therapeutic agents (2-4).

In the field of drug design and development, widely used molecular docking approaches such as AutoDock Vina and Glide usually employ strategies based on geometric and energy-based matching principles (5,6). The protein-ligand binding complex undergoes a series of conformational sampling, score ranking and energy-driven refinement (7). Nowadays, driven by the advancement of computational technology, artificial intelligence-driven drug design has emerged

as a prominent approach in drug development. Artificial intelligence approach like machine learning, deep learning, and related methodologies have been integrated in traditional virtual screening area. Recently, EQUIBIND, an SE(3)-equivariant geometric deep learning model was reported, which integrates Graph Matching Networks (GMN) (8) and E(3)-equivariant graph neural networks (E(3)-GNN) (9) to predict the binding conformations of ligand-receptor complexes (10). EQUIBIND significantly enhances predictive efficiency by bypassing the need for extensive sampling procedures. It provides direct predictions of binding sites on receptors (blind docking) and ligand binding conformations. A benchmark test demonstrates that EQUIBIND exhibits a processing efficiency of about nine times surpasses than currently prevalent commercial binding predicting programs (10,11).

Moreover, EQUIBIND capitalizes on a K-NN graph (k-nearest neighbor graph) to delineate three-dimensional structures. The input parameters predominantly encompass the rigid three-dimensional arrangement of the protein and the adaptable, optimizable conformations of small molecules, which are generated at random using RDKit. Subsequently, EQUIBIND employs Invariant Equivariant Graph Matching Networks (IEGMN) to transform the three-dimensional coordinates and predict the binding

conformation of the ligand. To ensure accuracy, EQUIBIND employs the SE(3)-equivariant mechanism to calculate the binding sites of receptors, in which the predictive sites are trained to match the actual binding sites. However, EQUIBIND does not guarantee the absolute correctness of complex structures, often resulting in bond lengths and bond angles that deviate from reasonable ranges. To address this issue, EQUIBIND aligns the initial conformations generated by RDKit with those generated by IEGMN. As this process involves only rotatable single bonds, it ensures the local structural integrity. The algorithm primarily focuses on aligning atomic positions around rotatable single bonds, each of which can be manipulated independently. In comparison to traditional docking methods, the EQUIBIND model demonstrates commendable predictive accuracy, enabling precise forecasts of ligand-target binding modes (10).

However, EQUIBIND is not devoid of its limitations. It indirectly models the atomic positions of side chains by encoding features within the receptor α -carbon graph utilizing localized frameworks, as a result, some predictions may manifest notable disparities. Stärk *et al.* have attempted surface atom refinements and fine-tuning approaches by incorporating atomic subgraphs of the receptor. Regrettably, these endeavors failed to yield significant enhancements to the performance and instead contributed to extended runtimes. Consequently, there remains efforts for the future advancement and refinement of EQUIBIND.

In conclusion, EQUIBIND serves as a novel deep learning-based protein-ligand binding prediction tool. By leveraging SE(3)-equivariant transformations and utilizing minimal input information, it can directly predict the binding sites on receptors and the binding modes of ligands. This capability ensures both high prediction accuracy and a substantial enhancement in prediction efficiency. In the future, whether employed in conjunction with existing virtual screening tools or utilized independently for protein-ligand binding prediction, EQUIBIND holds the potential to emerge as a crucial asset in the drug molecule screening and discovery process.

Funding: This work was supported by the Qingdao Marine Science and Technology Innovation Special Project (No. 22-3-3-HYGG-25-HY).

Conflict of Interest: The authors have no conflicts of interest to disclose.

References

- Reymond JL, Awale M. Exploring chemical space for drug discovery using the chemical universe database. *ACS Chem Neurosci.* 2012; 3:649-657.
- Evans R, O'Neill M, Pritzel A, *et al.* Protein complex prediction with AlphaFold-Multimer. *bioRxiv.* 2021; 2021.10.04.463034.
- Jindal A, Kotelnikov S, Padhorny D, Kozakov D, Zhu Y, Chowdhury R, Vajda S. Side-chain packing using SE(3)-transformer. *Pac Symp Biocomput.* 2021; 27:46-55.
- Ganea O-E, Huang X, Bunne C, Bian Y, Barzilay R, Jaakkola T, Krause A. Independent SE(3)-equivariant models for end-to-end rigid protein docking. *arXiv.* 2021; 2111.07786.
- Halgren TA, Murphy RB, Friesner RA, Beard HS, Frye LL, Pollard WT, Banks JL. Glide: A new approach for rapid, accurate docking and scoring. 2. enrichment factors in database screening. *J Med Chem.* 2004; 47:1750-1759.
- Trott O, Olson AJ. AutoDock Vina: improving the speed and accuracy of docking with a new scoring function, efficient optimization, and multithreading. *J Comput Chem.* 2010; 31:455-461.
- Hassan NM, Alhossary AA, Mu Y, Kwoh CK. Protein-ligand blind docking using QuickVina-W with inter-process spatio-temporal integration. *Sci Rep.* 2017; 7:15451.
- Li Y, Gu C, Dullien T, Vinyals O, Kohli P. Graph matching networks for learning the similarity of graph structured objects. *ICML.* 2019; 34:3835-3845.
- Satorras VG, Hoogeboom E, Welling M. E(n)-equivariant graph neural networks. *arXiv.* 2021; 2102.09844.
- Stärk H, Ganea O-E, Pattanaik L, Barzilay R, Jaakkola T. EQUIBIND: Geometric deep learning for drug binding structure prediction. *arXiv.* 2022; 2022.05146.
- McNutt AT, Francoeur P, Aggarwal R, Masuda T, Meli R, Ragoza M, Sunseri J, Koes DR. GNINA 1.0: molecular docking with deep learning. *J Cheminform.* 2021; 13:43.

Received August 19, 2023; Revised September 15, 2023; Accepted September 19, 2023.

*Address correspondence to:

Shuang Wang, Department of Medical Chemistry, School of Pharmacy, Qingdao University, Qingdao 266071, Shandong, China; Department of Stomatology, Huangdao District Central Hospital, Qingdao 266555, Shandong, China.
E-mail: ws1201youyou@163.com

Xiaowen Tang, Department of Medical Chemistry, School of Pharmacy, Qingdao University, Qingdao 266071, Shandong, China.
E-mail: xwtang1219@qdu.edu.cn

Released online in J-STAGE as advance publication September 26, 2023.

Complete trisomy 9 detected by noninvasive prenatal testing and confirmed by amniocentesis

Feixiang Huang¹, Jing Zhou², Zheyun Xu³, Qing Qi², Hongmei Sun², Lei Chen^{4,*}, Ling Wang^{2,*}

¹ Department of Traditional Chinese Medicine, Hangzhou Women's Hospital, Hangzhou, Zhejiang, China;

² Department of gynecology, Obstetrics and Gynecology Hospital of Fudan University, Shanghai, China;

³ Zhejiang Chinese medical university, Hangzhou, Zhejiang, China;

⁴ Ultrasonography Department, Hangzhou Women's Hospital, Hangzhou, Zhejiang, China.

SUMMARY Complete chromosome 9 trisomy (T9) is a rare and fatal chromosomal disorder. We performed non-invasive prenatal testing (NIPT) in a patient with threatened abortion symptoms and found that the fetal was at risk for complete chromosome 9 trisomy. This shows that NIPT has certain accuracy in detecting trisomy of chromosome 9, which provide options for prenatal diagnosis of rare chromosomal abnormalities.

Keywords noninvasive prenatal testing, amniocentesis, complete trisomy 9, early threatened abortion

Letter to the Editor,

Complete T9 which means trisomy of the whole chromosome 9 with no evidence of mosaicism is rarely been reported. This rare aneuploidy, accounts for only 2.7 percent of all trisomy, usually leads to early pregnancy miscarriage (1). In rare cases, when the babies are born alive, they usually die during the neonatal period (2,3).

On September 16, 2019, a 26-year old female (gravida 1, para 0) patient at 19 week of pregnancy was admitted to our hospital due to abnormality of chromosome 9. There was no history of present disease and the family history was unremarkable. Ultrasonography performed at 7, 3/7 and 12, 1/7 week of pregnancy showed normal results. Early serological screening at 12,3/7 week of pregnancy showed the risk of trisomy 18 was high at 1: 119 (Greater than or equal to 1/460 is high risk), and the risks of trisomy 21 and trisomy 13 were low. Non-invasive prenatal testing (NIPT) at 14,5/7 wk of pregnancy suggested an abnormal Z-score of fetal chromosome 9 at 15.340 (the normal range was Z-score > 3 or < 3). The result of amniocentesis performed at 19 week of pregnancy found the final karyotyping of the fetus was 47, XX, +9, and complete T 9 was confirmed. Transabdominal level II ultrasound performed at 21, 6/7 wk of gestation showed intrauterine growth restriction (IUGR), enlargement of anterior fontanelle (Figure 1A), widened eye distance (Figure 1B), cleft lip and palate (Figures 1C and 1D), high echo of left kidney has, widened renal

collecting system and missing image of right renal echo (Figure 1E). Transverse section of the bladder, with only one umbilical artery visible on the right side of the fetus. In transverse view of the bladder, only one umbilical artery was observed at the right (Figure 1F). The four-chamber view revealed heart enlargement (Figure 1G) and pulmonary artery broadening (Figure 1H). No gallbladder echo was found in this test, that means absence of the gallbladder.

The patient requested termination of the pregnancy. At 22,1/7 week of pregnancy, the patient received ultrasound-guided amniotic cavity 6, 9-diamino-2-ethoxylacridine lactate hydrate (Rivanol, Guangxi Hefeng Pharmaceutical Co., Ltd., China) injection for labor induction. The fetus was stillborn 1 day after Rivanol injection.

NIPT for fetal chromosome detection has been widely used in recent years for further prenatal confirmation (4). It is mainly used for screening T21, T18, and T13 (5) and the use of NIPT in detecting T9 is rarely reported. The chromosome 9 abnormality suggested by NIPT in our case was consistent with the results of late amniocentesis. It is suggested that NIPT has accuracy in the early detection of complete T9. In addition, compared with amniocentesis which is suitable at 15-22 weeks of gestation, and umbilical vein puncture which is suitable at late than18 weeks of gestation (6), NIPT can be used in early gestational weeks with higher security for it doesn't increase the rate of miscarriage and has no contraindications (7).

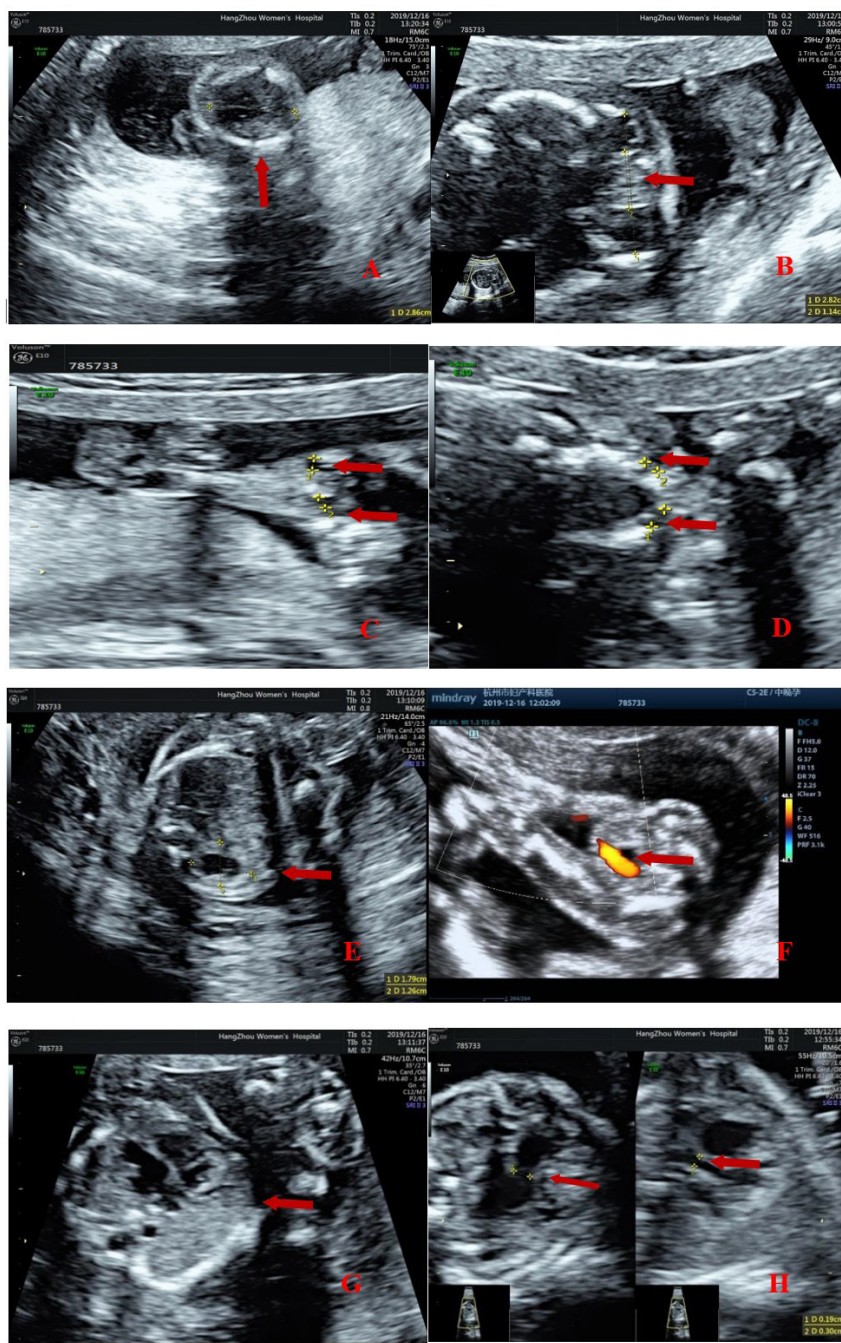


Figure 1 Imaging findings. (A) The arrow denotes the site of large anterior fontanelle, (B) widened eye distance, (C) cleft lip, (D) cleft palate, (E) widened renal collecting system, (F) Single umbilical artery, (G) large heart and (H) Widened pulmonary artery.

It has been reported that the fetal free DNA can be detected as early as 5 weeks of gestation in peripheral blood of pregnant women, and the detection rate is higher in the second trimester (8). Compared with transabdominal chorionic villus sampling (TA-CVS) that can be performed in the earlier gestational weeks (10-14 weeks) (9), NIPT is a non-invasive operation, while the TA-CVS has certain effects on the fetus such as fetal extremity developmental impairment, abortion, etc. (10). Our case reported a complete T9 with signs of threatened abortion, detected by NIPT, finally confirmed by amniocentesis and ultrasonic testing. To our knowledge, there is no similar literature at present. And it indicates that NIPT can be used for early detection of complete T9.

Funding: This work was supported by grants from a project from Kunpeng talent plan of Hangzhou Women's Hospital (to FX Huang), a project from Hangzhou municipal health commission for new talent in the medical industry (to FX Huang), a project of the National Science Foundation of Gansu province (grant No. 23JRRG0009 to HM Sun), a project of the Innovation Foundation of Higher Education of Gansu Province (grant No. 2021B-239 to HM Sun), a project of the Chinese Association of Integration of Traditional and Western Medicine special foundation for Obstetrics and Gynecology (grant No. FCK-ZSYTW-04 to Q Qi), a project under the Scientific and Technological Innovation Action Plan of the Shanghai Natural Science Fund (grant No. 20ZR1409100 to L Wang), a project

of the Chinese Association of Integration of Traditional and Western Medicine special foundation for Obstetrics and Gynecology-PuZheng Pharmaceutical Foundation (grant No. FCK-PZ-08 to L Wang), a project for hospital management of the Shanghai Hospital Association (grant No. X2021046 to L Wang) and a clinical trial project of the Special Foundation for Healthcare Research of the Shanghai Municipal Health Commission (grant No. 202150042 to L Wang).

Conflict of Interest: The authors have no conflicts of interest to disclose.

References

1. Chitayat D, Hodgkinson K, Luke A, Winsor E, Rose T, Kalousek D. Prenatal diagnosis and fetopathological findings in five fetuses with trisomy 9. *Am J Med Genet.* 1995; 56:247-251.
2. Feingold M, Atkins L. A case of trisomy 9. *J Med Genet.* 1973; 10:184-187.
3. Kannan TP, Hemlatha S, Ankathil R, Zilfalil BA. Clinical manifestations in trisomy 9. *Indian J Pediatr.* 2009; 76:745-746.
4. Du Y, Lin J, Lan L, Dong Y, Zhu J, Jiang W, Pan X, Lu Y, Li D, Wang L. Detection of chromosome abnormalities using current noninvasive prenatal testing: A multi-center comparative study. *Biosci Trends.* 2018; 12:317-324.
5. Faycal G, Bianchi DW. Noninvasive prenatal testing creates an opportunity for antenatal treatment of Down syndrome. *Prenat Diagn.* 2013; 33:614-618.
6. Alfirevic Z. Early amniocentesis versus transabdominal chorion villus sampling for prenatal diagnosis. *Cochrane Database Syst Rev.* 2007; 18:CD000077.
7. Odibo AO, Gray DL, Dicke JM, Stamilio DM, Macones GA, Crane JP. Revisiting the fetal loss rate after second-trimester genetic amniocentesis. *Obstet Gynecol.* 2008; 111:589-595.
8. Floyd E, Allyse MA, Michie M. Spanish and English-speaking pregnant women's views on cfDNA and other prenatal screening: Practical and ethical reflections. *J Genet Couns.* 2016; 25:965-977.
9. Firth HV, Boyd PA, Chamberlain PF, MacKenzie IZ, Morriss-Kay GM, Huson SM. Analysis of limb reduction defects in babies exposed to chorionic villus sampling. *Lancet.* 1994; 343:1069-1071.
10. Cederholm M, Haglund B, Axelsson O. Infant morbidity following amniocentesis and chorionic villus sampling for prenatal karyotyping. *BJOG.* 2005; 112:394-402.

Received July 18, 2023; Revised September 18, 2023; Accepted September 22, 2023

*Address correspondence to:

Lei Chen, Department of Hangzhou Women's Hospital, No. 369 Kunpeng Road, Shangcheng District, Hangzhou 310008, Zhejiang, China.

E-mail: fxhuang2009@163.com

Ling Wang, Laboratory for Reproductive Immunology, Obstetrics and Gynecology Hospital of Fudan University, 419 Fangxie Road, Shanghai 200011, China.

E-mail: dr.wangling@fudan.edu.cn.

Released online in J-STAGE as advance publication October 11, 2023.



Guide for Authors

1. Scope of Articles

Drug Discoveries & Therapeutics (Print ISSN 1881-7831, Online ISSN 1881-784X) welcomes contributions in all fields of pharmaceutical and therapeutic research such as medicinal chemistry, pharmacology, pharmaceutical analysis, pharmaceutics, pharmaceutical administration, and experimental and clinical studies of effects, mechanisms, or uses of various treatments. Studies in drug-related fields such as biology, biochemistry, physiology, microbiology, and immunology are also within the scope of this journal.

2. Submission Types

Original Articles should be well-documented, novel, and significant to the field as a whole. An Original Article should be arranged into the following sections: Title page, Abstract, Introduction, Materials and Methods, Results, Discussion, Acknowledgments, and References. Original articles should not exceed 5,000 words in length (excluding references) and should be limited to a maximum of 50 references. Articles may contain a maximum of 10 figures and/or tables. Supplementary Data are permitted but should be limited to information that is not essential to the general understanding of the research presented in the main text, such as unaltered blots and source data as well as other file types.

Brief Reports definitively documenting either experimental results or informative clinical observations will be considered for publication in this category. Brief Reports are not intended for publication of incomplete or preliminary findings. Brief Reports should not exceed 3,000 words in length (excluding references) and should be limited to a maximum of 4 figures and/or tables and 30 references. A Brief Report contains the same sections as an Original Article, but the Results and Discussion sections should be combined.

Reviews should present a full and up-to-date account of recent developments within an area of research. Normally, reviews should not exceed 8,000 words in length (excluding references) and should be limited to a maximum of 10 figures and/or tables and 100 references. Mini reviews are also accepted, which should not exceed 4,000 words in length (excluding references) and should be limited to a maximum of 5 figures and/or tables and 50 references.

Policy Forum articles discuss research and policy issues in areas related to life science such as public health, the medical care system, and social science and may address governmental issues at district, national, and international levels of discourse. Policy Forum articles should not exceed 3,000 words in length (excluding references) and should be limited to a maximum of 5 figures and/or tables and 30 references.

Case Reports should be detailed reports of the symptoms, signs, diagnosis, treatment, and follow-up of an individual patient. Case reports may contain a demographic profile of the patient but usually describe an unusual or novel occurrence. Unreported or unusual side effects or adverse interactions involving medications will also be considered. Case Reports should not exceed 3,000 words in length (excluding references).

Communications are short, timely pieces that spotlight new research findings or policy issues of interest to the field of global health and medical practice that are of immediate importance. Depending on their content, Communications will be published as "Comments" or

"Correspondence". Communications should not exceed 1,500 words in length (excluding references) and should be limited to a maximum of 2 figures and/or tables and 20 references.

Editorials are short, invited opinion pieces that discuss an issue of immediate importance to the fields of global health, medical practice, and basic science oriented for clinical application. Editorials should not exceed 1,000 words in length (excluding references) and should be limited to a maximum of 10 references. Editorials may contain one figure or table.

News articles should report the latest events in health sciences and medical research from around the world. News should not exceed 500 words in length.

Letters should present considered opinions in response to articles published in *Drug Discoveries & Therapeutics* in the last 6 months or issues of general interest. Letters should not exceed 800 words in length and may contain a maximum of 10 references. Letters may contain one figure or table.

3. Editorial Policies

For publishing and ethical standards, *Drug Discoveries & Therapeutics* follows the Recommendations for the Conduct, Reporting, Editing, and Publication of Scholarly Work in Medical Journals issued by the International Committee of Medical Journal Editors (ICMJE, <https://icmje.org/recommendations>), and the Principles of Transparency and Best Practice in Scholarly Publishing jointly issued by the Committee on Publication Ethics (COPE, <https://publicationethics.org/resources/guidelines-new/principles-transparency-and-best-practice-scholarly-publishing>), the Directory of Open Access Journals (DOAJ, <https://doaj.org/apply/transparency>), the Open Access Scholarly Publishers Association (OASPA, <https://oaspa.org/principles-of-transparency-and-best-practice-in-scholarly-publishing-4>), and the World Association of Medical Editors (WAME, <https://wame.org/principles-of-transparency-and-best-practice-in-scholarly-publishing>).

Drug Discoveries & Therapeutics will perform an especially prompt review to encourage innovative work. All original research will be subjected to a rigorous standard of peer review and will be edited by experienced copy editors to the highest standards.

Ethical Approval of Studies and Informed Consent: For all manuscripts reporting data from studies involving human participants or animals, formal review and approval, or formal review and waiver, by an appropriate institutional review board or ethics committee is required and should be described in the Methods section. When your manuscript contains any case details, personal information and/or images of patients or other individuals, authors must obtain appropriate written consent, permission and release in order to comply with all applicable laws and regulations concerning privacy and/or security of personal information. The consent form needs to comply with the relevant legal requirements of your particular jurisdiction, and please do not send signed consent form to *Drug Discoveries & Therapeutics* to respect your patient's and any other individual's privacy. Please instead describe the information clearly in the Methods (patient consent) section of your manuscript while retaining copies of the signed forms in the event they should be needed. Authors should also state that the study conformed to the provisions of the Declaration of Helsinki (as revised in 2013, <https://wma.net/what-we-do/medical-ethics/declaration-of-helsinki>). When reporting experiments on animals, authors should indicate whether the institutional and national guide for the care and use of laboratory animals was followed.

Reporting Clinical Trials: The ICMJE (<https://icmje.org/recommendations/browse/publishing-and-editorial-issues/clinical-trial-registration.html>) defines a clinical trial as any research project that prospectively assigns people or a group of people to an intervention, with or without concurrent comparison or control groups, to study the relationship between a health-related intervention and a health outcome. Registration of clinical trials in a public trial registry

at or before the time of first patient enrollment is a condition of consideration for publication in *Drug Discoveries & Therapeutics*, and the trial registration number will be published at the end of the Abstract. The registry must be independent of for-profit interest and publicly accessible. Reports of trials must conform to CONSORT 2010 guidelines (<https://consort-statement.org/consort-2010>). Articles reporting the results of randomized trials must include the CONSORT flow diagram showing the progress of patients throughout the trial.

Conflict of Interest: All authors are required to disclose any actual or potential conflict of interest including financial interests or relationships with other people or organizations that might raise questions of bias in the work reported. If no conflict of interest exists for each author, please state "There is no conflict of interest to disclose".

Submission Declaration: When a manuscript is considered for submission to *Drug Discoveries & Therapeutics*, the authors should confirm that 1) no part of this manuscript is currently under consideration for publication elsewhere; 2) this manuscript does not contain the same information in whole or in part as manuscripts that have been published, accepted, or are under review elsewhere, except in the form of an abstract, a letter to the editor, or part of a published lecture or academic thesis; 3) authorization for publication has been obtained from the authors' employer or institution; and 4) all contributing authors have agreed to submit this manuscript.

Initial Editorial Check: Immediately after submission, the journal's managing editor will perform an initial check of the manuscript. A suitable academic editor will be notified of the submission and invited to check the manuscript and recommend reviewers. Academic editors will check for plagiarism and duplicate publication at this stage. The journal has a formal recusal process in place to help manage potential conflicts of interest of editors. In the event that an editor has a conflict of interest with a submitted manuscript or with the authors, the manuscript, review, and editorial decisions are managed by another designated editor without a conflict of interest related to the manuscript.

Peer Review: *Drug Discoveries & Therapeutics* operates a single-anonymized review process, which means that reviewers know the names of the authors, but the authors do not know who reviewed their manuscript. All articles are evaluated objectively based on academic content. External peer review of research articles is performed by at least two reviewers, and sometimes the opinions of more reviewers are sought. Peer reviewers are selected based on their expertise and ability to provide quality, constructive, and fair reviews. For research manuscripts, the editors may, in addition, seek the opinion of a statistical reviewer. Every reviewer is expected to evaluate the manuscript in a timely, transparent, and ethical manner, following the COPE guidelines (https://publicationethics.org/files/cope-ethical-guidelines-peer-reviewers-v2_0.pdf). We ask authors for sufficient revisions (with a second round of peer review, when necessary) before a final decision is made. Consideration for publication is based on the article's originality, novelty, and scientific soundness, and the appropriateness of its analysis.

Suggested Reviewers: A list of up to 3 reviewers who are qualified to assess the scientific merit of the study is welcomed. Reviewer information including names, affiliations, addresses, and e-mail should be provided at the same time the manuscript is submitted online. Please do not suggest reviewers with known conflicts of interest, including participants or anyone with a stake in the proposed research; anyone from the same institution; former students, advisors, or research collaborators (within the last three years); or close personal contacts. Please note that the Editor-in-Chief may accept one or more of the proposed reviewers or may request a review by other qualified persons.

Language Editing: Manuscripts prepared by authors whose native language is not English should have their work proofread by a native English speaker before submission. If not, this might delay the publication of your manuscript in *Drug Discoveries & Therapeutics*.

The Editing Support Organization can provide English

proofreading, Japanese-English translation, and Chinese-English translation services to authors who want to publish in *Drug Discoveries & Therapeutics* and need assistance before submitting a manuscript. Authors can visit this organization directly at <https://www.iacmhr.com/iac-eso/support.php?lang=en>. IAC-ESO was established to facilitate manuscript preparation by researchers whose native language is not English and to help edit works intended for international academic journals.

Copyright and Reuse: Before a manuscript is accepted for publication in *Drug Discoveries & Therapeutics*, authors will be asked to sign a transfer of copyright agreement, which recognizes the common interest that both the journal and author(s) have in the protection of copyright. We accept that some authors (e.g., government employees in some countries) are unable to transfer copyright. A JOURNAL PUBLISHING AGREEMENT (JPA) form will be e-mailed to the authors by the Editorial Office and must be returned by the authors by mail, fax, or as a scan. Only forms with a hand-written signature from the corresponding author are accepted. This copyright will ensure the widest possible dissemination of information. Please note that the manuscript will not proceed to the next step in publication until the JPA Form is received. In addition, if excerpts from other copyrighted works are included, the author(s) must obtain written permission from the copyright owners and credit the source(s) in the article.

4. Cover Letter

The manuscript must be accompanied by a cover letter prepared by the corresponding author on behalf of all authors. The letter should indicate the basic findings of the work and their significance. The letter should also include a statement affirming that all authors concur with the submission and that the material submitted for publication has not been published previously or is not under consideration for publication elsewhere. The cover letter should be submitted in PDF format. For an example of Cover Letter, please visit: Download Centre (<https://www.ddtjournal.com/downcentre>).

5. Submission Checklist

The Submission Checklist should be submitted when submitting a manuscript through the Online Submission System. Please visit Download Centre (<https://www.ddtjournal.com/downcentre>) and download the Submission Checklist file. We recommend that authors use this checklist when preparing your manuscript to check that all the necessary information is included in your article (if applicable), especially with regard to Ethics Statements.

6. Manuscript Preparation

Manuscripts are suggested to be prepared in accordance with the "Recommendations for the Conduct, Reporting, Editing, and Publication of Scholarly Work in Medical Journals", as presented at <http://www.ICMJE.org>.

Manuscripts should be written in clear, grammatically correct English and submitted as a Microsoft Word file in a single-column format. Manuscripts must be paginated and typed in 12-point Times New Roman font with 24-point line spacing. Please do not embed figures in the text. Abbreviations should be used as little as possible and should be explained at first mention unless the term is a well-known abbreviation (e.g. DNA). Single words should not be abbreviated.

Title page: The title page must include 1) the title of the paper (Please note the title should be short, informative, and contain the major key words); 2) full name(s) and affiliation(s) of the author(s), 3) abbreviated names of the author(s), 4) full name, mailing address, telephone/fax numbers, and e-mail address of the corresponding author; 5) author contribution statements to specify the individual contributions of all authors to this manuscript, and 6) conflicts of interest (if you have an actual or potential conflict of interest to disclose, it must be included as a footnote on the title page of the manuscript; if no conflict of interest

exists for each author, please state "There is no conflict of interest to disclose").

Abstract: The abstract should briefly state the purpose of the study, methods, main findings, and conclusions. For article types including Original Article, Brief Report, Review, Policy Forum, and Case Report, a one-paragraph abstract consisting of no more than 250 words must be included in the manuscript. For Communications, Editorials, News, or Letters, a brief summary of main content in 150 words or fewer should be included in the manuscript. For articles reporting clinical trials, the trial registration number should be stated at the end of the Abstract. Abbreviations must be kept to a minimum and non-standard abbreviations explained in brackets at first mention. References should be avoided in the abstract. Three to six key words or phrases that do not occur in the title should be included in the Abstract page.

Introduction: The introduction should provide sufficient background information to make the article intelligible to readers in other disciplines and sufficient context clarifying the significance of the experimental findings.

Materials/Patients and Methods: The description should be brief but with sufficient detail to enable others to reproduce the experiments. Procedures that have been published previously should not be described in detail but appropriate references should simply be cited. Only new and significant modifications of previously published procedures require complete description. Names of products and manufacturers with their locations (city and state/country) should be given and sources of animals and cell lines should always be indicated. All clinical investigations must have been conducted in accordance with the Declaration of Helsinki (as revised in 2013, <https://wma.net/what-we-do/medical-ethics/declaration-of-helsinki>). All human and animal studies must have been approved by the appropriate institutional review board(s) and a specific declaration of approval must be made within this section.

Results: The description of the experimental results should be succinct but in sufficient detail to allow the experiments to be analyzed and interpreted by an independent reader. If necessary, subheadings may be used for an orderly presentation. All Figures and Tables should be referred to in the text in order, including those in the Supplementary Data.

Discussion: The data should be interpreted concisely without repeating material already presented in the Results section. Speculation is permissible, but it must be well-founded, and discussion of the wider implications of the findings is encouraged. Conclusions derived from the study should be included in this section.

Acknowledgments: All funding sources (including grant identification) should be credited in the Acknowledgments section. Authors should also describe the role of the study sponsor(s), if any, in study design; in the collection, analysis, and interpretation of data; in the writing of the report; and in the decision to submit the paper for publication. If the funding source had no such involvement, the authors should so state.

In addition, people who contributed to the work but who do not meet the criteria for authors should be listed along with their contributions.

References: References should be numbered in the order in which they appear in the text. Citing of unpublished results, personal communications, conference abstracts, and theses in the reference list is not recommended but these sources may be mentioned in the text. In the reference list, cite the names of all authors when there are fifteen or fewer authors; if there are sixteen or more authors, list the first three followed by *et al.* Names of journals should be abbreviated in the style used in PubMed. Authors are responsible for the accuracy of the references. The EndNote Style of *Drug Discoveries & Therapeutics* could be downloaded at **EndNote** (https://www.ddtjournal.com/examples/Drug_Discoveries_Therapeutics.ens).

Examples are given below:

Example 1 (Sample journal reference):

Nakata M, Tang W. Japan-China Joint Medical Workshop on Drug Discoveries and Therapeutics 2008: The need of Asian pharmaceutical researchers' cooperation. *Drug Discov Ther.* 2008; 2:262-263.

Example 2 (Sample journal reference with more than 15 authors):

Darby S, Hill D, Auvinen A, *et al.* Radon in homes and risk of lung cancer: Collaborative analysis of individual data from 13 European case-control studies. *BMJ.* 2005; 330:223.

Example 3 (Sample book reference):

Shalev AY. Post-traumatic stress disorder: Diagnosis, history and life course. In: Post-traumatic Stress Disorder, Diagnosis, Management and Treatment (Nutt DJ, Davidson JR, Zohar J, eds.). Martin Dunitz, London, UK, 2000; pp. 1-15.

Example 4 (Sample web page reference):

World Health Organization. The World Health Report 2008 – primary health care: Now more than ever. <https://apps.who.int/iris/handle/10665/43949> (accessed September 23, 2022).

Tables: All tables should be prepared in Microsoft Word or Excel and should be arranged at the end of the manuscript after the References section. Please note that tables should not be in image format. All tables should have a concise title and should be numbered consecutively with Arabic numerals. If necessary, additional information should be given below the table.

Figure Legend: The figure legend should be typed on a separate page of the main manuscript and should include a short title and explanation. The legend should be concise but comprehensive and should be understood without referring to the text. Symbols used in figures must be explained. Any individually labeled figure parts or panels (A, B, etc.) should be specifically described by part name within the legend.

Figure Preparation: All figures should be clear and cited in numerical order in the text. Figures must fit a one- or two-column format on the journal page: 8.3 cm (3.3 in.) wide for a single column, 17.3 cm (6.8 in.) wide for a double column; maximum height: 24.0 cm (9.5 in.). Please make sure that artwork files are in an acceptable format (TIFF or JPEG) at minimum resolution (600 dpi for illustrations, graphs, and annotated artwork, and 300 dpi for micrographs and photographs). Please provide all figures as separate files. Please note that low-resolution images are one of the leading causes of article resubmission and schedule delays.

Units and Symbols: Units and symbols conforming to the International System of Units (SI) should be used for physicochemical quantities. Solidus notation (e.g. mg/kg, mg/mL, mol/mm²/min) should be used. Please refer to the SI Guide www.bipm.org/en/si/ for standard units.

Supplemental data: Supplemental data might be useful for supporting and enhancing your scientific research and *Drug Discoveries & Therapeutics* accepts the submission of these materials which will be only published online alongside the electronic version of your article. Supplemental files (figures, tables, and other text materials) should be prepared according to the above guidelines, numbered in Arabic numerals (e.g., Figure S1, Figure S2, and Table S1, Table S2) and referred to in the text. All figures and tables should have titles and legends. All figure legends, tables and supplemental text materials should be placed at the end of the paper. Please note all of these supplemental data should be provided at the time of initial submission and note that the editors reserve the right to limit the size

and length of Supplemental Data.

7. Online Submission

Manuscripts should be submitted to *Drug Discoveries & Therapeutics* online at <https://www.ddtjournal.com/login>. Receipt of your manuscripts submitted online will be acknowledged by an e-mail from Editorial Office containing a reference number, which should be used in all future communications. If for any reason you are unable to submit a file online, please contact the Editorial Office by e-mail at office@ddtjournal.com

8. Accepted Manuscripts

Page Charge: Page charges will be levied on all manuscripts accepted for publication in *Drug Discoveries & Therapeutics* (Original Articles / Brief Reports / Reviews / Policy Forum / Communications: \$140 per page for black white pages, \$340 per page for color pages; News / Letters: a total cost of \$600). Under exceptional circumstances, the author(s) may apply to the editorial office for a waiver of the publication charges by stating the reason in the Cover Letter when the

manuscript online.

Misconduct: *Drug Discoveries & Therapeutics* takes seriously all allegations of potential misconduct and adhere to the ICMJE Guideline (<https://icmje.org/recommendations>) and COPE Guideline (https://publicationethics.org/files/Code_of_conduct_for_journal_editors.pdf). In cases of suspected research or publication misconduct, it may be necessary for the Editor or Publisher to contact and share submission details with third parties including authors' institutions and ethics committees. The corrections, retractions, or editorial expressions of concern will be performed in line with above guidelines.

(As of December 2022)

Drug Discoveries & Therapeutics

Editorial and Head Office
Pearl City Koishikawa 603,
2-4-5 Kasuga, Bunkyo-ku,
Tokyo 112-0003, Japan.
E-mail: office@ddtjournal.com

